การสังเคราะห์อนุพันธ์ทรุกซีนชนิดใหม่เพื่อเป็นคีโมเซ็นเซอร์สำหรับไนโตรแอโรแมติกและไอออนโลหะ

นางสาวภรภัทร สำอางค์

วิทยานิพนธ์นี้เป็นส่วนหนึ่งของการศึกษาตามหลักสูตรปริญญาวิทยาศาสตรดุษฎีบัณฑิต
สาขาวิชาเคมี ภาควิชาเคมี
คณะวิทยาศาสตร์ จุฬาลงกรณ์มหาวิทยาลัย
ปีการศึกษา 2558

SYNTHESIS OF NOVEL TRUXENE DERIVATIVES AS CHEMOSENSORS FOR NITROAROMATICS AND METAL IONS

Miss Pornpat Sam-ang

A Dissertation Submitted in Partial Fulfillment of the Requirements
for the Degree of Doctor of Philosophy Program in Chemistry
Department of Chemistry
Faculty of Science
Chulalongkorn University
Academic Year 2015

Thesis Title	SYNTHESIS OF NOVEL TRUXENE DERIVATIVES AS CHEMOSENSORS FOR NITROAROMATICS AND METAL IONS
By	Miss Pornpat Sam-ang
Field of Study	Chemistry
Thesis Advisor	Associate Professor Paitoon Rashatasakhon, Ph.D.
Thesis Co-Advisor	Professor Mongkol Sukwattanasinitt, Ph.D.

Accepted by the Faculty of Science, Chulalongkorn University in Partial Fulfillment of the Requirements for the Doctoral Degree

.....Dean of the Faculty of Science
(Associate Professor Polkit Sangvanich, Ph.D.)

THESIS COMMITTEE

.....Chairman
(Associate Professor Vudhichai Parasuk, Ph.D.)

.....Thesis Advisor
(Associate Professor Paitoon Rashatasakhon, Ph.D.)

.....Thesis Co-Advisor
(Professor Mongkol Sukwattanasinitt, Ph.D.)

.....Examiner
(Assistant Professor Anawat Ajavakom, Ph.D.)

.....Examiner
(Professor Thawatchai Tuntulani, Ph.D.)

.....External Examiner
(Professor Ngampong Kongkathip, Ph.D.)

ภรภัทร สำอางค์ : การสังเคราะห์อนุพันธ์ทรุกซีนชนิดใหม่เพื่อเป็นคีโมเซ็นเซอร์สำหรับไนโตรแอโรแมติกและไอออนโลหะ (SYNTHESIS OF NOVEL TRUXENE DERIVATIVES AS CHEMOSENSORS FOR NITROAROMATICS AND METAL IONS) อ.ที่ปรึกษาวิทยานิพนธ์หลัก: รศ. ดร.ไพฑูรย์ รัชตะสาคร, อ.ที่ปรึกษาวิทยานิพนธ์ร่วม: ศ. ดร.มงคล สุขวัฒนาสินิทธิ์, 87 หน้า.

สารประกอบเรืองแสง 2 ชนิดซึ่งมีทรุกซีนเป็นหน่วยเรืองแสงถูกสังเคราะห์และพัฒนาเพื่อใช้เป็น turn-off ฟลูออเรสเซนต์เซ็นเซอร์สำหรับสารประกอบไนโตรอะโรมาติก (T1) และไอออนของทองแดง (T2) หมู่ไม่ชอบน้ำชนิดนอร์มอลบิวทิลหรือ หมู่ชอบน้ำที่เป็นสายโซ่ไดไกลคอลที่อยู่ในโครงสร้าง T1 และ T2 สามารถยับยั้งการซ้อนทับของทรุกซีนแบบไพ-ไพ อีกทั้งยังช่วยให้สารมีความสารถในการละลายได้ในตัวทำละลายอินทรีย์หรือในน้ำ การสังเคราะห์สารแต่ละชนิดสามารถทำได้โดยใช้ปฏิกิริยาควบคู่โซโนกาชิราเป็นหลัก ซึ่งสามารถให้ผลิตภัณฑ์ที่ต้องการ T1 และ T2 ได้ในร้อยละผลผลิตที่ 14 และ 18 ตามลำดับ สมบัติเชิงแสงและความสามารถในการตรวจวัดของ T1 ขึ้นอยู่กับชนิดของตัวทำละลาย ในคลอโรฟอร์ม สาร T1 สามารถระงับสัญญาณการเรืองแสงอย่างจำเพาะเจาะจงโดย 2-ไนโตรฟีนอล อย่างไรก็ตาม การระงับสัญญาณฟลูออเรสเซนต์จะเลือกจำเพาะเจาะจงกับกรดพิคริกในของผสมระหว่างน้ำและเตตระไฮโดรฟิวแรนเป็นตัวทำละลาย ความเข้มข้นต่ำสุดที่สามารถตรวจวัดได้เท่ากับ 1.54 และ 0.15 ส่วนในล้านส่วนสำหรับ 2-ไนโตรฟีนอลและกรดพิคริก ตามลำดับ จากการพิจารณาการซ้อนทับของสเปกตรัมการดูดกลืนแสงของ T1 และสารที่ถูกวิเคราะห์สัมพันธ์กับเศษส่วนของโฟตอนที่ถูกดูดกลืนโดย T1 และประสิทธิภาพการระงับสัญญาณ บ่งชี้ว่ากลไกการตรวจวัดเกี่ยวข้องกับปรากฏการณ์บดบังการดูดกลืนแสงของ T1 ด้วยสารที่ถูกวิเคราะห์ อย่างไรก็ตามประสิทธิภาพในการตรวจวัดที่ลดลงเมื่ออุณหภูมิเพิ่มสูงขึ้นแสดงให้เห็นว่ายังมีกลไกในการระงับสัญญาณแบบการถ่ายเทพลังงานเข้ามาเกี่ยวข้องด้วย

สาร T2 สามารถละลายได้ดีในเตตระไฮโดรฟิวแรนที่มีน้ำมากถึง 70% และแสดงการถูกระงับสัญญาณการเรืองแสงอย่างจำเพาะต่อไอออนทองแดง โดยปราศจากการรบกวนจากไอออนของโลหะชนิดอื่นๆ ระบบการตรวจวัดนี้มีขอบเขตของการตรวจวัดไอออนทองแดงที่ 0.06 ส่วนในล้านส่วน ผลการศึกษาพบว่าเศษส่วนโมลระหว่าง T2 กับไอออนทองแดงที่ 0.5 จะให้ประสิทธิภาพในการระงับสัญญาณสูงที่สุด และการวิเคราะห์มวลในสารละลายผสมระหว่าง T2 กับไอออนทองแดงพบมวลโมเลกุลที่สอดคล้องกับสารประกอบเชิงซ้อนระหว่าง T2 และทองแดงในสัดส่วน 1:1 กลไกการตรวจวัดอาจเกี่ยวข้องกับการระงับสัญญาณของการเกิดสารเชิงซ้อนที่สภาวะพื้น นอกจากนี้ สามารถพัฒนาระบบตรวจวัดแอนไอออนที่มีความจำเพาะได้จากสารละลายผสมระหว่าง T2 กับไอออนทองแดง ซึ่งแสดงการกลับคืนมาของสัญญาณเมื่อเติมไฮโดรเจนฟอตเฟตและสารประกอบฟอตเฟตชีวภาพต่างๆ โดยการได้รับสัญญาณการเรืองแสงกลับคืนมาเกิดจากการโคออดิเนชันระหว่างหมู่ฟอตเฟตกับไอออนทองแดงในสารประกอบเชิงซ้อน

ภาควิชา เคมี	ลายมือชื่อนิสิต .....
สาขาวิชา เคมี	ลายมือชื่อ อ.ที่ปรึกษาหลัก .....
ปีการศึกษา 2558	ลายมือชื่อ อ.ที่ปรึกษาร่วม .....

5373927523 : MAJOR CHEMISTRY
KEYWORDS: TRUXENE / NITROAROMATIC COMPOUNDS / COPPER(II) ION / FLUORESCENT SENSORS

PORNPAT SAM-ANG: SYNTHESIS OF NOVEL TRUXENE DERIVATIVES AS CHEMOSENSORS FOR NITROAROMATICS AND METAL IONS. ADVISOR: ASSOC. PROF. PAITOON RASHATASAKHON, Ph.D., CO-ADVISOR: PROF. MONGKOL SUKWATTANASINITT, Ph.D., 87 pp.

Two fluorescent compounds with truxene as a fluorophore are synthesized and developed as turn-off fluorescent sensors for nitroaromatic compounds (T1) and copper(II) ion (T2). Six hydrophobic *n*-butyl groups in T1 and six hydrophilic diglycol chains in T2 prevent pi-pi stacking of truxene core and enhance their solubilities in organic or aqueous media. The synthesis of each compound is based primarily on the Sonogashira coupling reactions, which produced the desired compounds T1 and T2 in the overall yields of 14 and 18 %, respectively. The photophysical and sensing properties of T1 depend on the solvents. In chloroform, T1 is selectively quenched by 2-nitrophenol. However, the quenching is the fluorescence signal of selectively observed with picric acid in aqueous tetrahydrofuran. The detection limits are determined as 1.54 and 0.15 ppm for 2-nitrophenol and picric acid, respectively. The considerable overlapping of the absorption spectra of T1 and that of the analytes, along with the correlation of the fraction of photons absorbed by T1 and quenching efficiencies, the sensing mechanism significantly involves inner-filter effect, where the analytes compete with T1 during the absorption process. However, the lower quenching efficiency at higher temperature suggested that energy transfer via static quenching may also involve.

Compound T2 can dissolve well in tetrahydrofuran containing up to 70% of water and shows effective and selective fluorescence quenching towards copper(II) ion without any interference from other metal ions. The detection limit of this sensing system is 0.06 ppm. The mass analysis using a mixture between T2 and copper(II) ion corresponds to the mass of a 1:1 complex between T2 and copper(II), as verified by a Job's plot. Thus, the quenching mechanism should involves the formation of such non fluorescent ground state complex. In addition, an anion sensing system is developed from the complex of T2 and copper(II) ion, which shows fluorescence recovery upon the addition of hydrogen phosphate and several biological phosphate compounds. The signal restoration involves the coordination of phosphate group to copper(II) preventing the complexation of copper(II) ion with T2.

Department:	Chemistry	Student's Signature	.....
Field of Study:	Chemistry	Advisor's Signature	.....
Academic Year:	2015	Co-Advisor's Signature	.....

ACKNOWLEDGEMENTS

Firstly, I would like to express my deepest gratitude to my supervisors, Assoc. Prof. Dr. Paitoon Rashatasakhon and my co-advisor, Prof. Dr. Mongkol Sukwattanasinitt for the continuous support, excellent guidances, stimulation, helpful discussions, valuable suggestions and providing me with an excellent atmosphere for doing research and writing of this thesis. Without these two persons I could not reach my goal.

Secondly, My appreciation is given to Assoc. Prof. Dr. Vudhichai Parasuk, Prof. Dr. Thawatchai Tuntulani and Asst. Prof. Dr. Anawat Ajavakom by serving as the chairman and members of thesis defense committee. Thank you for their kind attentions and advices in this thesis. I gratefully thank Prof. Dr. Ngampong Kongkathip, the external examiner from Kasetsart University for her kind suggestions and many useful remarks.

I truly thank Prof. Dr. Quan Jason Cheng from the Department of Chemistry, University California Riverside, USA for the stimulating discussions, supporting by giving me a good opportunity to join his group for two months. I also thank my great friends at Riverside campus for fun times and great memories and during I was there as a visiting student.

My sincere thank the financial support from the Pibulsongkram Rajabhat University and the commission on Higher Education (CHE) under the Strategic Scholarships program for Frontier Research Network for the joint Ph.D Program Thai Doctoral degree. Also, I would like to thank Overseas Research Experience Scholarship for giving me a chance to doing research at California Riverside University and the 90th Anniversary of Chulalongkorn University Fund (Ratchadapisek Sompote Fund) for their financial support of my study.

Besides, I would sincerely like to thank Asst. Prof. Dr. Anawat Ajavakom, Asst. Prof. Dr. Sumrit Wacharasindhu, and Dr. Sakulsuk Unarunthai for their challenging ideas, advices and giving me good suggestions during our research group meeting.

In addition, I would like to thank my fellow labmates in MAPS Group: Dr. Nakorn Niamnont, Dr. Wisuttaya Worawalai, Miss Rungthiwa Arunchai, Mr. Thanachart Techajaroonjit, Mr. Rangsarit Sukato, Mr. Bhobnibhit Chatmaneerungcharoen, Mr. Waroton Paisuwan, Mr. Apiratt Thitimon, Mr. Jadetapong Klahan and all those others that have not been mentioned above. They have always been hugely supportive and encouraging me with their best wishes. I especially thank all my friends at Pibulsongkram Rajabhat University for our friendship and their helps in everything. I will never forget.

Finally, my heartfelt thank to my parents, my sister and Dr. Thongchai Chinkatham for their moral principal, love, care and supporting me spiritually throughout my life.

CONTENTS

Page

Page

Page

Page

LIST OF TABLES

Table Page

LIST OF FIGURES

Figure Page

LIST OF SCHEMES

Scheme Page

LIST OF ABBREVIATIONS

Ar	aromatic
calcd	calculated
^{13}C NMR	carbon-13 nuclear magnetic resonance
$CDCl_3$	deuterated chloroform
DMSO- d_6	deuterated dimethyl sulfoxide
DMSO	dimethylsulfoxide
d	doublet (NMR)
dd	doublet of doublet (NMR)
ESIMS	electrospray ionization mass spectrometry
equiv	equivalent (s)
FT-IR	fourier transform infrared spectroscopy
g	gram (s)
^{1}H NMR	proton nuclear magnetic resonance
Hz	Hertz
HRMS	high resolution mass spectrum
h	hour (s)
IR	*infrared*
J	coupling constant
mg	milligram (s)
mL	milliliter (s)
mmol	millimole (s)
m/z	mass per charge

m	multiplet (NMR)
M.W.	molecular weight
M	molar
MHz	megaHertz
rt	room temperature
s	singlet (NMR)
THF	tetrahydrofuran
TLC	thin layer chromatography
UV	ultraviolet
δ	chemical shift
°C	degree celsius
μL	microliter (s)
μM	micromolar (s)
Φ	quantum yield
% yield	percentage yield

CHAPTER I
INTRODUCTION

1.1 Overview

The contamination of air, soil, and water by pollutants such as heavy metal ions or nitroaromatic compounds (NACs) has been major environmental concerns. Therefore, qualitative and quantitative detections of these hazardous compounds in environmental sources or ecosystem are of great importance. Various analytical techniques such as gas chromatography coupled mass spectrometry (GC-MS), ion-mobility spectroscopy (IMS), and surface enhanced Raman spectroscopy (SARS) have been used for these purposes. However, these techniques usually require costly equipment, complicated instrument operation, tedious sample preparation, and well-trained instrument users. In comparison to those techniques, fluorescence spectroscopy is more user-friendly, requires less expensive instrument, yet provides high selectivity and comparable sensitivity in short response time. As the portable fluorometers have become commercially available, the real-time monitoring and on-site detection can also be performed [1-3].

1.1.1 Nitroaromatic compounds

Nitroaromatic compounds (NACs) such as nitrobenzene (NB), trinitrobenzene (TNB) and picric acid (PA) are widely used as industrial solvents, insecticides, dyes, and herbicides, while trinitrotolulene (TNT) is the explosive chemical commonly involves in terrorist or criminal activities [4-8] **(Figure 1.1)**. For the bioenvironmental issues, contamination of NACs in water and soil can be seriously dangerous, especially to the chemically sensitive animals and plants [9-11]. In term of human exposure, NACs are known to cause the formation of methemoglobin upon acute exposure while the chronic exposure can cause anemia, bladder tumors, and liver damages [12, 13].

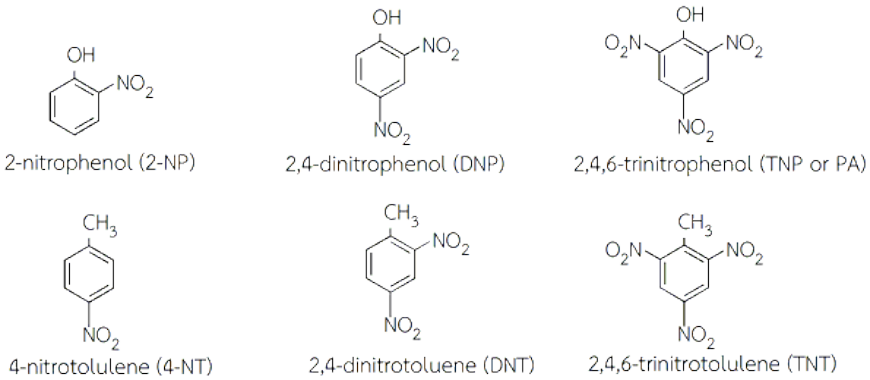

Figure 1.1 Structure of nitroaromatic compounds

1.1.2 Heavy metals

Heavy metal ions are the cationic forms of transition elements such as copper, lead, iron, mercury, zinc, and manganese. They have high atomic weights and relatively high stabilities. Most importantly, they can accumulate in the air, water, soil, and living organisms through food chains. These metal ions are usually toxic to the environment and living organisms such as algae, fungi, bacteria or viruses. Their accumulation in human bodies often lead to sickness or health problems. Common sources of heavy metal ions contaminated in environment include agricultural and industrial wastes. For human body, some of these metals are essential to maintain the metabolism or biological functions of cells and organs, while some are highly toxic. For example, Cu^{2+} ions are essential for human body. They are distributed in liver, muscle, and bone, and they can facilitate the process of iron uptake. Therefore, Cu^{2+} deficiency often results in anemia-like symptoms as well as hypopigmentation, bone abnormalities, impaired growth, and irregularity in glucose and cholesterol metabolisms. In contrast, excessive accumulation of copper in tissues can cause Wilson's disease—an autosomal recessive genetic disorder [14-18].

1.2 Fluorescence spectroscopy

Fluorescence spectroscopy, also known as fluorometry or spectrofluorometry, is widely used as analytical techniques in chemical, biological, and environmental studies. It is a precise quantitative and qualitative technique that have many

advantages over other spectroscopic methods such as simplicity, high sensitivity, high specificity, inexpensive, easy to operate and can be used as various applications [19].

The fluorescence process is usually illustrated by the Jablonski diagram [19] as shown in **Figure 1.2**. Fluorescence occurs when a molecule in ground state (S_0) absorbs light. One electron in the highest occupied molecular orbital (HOMO) is then excited to a higher molecular orbital, causing the molecule to change its electronic state from ground (S0) to excited states (S_1, S_2, or S_3) depending on the amount of absorbed energy. At the excited state, the molecule would quickly release energy by internal conversion (vibration or rotation) to the lowest excited state. After that, the fluorescence signal is observed when molecule release the last portion of energy when it changes from the lowest electronic excited state back to the ground state.

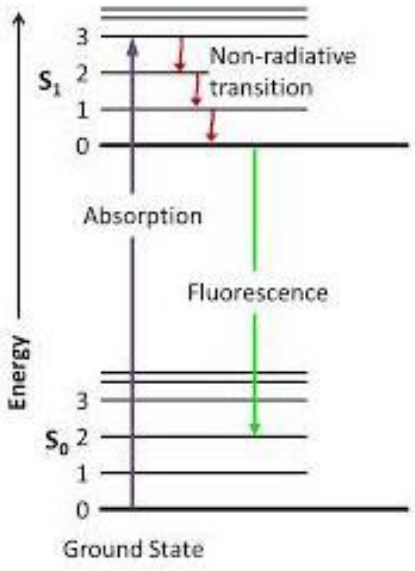

Figure 1.2 Jablonski diagram illustrating the fluorescence process

1.3 Fluorescence chemosensor

A molecular sensor or chemosensor is a molecule that specifically interacts with an analyte led to changing of fluorescent signal. Three major components in most of the fluorescent sensors are 1) a receptor which selectively and binds with analyte of interest, 2) a fluorophore that provides optical communication between sensor and the outer world, and 3) a spacer (linker) that binds both components together. In terms

of detection modes, fluorescence sensors can be classified into three categories; quenching of emission by the target (“turn-off”), increase or restoration of emission (“turn-on”), and changes in the emission wavelength (“ratiometric”) **(Figure 1.3)**. In this research, the turn-off process will be the chosen mode of detection.

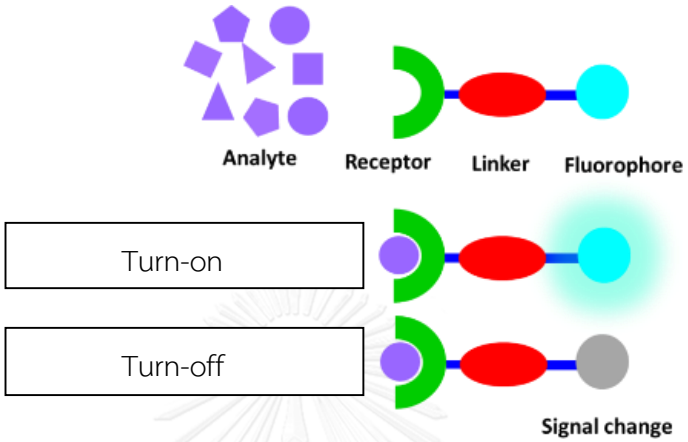

Figure 1.3 Schematic illustration of a fluorescence sensor device

1.4 Fluorescence quenching

Fluorescence quenching refers to any process which decreases the fluorescence intensity of a fluorescent material. Several interactions or mechanisms between fluorophore and the analyte can cause the excited fluorophore to return from excited state back to ground state without emission of light, for examples the rotation or vibration decay, photo-induced electron transfer (PET) and energy transfer.

1.4.1 Mechanism of fluorescence quenching

Photo induced electron transfer (PET) process often results in signal quenching fluorescence from excited fluorophores which described by molecular orbital energy diagram **(Figure 1.4)**. In the absence of analyte, the electron in the HOMO of receptor has higher energy than HOMO of fluorophore; as a result, the PET process can transfer an electron to the acceptor’s HOMO. If the electron pair on the receptor atom is coordinated to some electron-deficient species such as a transition

metal cation, the energy of the electron pair is lowered and the fluorescence will be turn on.

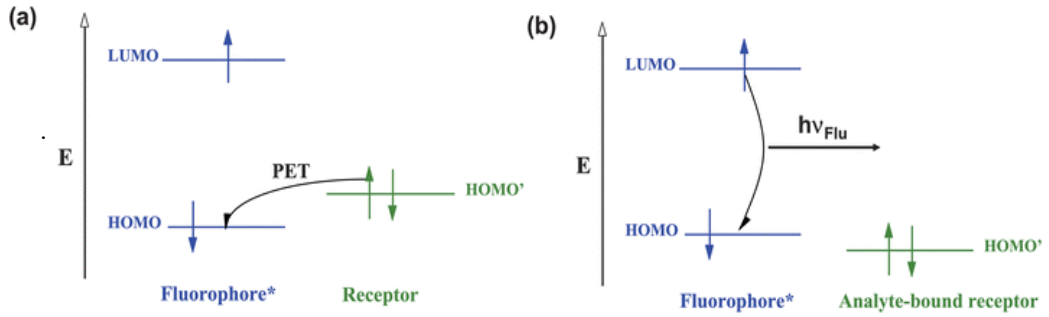

Figure 1.4 Energy level diagrams illustrating PET process in case (a) Free (b) coupled with analyte [20]

Another mechanism, **photo induced energy transfer** from the excited state of fluorophores to quenchers consists of three modes; Forster resonance energy transfer mechanism (FRET), dynamic (collisional) quenching, and static quenching (ground-state complex formation).

Forster resonance energy transfer mechanism (FRET) occurs when a donor molecule in the excited state transfers its excitation energy to a nearby chromophore, the acceptor molecule in the ground state. If the fluorescence emission spectrum of the donor molecule overlaps with the absorption spectrum of the acceptor, the energy transfer will happen as the result of long-range dipole-dipole intermolecular coupling between the donor and acceptor. The emission signal of the acceptor (solid yellow arrow, **Figure 1.5**) appears through the excitation of the donor molecule (solid purple arrow), while the emission of the donor molecule is reduced (dashed blue arrow). The donor fluorescence (solid blue arrow) is diminished during the transition to a lower quantum state. The efficiency of the transferred energy depends on the molecular distance between 1-10 nm, the extent of spectral overlap of the emission spectrum of the donor with the absorption of the acceptor, the quantum yield of the donor, the relative orientation of the donor and acceptor transition dipoles, and the distance between the donor and acceptor molecules [20].

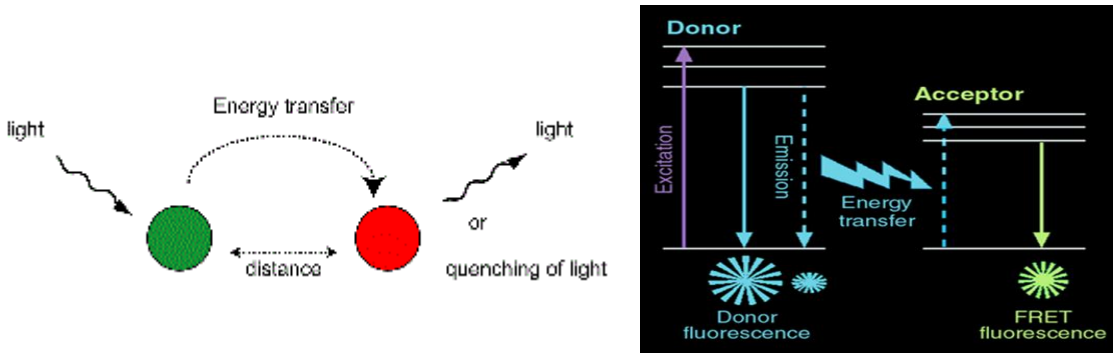

Figure 1.5 (left) FERT model and (right) Jablonski diagram showing the energy transfer between the fluorescence donor and acceptor involved in FRET [20].

Dynamic quenching is a collision between the quencher and fluorophore. As shown in **Fiqure 1.6A,** dynamic quenching takes place when the excited fluorophore (F*) is deactivated upon contact with quencher (Q) and the fluorophore returns to the ground state without emission of fluorescence light, while Q is not chemically altered in the process. On the other hand, **Figure 1.6B** illustrates *the static quenching* which results from the formation of a non-fluorescent complex between the F and Q (F•Q) in the ground state. When this complex absorbs energy from light, the excited state immediately returns to ground state without emission of a photon and the molecules do not emit fluorescent light. A characteristic of static quenching is a change in the absorption spectra of the two molecules when they form a complex.

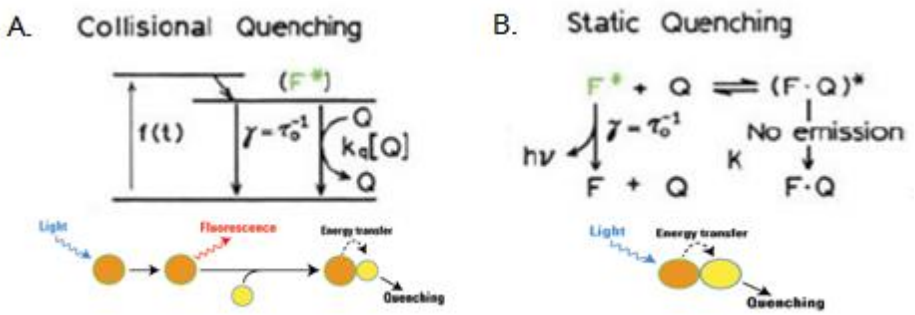

Figure 1.6 Dynamic and static quenching mechanisms

Static and dynamic quenching can be distinguished by their differing dependence on temperature and fluorescence lifetime decay. First, the lifetime of static quenching will not change; because, the fluorescence occurs from the uncomplexed fluorophore which remains the same during the quenching process. In contrast, the lifetime of dynamic quenching decreases in proportion to the intensity **(Figure 1.7)**.

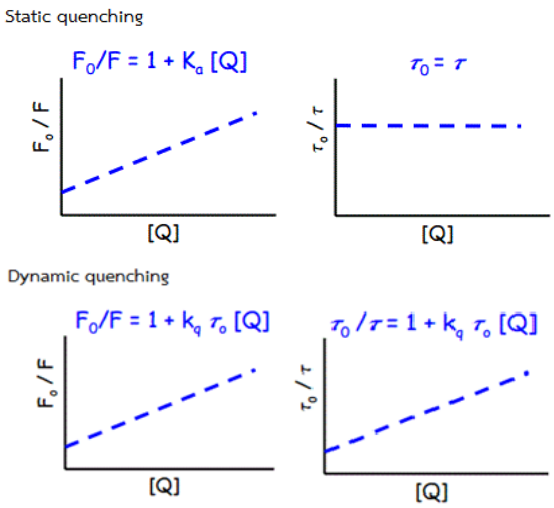

Figure 1.7 Fluorescence life of static and dynamic quenching

Second, the effect of temperature increasing can be used to distinguish the two forms of quenching. At higher temperature, diffusion rates and the frequency of collision increase in dynamic quenching. On the other hand, static quenching decrease due to the dissociation of weakly bound complexed **(Figure 1.8)**.

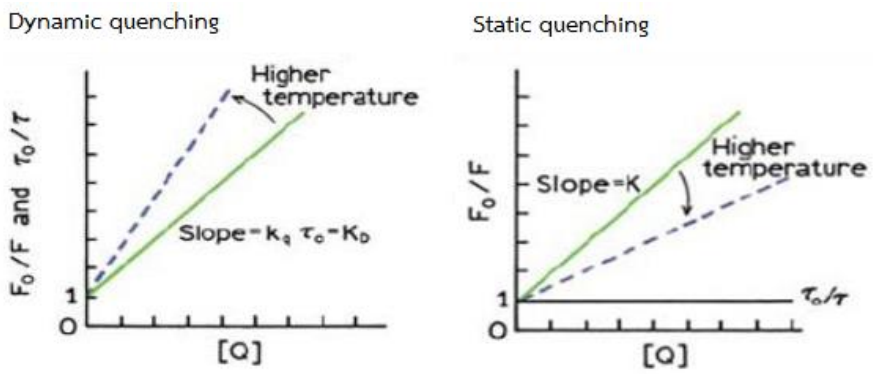

Figure 1.8 Temperature effect of static and dynamic quenching

1.4.2 Stern-Volmer equation

Static and dynamic quenching require molecular contract between the fluorophore and quencher. In case of this quenching, it exhibits a quencher-concentration that is described by Stern-Volmer equation given by

$$\frac{I_0}{I} = 1 + K_{SV}[Q]$$

Where I_0 and I are the fluorescence intensities observed in the absence and presence of quencher, respectively. [Q] is the quencher concentration and K_{sv} is the Stern-Volmer quenching constant – a parameter that determines the efficiency of quenching process. K_{sv} obtained from a slope that a plot of I_0/I verse [Q] would give a straight line. A linear relationship may indicate either a dynamic or static quenching modes. The moderate to large binding constants give rise to K_{sv} that exceed the rate achievable at the diffusion limit, and hence, static quenching can be inferred.

1.5 Truxene

Truxene or 10,15- dihidro-5H-dihidro-5*H*-diindenal[1,2-α;1',2'-c]-fluorene is highly hydrophobic and relatively planar heptacyclic polyarene structure **(Figure 1.9)** which led to a poor water solubility and lower quantum efficiency due to aggregation. The structure of truxene has attracted a great deal of interest due to their structural rigidity, high thermal stability, and strongly emissive properties. Moreover, the truxene core can easily be functionalized by the alkylation at C2, C7, and C12 positions in order to extend the π-conjugation system and shift the emission wavelength into the visible region. Nucleophilic addition at the C5, C10, and C15 carbons of truxene could prevent the π-π stacking and enhance the solubility of molecule in organic solvent [21-25].

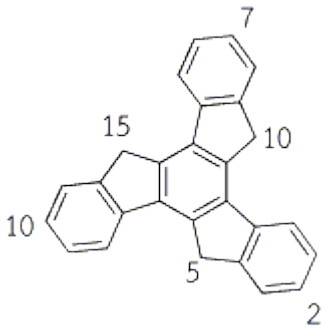

Figure 1.9 The structure of truxene

1.6 Literature review on Truxene derivatives

In 2009, S.C. Yuan and co-workers [26] designed and synthesized four monodisperse, well-defined, star-shaped truxene derivatives bearing oligo (fluorene, ethynylene) (OFE) branches; **TOFE1-TOFE4 (Figure 1.10)**. These molecules show highly efficient greenish-blue light emissions, and excellent thermal and electrochemical stabilities. In addition, all compounds can be used as active materials a light-emitting layer for OLED to give a device emitting blue color.

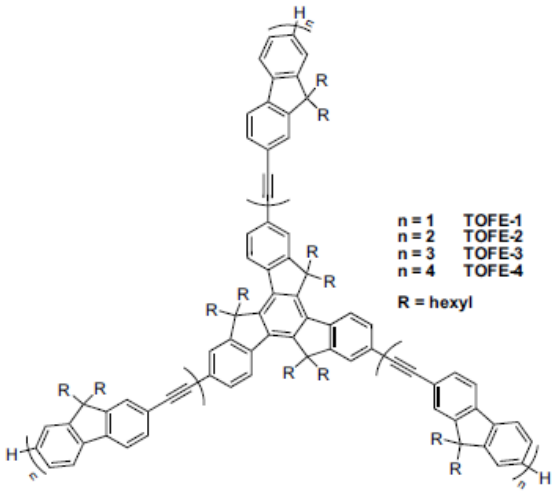

Figure 1.10 The structure of star-shaped molecules **TOFE1-TOFE4** [26]

In 2009, Z. Yang and co-workers [27] synthesized two solution-processable triphenylamine-based dendrimers with truxene core as hole-transporting materials for

organic light-emitting diodes; **Tr-TPA3** and **Tr-TPA9 (Figure 1.11)**. The dendrimers showed excellent solubility in organic solvents, high thermal stability, and high glass transition temperature, Tg, of 110 °C.

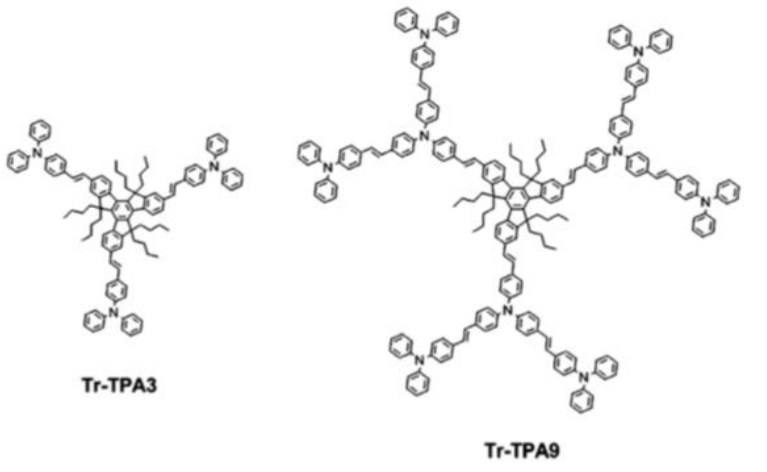

Figure 1.11 The structure of **Tr-TPA3** and **Tr-TPA9** [27]

In 2012, N. Earmrattana and co-workers [28] successfully synthesized two new water-soluble fluorophores 1 and 2 **(Figure 1.12)** containing a truxene core and ester-substituted aryl acetylenes peripheries as turn-off fluorescence sensor for cytochrome C and myoglobin detection. Both compounds possessed excellent solubility in aqueous media. They also exhibited outstanding emission quantum efficiencies typical for truxene derivatives.

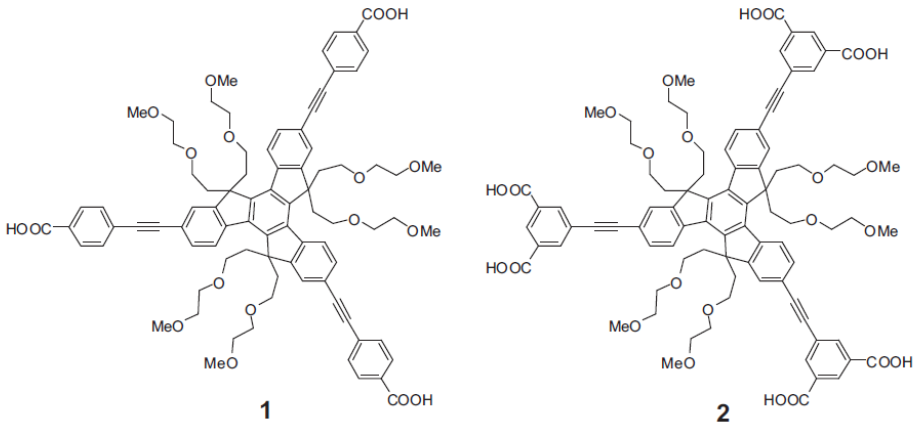

Figure 1.12 The structure of fluorophores **1** and **2** [28]

From the literature reviews, most of truxene derivatives consisting of the π-conjugated commonly showed highly fluorescent quantum yield. The absorption and emission in visible range of truxene derivatives benefited its applications as naked-eye. There are numerous researches containing truxene as core structure for OLEDs, liquid crystals, organic solar cells but for the application of fluorescence sensor has a few. Therefore, this research focuses on synthesis of fluorescence chemosensors by using truxene as a core for detection of nitroaromatic compounds and metal ions.

1.7 Literature reviews on nitroaromatic compounds and metal ions applications

In 2010, Lee and co-workers [29] designed a dipyrenylcalix [4] arene (**L**) containing a calix [4] arene as core structure and two pyrene peripheries for the detection of nitroaromatic species at low concentration in CH_3CN **(Figure 1.13)**. **L** molecule exhibited a selective fluorescent quenching with TNT and TNB; but, TNB can quench the fluorescence more effective than TNT. The mechanism, in which TNB that has the greater the number of electron-withdrawing nitro ($-NO_2$) group on the toluene core occurs intermolecular π-π interaction with the two pyrene moieties as the result of a charge-transfer process.

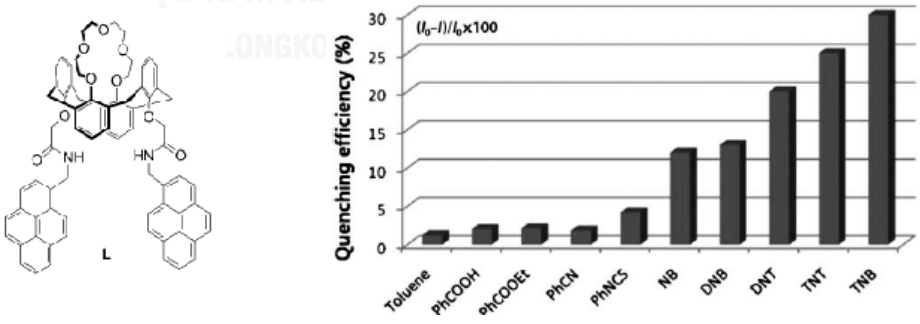

Figure 1.13 (left) Structure of dipyrenyl calix [4] arene (**L**) (right) Quenching efficiency of **L** towards various analytes in CH_3CN [29]

In 2012, Bhalla and co-workers [30] successfully synthesized novel pentacenequinone derivative that incorporate a pentacenequinone as donor and

thiophene as acceptor unit causing the intramolecular charge-transfer (ICT) process resulting in itself is weakly fluorescence. Interestingly, this compound exhibited fluorescent organic nanoaggregates in solvent mixture of H_2O/THF (9:1) due to its aggregation-induced emission enhancement attributes. Then, pentacenequinone derivative was applied to detect nitroaromatic compounds. The compound showed a selective fluorescence quenching in the presence of picric acid (PA) with a detection limit of 500 ppb **(Figure 1.14)**.

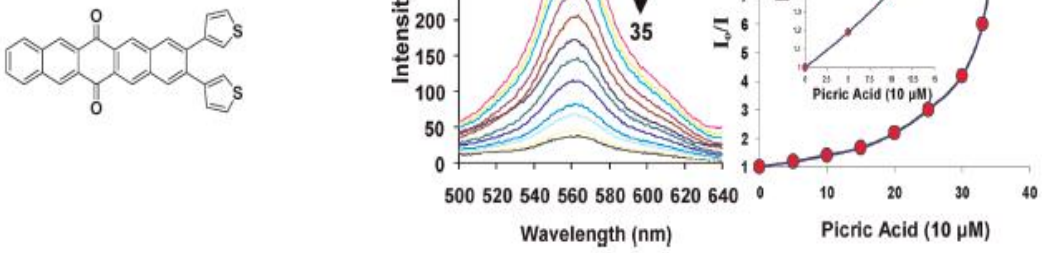

Figure 1.14 (left) Structure of pentacenequinone derivative (right) A) Change in fluorescence spectra of compound (10 μM) with the addition of PA in H_2O/THF (9:1) mixture; B) Stern-Volmer plot in response to PA. Inset: Stern-Volmer plot obtained at lower concentration of PA [30]

In 2012, Park and co-workers [31] reported a new fluorescent macrocyclic host, calix-[2]pyreno[2]-pyrrole, and its guest binding properties. This molecule exhibited high binding affinity for polynitroaromatic compounds including TNT. Accordingly, they carried out the fluorescent titration of this molecule with 2,4,6-trinitrotoluene (TNT) in toluene. As shown in **Figure 1.15**, the gradual addition of TNT resulted in complete quenching of fluorescence with the Stern-volmer constant (K_{sv}) of 1.2×10^6 M^{-1}. They suggested that the quenching mechanism is the π-π interaction between electron rich-pi system with electron deficient or electron poor (TNT), which was further confirmed by a Job's plot analysis. From a job's plot data was found to exhibit a maximum at 0.5 molar fractions which was consistent the formation of a 1:1 complex. These results

indicated the complex formation between calix [2]pyreno[2]-pyrrole and nitroaromatic was directed by electronic nature of the host and guest.

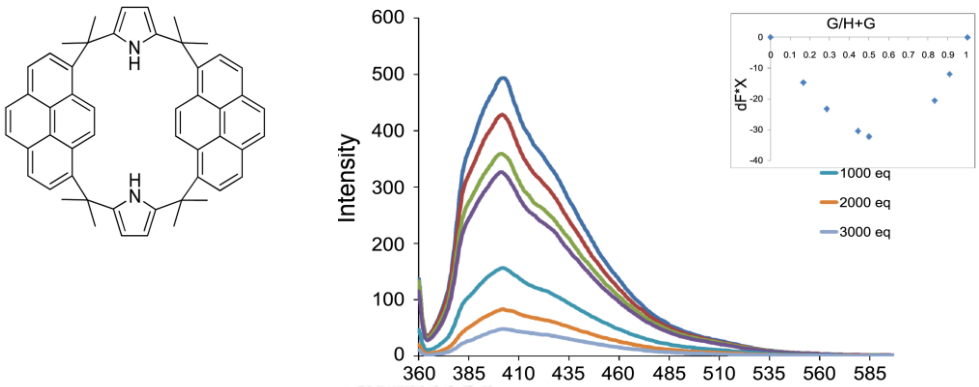

Figure 1.15 (left) Structure of Calix[2]pyreno[2]pyrrole (Right) Fluorescence spectral changing of this compound upon addition of TNT and (inset) a Job's plot experiment [31]

In 2013, Bhally and co-workers [12] designed and synthesized π-electron rich triphenylene derivatives **3** and **5** as chemosensors for various elctron deficient nitroaromatic explosives such as picric acid, trinitrotoluene, dinitrotolulene and dinitrobenzene in a THF: H_2O (9.5:0.5). Derivative **5** showed a more sensitive response towards the nitroaromatic derivatives than derivative **3** due to the spectral overlap between the emission spectrum of derivative **5** and the absorption spectrum of picric acid is much more than that in derivative **3**. The calculated Stern-Volmer constant (K_{sv}) of **3** and **5** were found to be 2.91×10^5 and 2.93×10^5 M^{-1} for PA, respectively. The quenching of the fluorescence involves the energy transfer from photo-excited π-electron rich both derivatives to ground state electron deficient picric acid. Moreover, the solution coated strips of derivative **3** and gel coated strips of derivative **5** can detect easily to picric acid by the naked eye which was up to 14 pg cm^{-2} **(Figure 1.16)**.

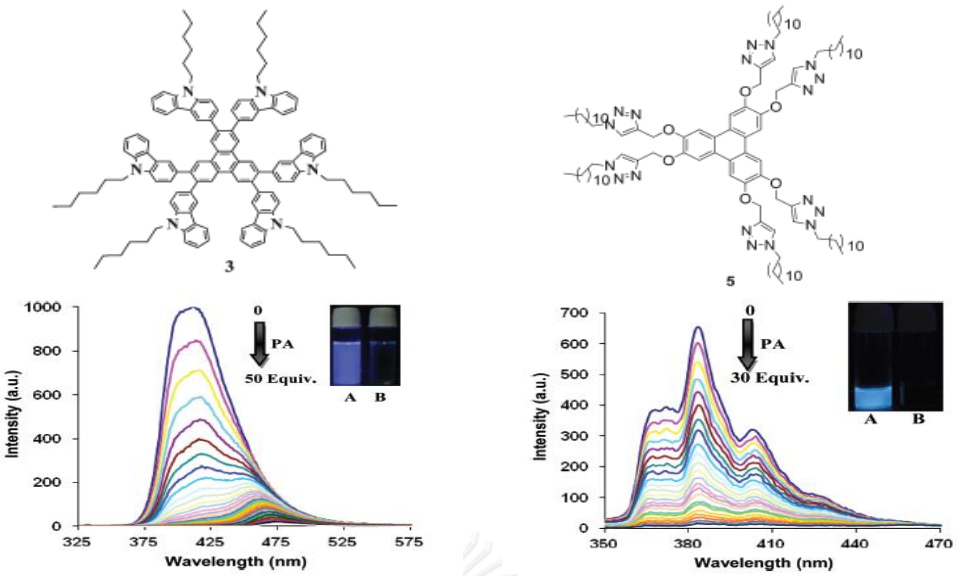

Figure 1.16 (above) Structure of triphenylene derivatives **3** and **5** (bottom) Fluorescence emission spectra of **3** and **5** (5 μM) upon the addition of PA (0-50 equiv.) in a THF : H_2O (9.5 : 0.5) mixture. The inset shows the fluorescence of both **3** and **5** before (A) and after (B) the addition of picric acid [12]

In 2013, Niamnont and co-workers [32], had successfully synthesized four novel triphenylamine derivatives (TEP, TAP, TEP and TAC) containing an electron donating triphenylamine core and three ethylnylpyrene or ethynylcorannulene peripheries **(Figure 1.17)**. The fluorescence quenching of TAP and TAC showed clearly much more sensitive than TEP and TEC. The results suggested that hydrogen of the triazole bridge can interact with the nitro group which confirmed by ^{1}H-NMR titration. TAP showed the higher sensitivity toward TNT than TAC in $CHCl_3$ due to the shape geometry of the corannulene does not well accommodate π-π interaction with TNT causing no PET process. The K_{SV} value at 5°C to 45°C of TAP were 1.4 x10^4 M^{-1} and 2.0 x 10^4 M^{-1}, respectively. The increasing of K_{SV} value upon temperature indicated that it is kind of dynamic quenching. Furthermore, TAP has the level of the visual detecting of TNT down to 0.58 ng mm^{-2} which is about ten times lower than the lowest number previously reported.

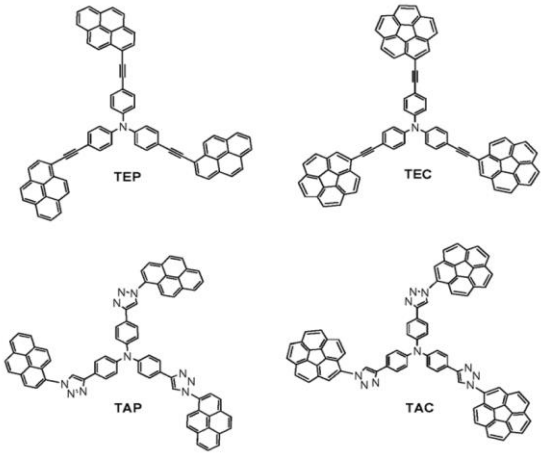

Figure 1.17 Structure of fluorophores [32]

In 2011, Zhang and co-workers [18] reported a novel fluorescence PPi sensor based on 1,8-naphthalimide bearing two dipicolylamine arms. Fluorescence enhancement and a 29 nm red-shift were observed when Zn^{2+} was added to this novel compound solution. The result could be explained by the coordination of Zn^{2+} and a lone pair electron of the tertiary amine (DPA), leading to suppression of photoinduced electron transfer process (PET). A binding mode of 1,8-naphtalimide derivative with Zn^{2+} studied by Job's plot analysis was 1:2 ratio. Moreover, the complex 1,8-naphthalimide derivative ·Zn^{2+} was selectively quenched by addition of PPi and a 23 nm blue-shift emission (from 505 to 481 nm) in CH_3CN-HEPES buffer (0.02 M, pH 7.4) with a detection limit of 1.5 μM **(Figure 1.18)**.

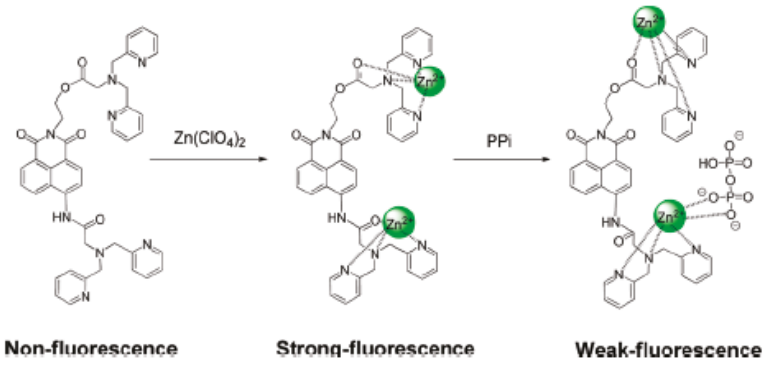

Figure 1.18 Proposed binding modes of 1,8-naphthalimide derivative and Zn^{2+} with PPi [18]

In 2012, Yuan and co-workers [24] successfully designed and synthesized two truxene derivatives (C_3B_3 and N_2S_3) as fluorescent probes for fluoride anion (F^-) detection. C_3B_3 that containing three branches of demesitylboryl as acceptors displays selective turn-off fluorescence probe with F^- which was resulting from the strong binding of trivalent organic boron with the most electronegative F^-. In contrast, N_2S_3 exhibited the fluorescence enhancement upon the addition of F^-, thus, it is a turn-on fluorescence probe. N_2S_3 consist of two diphenylamine as donors and demesitylboryl as acceptors resulting in photon induced electron transfer (PET) quenching and gave a low fluorescence signal. When F^- was added to the solution of the complex, the fluorescence signal was increased since PET process was inhibited as shown in **Figure. 1.19**.

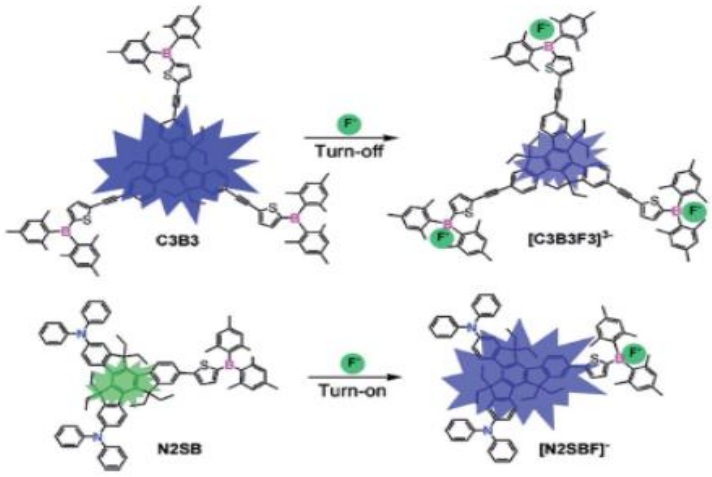

Figure 1.19 Schematic illustration of F^- sensing process of C_3B_3 and N_2S_3 and their fluorescenct changes [24]

Until now, there have been various researches working on design and synthesis of small molecules containing of receptor unit which specifically interacts with analyte and used as fluorescence sensor for detection of nitroaromatic compounds and metal ions. Interestingly, there are not many reports about the application of truxene derivative as chemosensor and no report that used as a fluorescent sensor for nitroaromatic compounds and metal ions.

Therefore, in our current study, we designed and synthesis of water-soluble and -insoluble truxene derivatives used as metal ions and nitroaromatic compounds sensor, respectively.

1.8 Objective of this research

(1) To synthesize novel fluorophores composed of truxene as core structure connecting to three ethylnyl pyrene (**T1**) or dipicolylamine (**T2**) as receptors **(Figure 1.20)**.

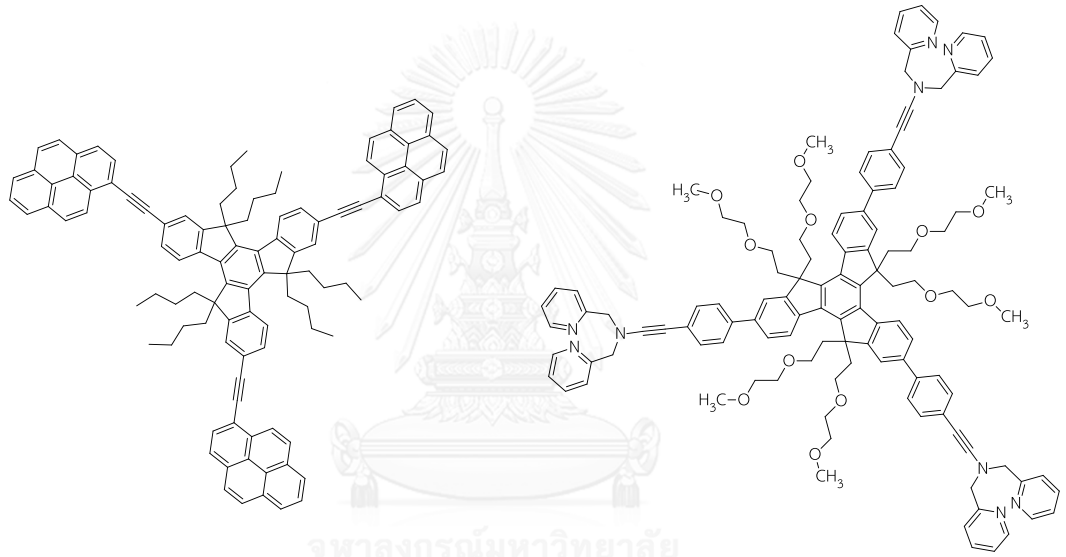

T1 **T2**

Figure 1.20 The target molecules (**T1** and **T2**)

(2) To characterize and study photophysical properties of the target molecules.

(3) To apply these novel fluorophores as nitroaromatic compounds and metal ion sensors by using UV-vis spectrometry and fluorescence spectrometry.

CHAPTER II

EXPERIMENTAL

2.1 Chemicals and materials

All reagents and solvents used in the reactions were standard analytical grade purchased from Sigma-Aldrich (USA), Fluka® (Switzerland), or Merck® (Germany) and other chemical suppliers.

Laboratory grade solvents, dichloromethane, ethyl acetate, and hexane were usually redistilled before use.

In anhydrous reactions, solvents such as tetrahydrofuran (THF) and tolulene were dried and distilled before use according to the standard procedures.

2.2 Instrumentation

Melting points were measured on a Fisher John Apparatus, Electrothermal MEL-TEMP®.

All ^{1}H NMR and ^{13}C NMR spectra were determined on a Varian Mercury NMR spectrometer, which operated at 400 MHz for ^{1}H and 100 MHz for ^{13}C nuclei (Bruker 400 MHz NMR spectrometer). All chemical shifts were reported in parts per million, ppm (δ scale) relative to tetramethylsilane (TMS) as an internal reference. Deuterochloroform ($CDCl_3$) was used as solvent. The following abbreviations are used for multiplicity: s=singhlet, d=doublet, t=triplet, q=quartet, brs=broad singlet, dd=double of doublet, dt=double of triplet, and m=multiplet. Coupling constants (*J*) are reported in Hertz (Hz).

Mass spectra were recorded on a Microflex MALDI-TOF mass spectrometer (Bruker Daltonics) using doubly recrystallized a-cyano-4-hydroxycinnamic acid (CCA) and dithranol as a matrix. The HRMS was obtained by using Mass spectrometer (microTOF, Bruker Daltonics) at an electron impact (EI) of 70 ev.

Fourier transform infrared spectra (FTIR) were obtained on Nicolet 6700 FTIR spectrometer equipped with a mercury-cadmium telluride (MCT) detector (Nicolet USA).

All absorption spectra were measured by using Shimadzu UV-2550 UV-Vis spectrophotometer (Varian, USA). Fluorescence spectra were recorded on a Varian Cary Eclipse spectrofluorometer. The maximum absorption wavelength was used as the excitation wavelength of each fluorophore and the emission was recorded from the wavelength at 390 to 600 nm. The solution of fluorophores were prepared in $CHCl_3$ and aqueous THF for nitroaromatic sensing and 30%THF-HEPES buffer (0.002M, pH 7.4) for metal ion sensing.

2.3 Chromatographic System

Analytical thin layer chromatography (TLC) was carried out on Merck Kieselgel 60, $F_{254,}$ 1mm aluminium-backed silica plates (Merck KgaA, Darmstadt, Germany) impregnated with 254 nm fluorescent indicator. The chromatogram was visualized under 254 nm ultraviolet (UV) light and 356 nm Black light.

Column chromatography was performed on glass column using Merck silica gel 60 (60-230 mesh). The size of the chromatographic column used depended on the amount (weight) of the sample. The ratio of sample and the adsorbent was about 1:40-80 by weight. The column was eluted with some suitable solvents which best separated the sample and each fraction was monitored by Thin-Layer Chromatography (TLC).

Flash column chromatography was performed using Merck Kieselgel 60G silica gel and eluting with the solvent system stated.

Preparative Thin Layer Chromatography (PLTC) was prepared by spreading aqueous slurry of silica gel $PF_{254+366}$ onto plate which was then left standing at room temperature to dry and subsequently activated for 2 h at 120^{o}C in the oven.

Milli-Q water was used in all experiments unless specified otherwise. The most reactions were carried out under positive pressure of N_2 filled in rubber balloons.

2.4 Synthesis of fluorophores and Characterizations

2.4.1 Synthesis of Truxene

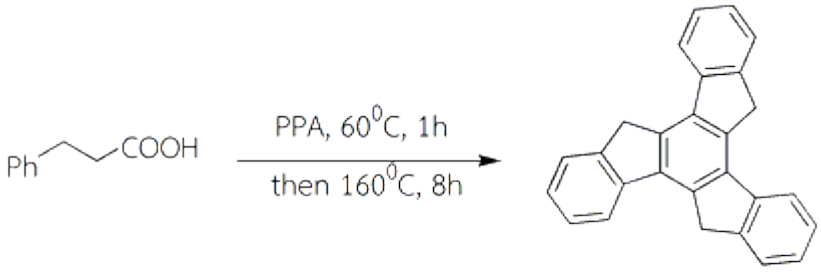

Truxene

A mixture of 3-phenylpropionic acid (10.0 g, 66.72 mmol) and polyphosphoric acid (50 g) was heated at 90 °C for 60 min under nitrogen atmosphere. Water (5 mL) was then added to the reaction mixture which was allowed to stir at 160 °C for 8 h. After the reaction was cooled to room temperature, the mixture was poured into ice water. The gray powder filtered was washed with water, and the crude product was purified by recrystallization from toluene to yield 3 as a light-yellow crystal (11.17 g, 49%). m.p. >300 °C. IR (KBr) ν_{max} cm^{-1}: 3044, 3024, 2871, 1609, 1469, 1393, 1021, 726. ^{1}H NMR (400 MHz, $CDCl_3$, ppm): δ 7.98 (d, *J* = 7.1 Hz, 1H), 7.71 (d, *J* = 6.8 Hz, 1H), 7.51 (t, *J* = 7.2 Hz, 1H), 7.40 (t, *J* = 7.0 Hz, 1H), 4.30 (s, 2H). ^{13}C NMR (100 Mz, $CDCl_3$, ppm): δ 143.8, 141.2, 137.0, 135.2, 128.3, 126.9, 126.2, 125.0, 121.9, 36.5. MALDI-TOF calcd for $C_{27}H_{18}$ 342.1409, found: 342.535 (M). [33]

2.4.2 Synthesis of 5,5′,10,10′,15,15′-hexabutyl truxene (1)

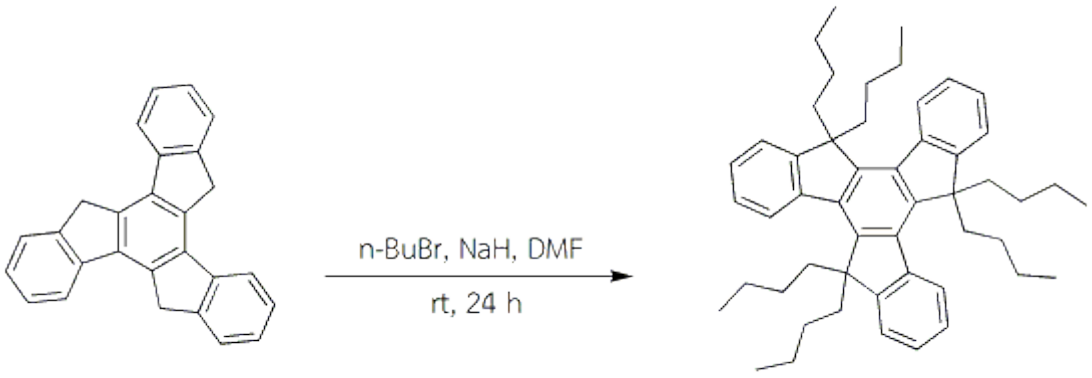

Truxene

1, 75%

Truxene (1.5 g, 4.54 mmol) in DMF (50 mL) was stirred at 0°C under nitrogen atmosphere and sodium hydride (2.2 g, 54.49 mmol) was added. The solution was allowed to warm until room temperature and stirred for 30 min and then followed by an addition of *n*-butyl bromide (5.8 mL). The reaction mixture stirred overnight at room temperature was poured into water and extracted with EtOAc. The combined organic layer was dried over $MgSO_4$, filtered, and concentrationed *in vacuo*. The crude product was purified by flash column chromatography using hexane as eluent to yield **1** as a while solid (2.3 g, 75%). m.p. 193-194 °C. IR (KBr) ν_{max} cm^{-1}: 2956, 2918, 2858, 1463, 1372, 1033. ^{1}H NMR (400 MHz, $CDCl_3$, ppm): δ 8.38 (d, *J* = 7.4 Hz, 3H), 7.46 (dd, *J* = 7.1 and 1.3 Hz, 3H), 7.40-7.35 (m, 6H), 3.02-2.94 (m, 6H), 2.12-2.07 (m, 6H), 0.91-0.85 (m, 12H), 0.52-0.42 (m, 30H). ^{13}C NMR (100 Mz, $CDCl_3$, ppm): δ 153.7, 145.0, 140.4, 138.5, 126.4, 126.0, 124.7, 122.3, 55.6, 36.7, 26.6, 22.9, 13.8. MALDI-TOF calcd for $C_{51}H_{66}$, 678.52, found: 677.85 (M+1). [28]

2.4.3 Synthesis of 5,5′,10,10′,15,15′-hexabutyl-2,7,12-triiodo-truxene (2)

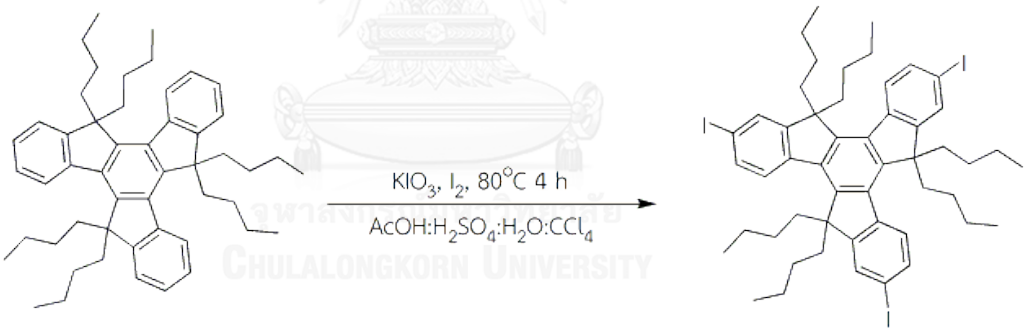

1 2, 93%

Carbon tetrachloride (CCl_4) (1 mL) was added dropwise into a solution of **1** (0.26 g, 0.38 mmol) in a 100: 40: 1.5 mixture of CH_3COOH-H_2SO_4-H_2O (5 mL). Potassium iodate (KIO_3) (0.08 g, 0.32 mmol) and I_2 (0.5 g, 1.91 mmol) were then added to the reaction mixture and allowed to heat at 80°C for 4 h. The reaction mixture was cooled to room temperature and poured into water. The crude product obtained by filtration was purified by precipitation in ethanol to afford **2** as a white powder (3.7g, 93%). m.p. 312-314 °C. IR (KBr) ν_{max} cm^{-1}: 2953, 2915, 2849, 1453, 1353, 1180, 873, 823, 788. ^{1}H NMR (400 MHz, $CDCl_3$, ppm): δ 8.07 (d, *J* = 8.4 Hz, 3H), 7.76 (s, 3H), 7.71 (d, *J* = 8.4 Hz, 3H),

2.88-2.81 (m, 6H), 2.05-2.00 (m, 6H), 0.92-0.84 (m, 12H), 0.52-0.41 (m, 30H). ^{13}C NMR(100 Mz, $CDCl_3$, ppm): δ 156.4, 145.6, 140.0, 138.2, 135.8, 132.1, 126.8, 93.2, 56.1, 36.9, 26.9, 22.7, 13.8. Elemental analysis: calcd for $C_{51}H_{63}I_3$: C 57.96, H 6.01, I 36.03, found: C 57.56, H 6.03, I 36.41.

2.4.4 Synthesis of fluorophore T1

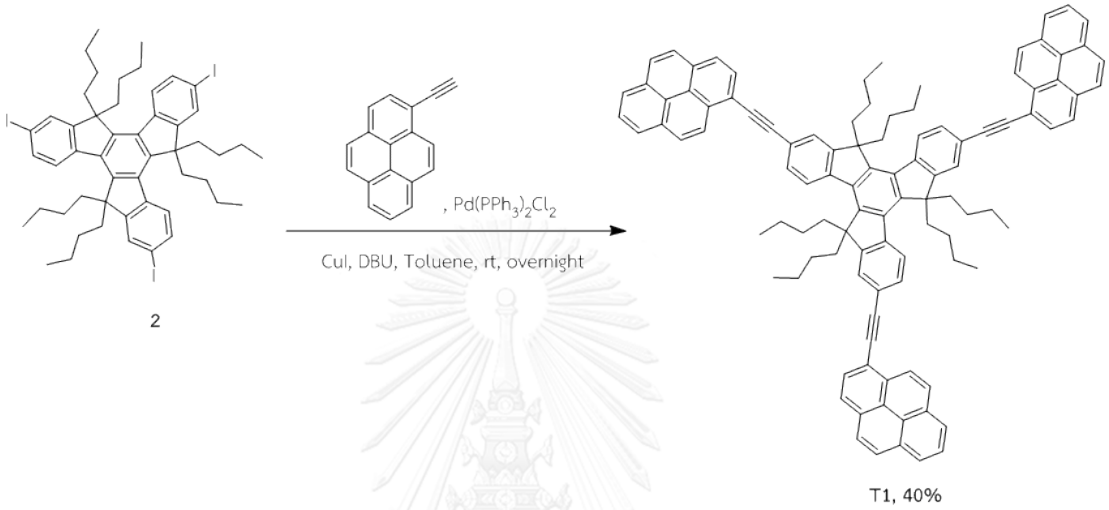

A mixture of **2** (0.30 g, 0.28 mmol), $Pd(PPh_3)_2Cl_2$ (18 mg, 0.03 mmol), CuI (5.0 mg, 0.03 mmol), 1-ethynylpyrene (0.23 g, 1.02 mmol) in tolulene (10 mL) and 1,8-diazabicyclo[5.4.0]undec-7-ene (DBU) (0.23 mL) was stirred at room temperature for 24 h. The reaction mixture was concentrated *in vacuo*, the residue was eluted through a flash column chromatography using hexane to give **T1** as a dark yellow solid (15 mg, 40%). m.p. >300 °C. IR (KBr) ν_{max} cm^{-1}: 2918, 2849, 1453, 1374, 840, 710. ^{1}H NMR (400 MHz, $CDCl_3$, ppm): δ 8.82 (d, *J* = 9.1 Hz, 3H), 8.51 (d, *J* = 8.7 Hz, 3H), 8.35-8.03 (m, 24H), 7.86-7.84 (m, 6H), 3.11-3.04 (m, 6H), 2.30-2.22 (m, 6H), 1.09-0.93 (m, 12H), 0.55-0.49 (m, 30H). ^{13}C NMR(100 Mz, $CDCl_3$, ppm): δ 154.1, 146.4, 140.7, 138.4, 132.1, 131.52, 131.47, 131.36, 130.37, 129.9, 128.6, 128.4, 127.48, 126.45, 125.9, 125.83, 125.78, 125.5, 125.0, 124.8, 124.6, 121.6, 118.2, 96.2, 89.4, 56.0, 36.9, 29.8, 26.8, 23.1, 14.0. MALDI-TOF calcd for $C_{105}H_{90}$ 1351.71, found: 1352.91 (M+1).

2.4.5 Synthesis of 4-iodo-2,2′-dipicolylamine (3)

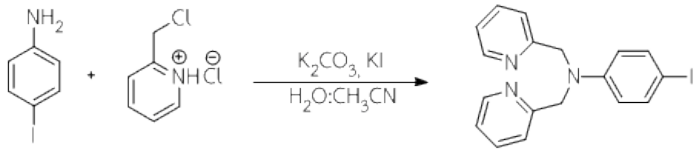

3, 44%

A solution of 2-(Chloromethyl) pyridinium chloride (1.30 g, 8.00 mmol) in water (3 mL) was added with potassium iodide (0.70 g, 4.80 mmol). Potassium carbonate was dissolved in water (3 mL) and slowly added to the solution. Then, a solution of 4-iodoaniline (0.70 g, 4.80 mmol) in acetonitrile (2 mL) was added to the stirred mixture. The reaction mixture was stirred at room temperature for 4 days. Next step was addition of water. The organic layer was separated and the aqueous phase was extracted with dichloromethane (3 × 20 mL) and was then dried over anhydrous $MgSO_4$. The filtrate was evaporated and the residue was purified by a silica gel column using gradient solvents starting from 10% EtOAC to CH_2Cl_2 and to EtOAc as eluents to afford **3** as a yellow needle crystal (0.57 g, 44%). IR (KBr) ν_{max} cm^{-1}: 3269, 2099, 1513, 1435, 1344, 1174, 810, 751. ^{1}H NMR (400 MHz, $CDCl_3$): δ 8.58 (d, *J* = 4.8 Hz, 2H), 7.62 (t, *J* = 8.0 Hz, 2H), 7.38 (d, *J* = 8 Hz, 2H), 7.25-7.10 (m, 2H), 6.48 (d, *J* = 8 Hz, 2H), 4.79 (s, 4H). ^{13}C NMR (100 MHz, $CDCl_3$): δ 158.2, 149.7, 147.8, 137.8, 136.8, 122.2, 120.7, 114.9, 78.3, 57.3. LR-ESI-MS m/z calcd for $C_{18}H_{16}IN_3$: 401.2442, found: 401.98 (M) [34].

2.4.6 Synthesis of 4-(trimethylsilyl)-ethynyl-2,2′-dipicolylamine (4)

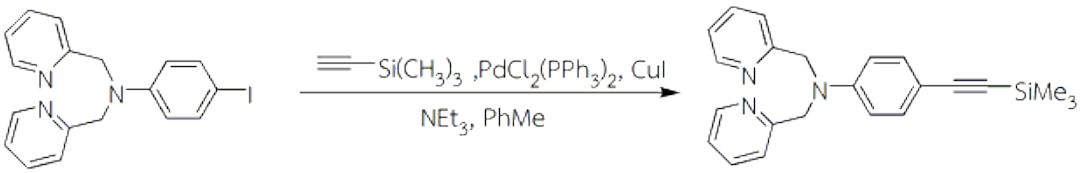

3 4, 75%

A mixture of **3** (0.30 g, 0.75 mmol), $Pd(PPh_3)_2Cl_2$ (0.03 g, 0.04 mmol) and CuI (0.01 g, 0.04 mmol) in mixed solvent (5 mL, NEt_3/toluene 1:4 v/v) was purged with nitrogen for 15 min. After that, a portion of trimethylsilylacethylene (TMSA, 0.13 mL, 0.90 mmol) was added into the mixture and the stirring was continued overnight under

nitrogen atmosphere at room temperature. The solvent was evaporated and the residue was diluted with dichloromethane (30 mL) and poured into water (20 mL). The organic layer was washed with saturated solution of sodium chloride and water, dried over anhydrous $MgSO_4$, and filtered. The solvent was evaporated and the crude product was purified by column chromatography on neutral Alumina using hexane as solvent to afford **4** as a pale yellow solid (0.21 g, 75%). ^{1}H NMR (400 MHz, $CDCl_3$): δ 8.39 (d, *J* = 4.8 Hz, 2H), 7.42 (t, *J* = 7.7 Hz, 2H), 7.06 (d, 8.0 Hz, 2H), 7.01-6.99 (m, 4H), 6.40 (d, *J* = 8.9 Hz, 2H), 4.62 (s, 4H), 0.00 (s, 9H). ^{13}C NMR (100 MHz, $CDCl_3$): δ 158.65, 150.1, 148.6, 137.5, 133.8, 122.7, 121.4, 112.7, 111.9, 106.3, 92.1, 57.6, 0.5. LR-ESI-MS m/z calcd for $C_{23}H_{25}N_3Si$: 371.5502, found: 372.07 (M+1).

2.4.7 Synthesis of 4-ethynyl-2,2′-dipicolylamine (5)

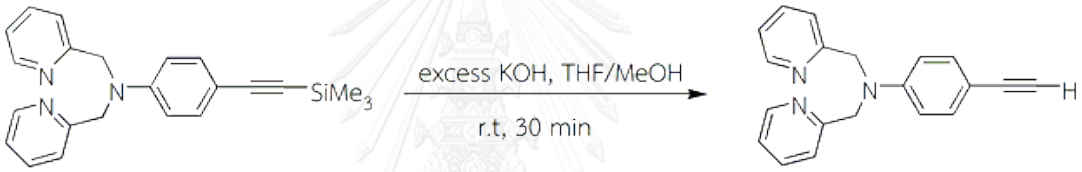

4 **5, 89%**

An excess KOH solution in THF/MeOH 1:10 v/v (10 mL) was added into a solution of **4** (0.24 g, 0.65 mmol) in THF/MeOH 1:10 v/v and the mixture was stirred at room temperature for 30 min. The solvent was removed under reduced pressure and the residue was dissolved in CH_2Cl_2 (30 mL) and washed with NH_4Cl solution, water (20 mL), and brine solution (20 mL). The organic layer was separated and the aqueous phase was extracted with CH_2Cl_2 (2 x 20 mL) and was then dried over anhydrous $MgSO_4$. The filtrate was evaporated and the residue was eluted through a neutral alumina column by using hexane to provide **5** as a pale yellow crystal (0.17 g, 89%). ^{1}H NMR (400 MHz, $CDCl_3$): δ 8.57 (d, *J* = 4.8 Hz, 2H), 7.61 (td, *J* = 7.7, 1.7 Hz, 2H), 7.29-7.24 (m, 2H), 7.21-7.14 (m, 4H), 6.62 (d, *J* = 9.0 Hz, 2H), 4.81 (s, 4H), 2.92 (s, 1H). ^{13}C NMR (100 MHz, $CDCl_3$): δ 158.55, 150.2, 148.8, 137.2, 133.8, 122.5, 121.1, 112.6, 110.5, 84.7, 75.4, 57.6. LR-ESI-MS m/z calcd for $C_{20}H_{17}N_3$: 299.1412, found: 300.07 (M+1) [35].

2.4.8 Synthesis of 5, 5′, 10, 10′, 15, 15′-hexa-2-(2-methoxyethoxy) ethyltruxene (6)

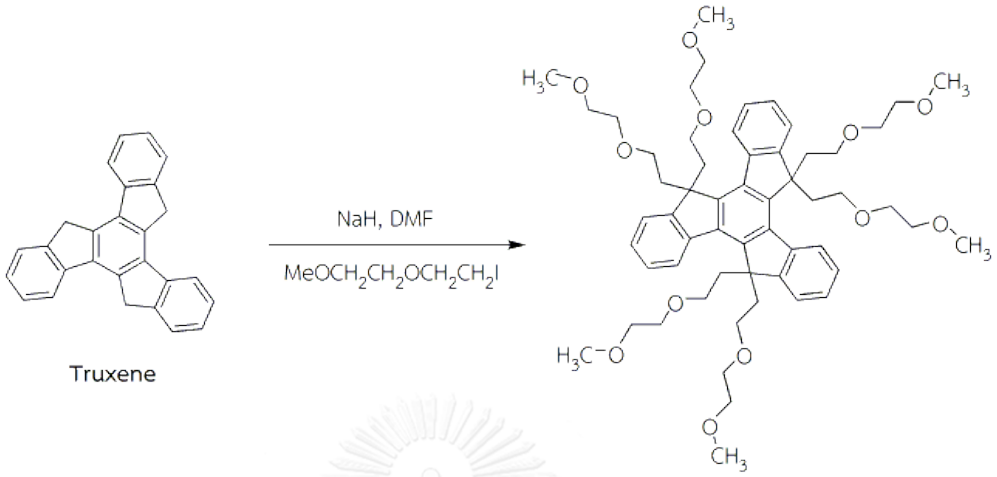

To a stirred solution of truxene (0.10 g, 0.29 mmol) in DMF (10 mL) at 0 °C under nitrogen, NaH (0.09 g, 2.32 mmol) was added. Then the solution was allowed to warm to room temperature and stirred for 30 min and then 1-iodo-2-(2-methoxyethoxy)ethane (0.53 g, 2.32 mmol) was added. After stirring for 24 h, the mixture was poured into water and extracted with EtOAc. The volatile solvents were removed under reduced pressure and the crude product was purified by column chromatography on silica gel using with EtOAc as the eluent to yield **6** (182 mg, 66%) as a white crystalline solid. ^{1}H NMR ($CDCl_3$, 400 MHz, ppm) d 8.34 (d, J = 8.3, 3H), 7.58 (d, J = 8.3 Hz, 3H), 7.41 (m, 6H), 3.19-3.28 (m, 36H), 3.06 (m, 12H), 2.50-2.72 (m, 18H). ^{13}C NMR (CDCl3, 100 MHz, ppm) d 151.5, 143.0, 138.1, 127.4, 127.3, 125.1, 122.8, 71.5, 69.7, 67.1, 58.8, 51.2, 36.0. MALDI-TOF calcd for $C_{57}H_{78}O_{12}$: 955.2220, found: 955.570 (M).

2.4.9 Synthesis of 2, 7, 12-Triiodo-5, 5′, 10, 10′, 15, 15′-hexa-2-(2-methoxyethoxy) ethyltruxene (7)

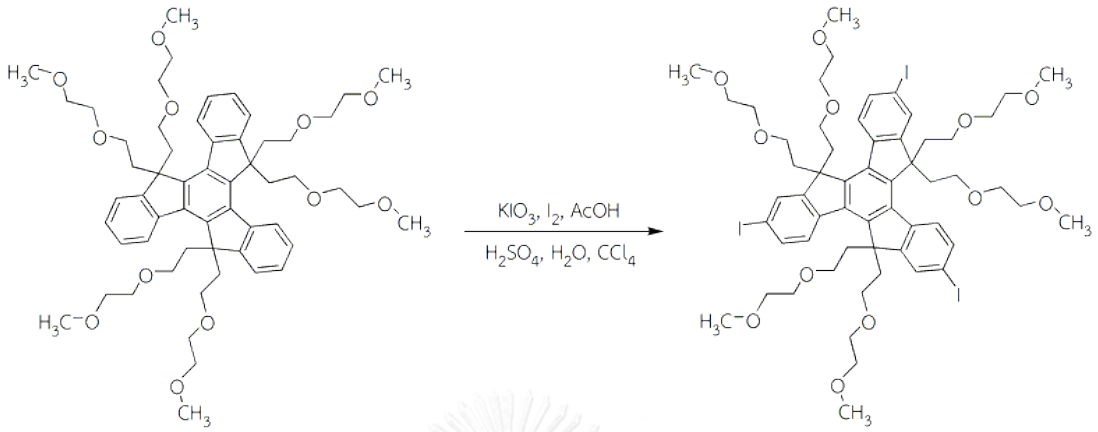

6 7, 96%

A solution of **6** (0.20 g, 0.20 mmol) in 20 mL of mixed solvent (CH_3COOH : H_2SO_4 : H2O : CCl_4 = 100 : 5 : 20 : 8) was heated to 40 °C with stirring. After adding KIO_3 (0.05 g, 0.23 mmol) and I_2 (0.08 g, 0.32 mmol), the mixture was heated to 80°C and stirred for 3 h. After the reaction mixture was cooled to room temperature, it was poured into water and extracted with EtOAc. The volatile solvents were removed under reduced pressure and the crude product was purified by column chromatography on silica gel eluting with EtOAc to yield **7** (0.26 g, 93%) as a yellow solid. ^{1}H NMR ($CDCl_3$, 400 MHz, ppm) d 7.97 (d, J = 8.1 Hz, 3H), 7.85 (s, 3H), 7.68 (d, J = 8.1, 3H), 3.01 (m, 18H), 2.63 (m,12H), 2.44 (m, 6H). ^{13}C NMR ($CDCl_3$, 400 MHz, ppm) d 154.0, 143.5, 137.4, 137.3, 136.5, 132.4, 126.6, 93.5, 71.6, 69.9, 67.0, 58.9, 51.7, 35.8, 29.7. MALDI-TOF calcd for $C_{57}H_{75}I_3O_{12}$: 1332.9116, found: 1355.550 (M+Na).

2.4.10 Synthesis of fluorophore T2.

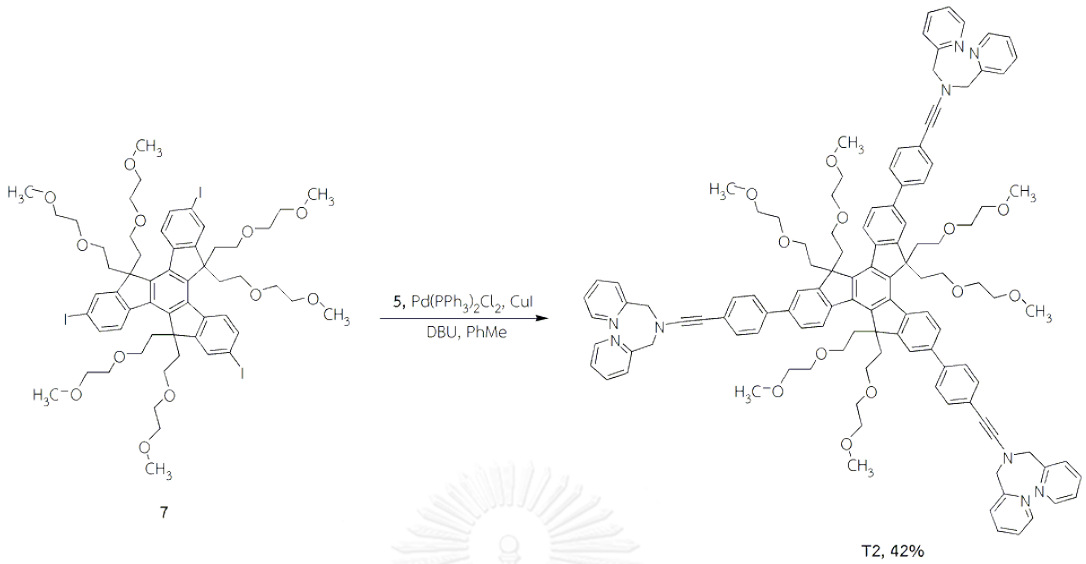

A mixture of 2,7,12-triiodo-5,5′,10,10′,15,15′-hexa-2-(2-methoxyethoxy) ethyl truxene **(7)** (0.15 g, 0.11 mmol), $Pd(PPh_3)Cl_2$ (4 mg, 0.05 mmol), CuI (2 mg, 0.05 mmol), and compound **5** (0.13 g, 0.45 mmol) was dissolved in toluene (10 mL). Then, 1,8-diazabicyclo[5.4.0] undec-7-ene (DBU) (0.13 mL) was added into the reaction mixture and the stirring was continued at room temperature for 24 h. After the combined filtrate was evaporated and the residue was eluted through a silica gel column by gradient solvents from dichloromethane chloride to ethyl acetate as the eluents to give **T2** as a yellow solid (0.87 g, 42%). IR (KBr) ν_{max} cm^{-1}: 2921, 2857, 2184, 1590, 1518, 1434, 1347, 1096, 814, 751. ^{1}H NMR (400 MHz, $CDCl_3$): δ 8.59 (d, J = 4.5 Hz, 2H), 8.21 (d, J = 8.4 Hz, 1H), 7.66-7.62 (m, 3H), 7.45 (dd, J = 15.2 Hz, 7.1 Hz), 7.39 (d, J = 8.4, 2H), 7.26-7.12 (m, 4H), 6.68 (d, 8.8 Hz, 2H), 4.86 (s, 4H), 3.20-3.16 (m, 12H), 3.07-2.98 (m, 4H), 2.69-2.64 (m, 4H), 2.54-2.47 (m, 4H). ^{13}C NMR (100 MHz, $CDCl_3$): δ 158.3, 151.9, 149.8, 148.3, 143.9, 137.9, 137.6, 137.2, 133.2, 130.7, 125.8, 125.1, 123.2, 122.4, 121.1, 112.6, 111.5, 91.6, 88.1, 71.7, 70.0, 67.3, 59.0, 57.3, 51.6, 36.2. MALDI-TOF calcd for $C_{117}H_{123}N_9O_{12}$: 1846.9325, found: 1844.441 (M+2). HR-ESI-MS m/z calcd for $C_{117}H_{123}N_9O_{12}$: 1846.9325, found: 1847.9404 (M+1).

2.5 Photophysical Property Study

A 100 μM solution of fluorophore **T1** in $CHCl_3$ and aqueous THF and a 50 μM solution of fluorophore **T2** in 30%THF-HEPES buffer (0.002M, pH 7.4) were prepared at room temperature for spectrophotometric experiments.

2.5.1 UV-Visible spectroscopy

The UV-Visible absorption spectra of the stock solutions of **T1** and **T2** were recorded from the wavelength at 250 nm to 600 nm at ambient temperature.

Molar extinction coefficient (ε)

The molar extinction coefficient (ε, epsilon) of **T1** and **T2** were usually based on concentrations measured from UV-Visible absorption spectra which reported in $M^{-1}cm^{-1}$. The maximum absorbance of all fluorophores should not be more than value of 1. The wavelength of maximum absorbance (λ_{max}) of each compound was plotted versus the concentrations (C) at the respective excitation wavelengths (λ_{ex}). Each plot should be a linear line that runs through the origin position (0, 0). The molar extinction coefficient (ε) can also be calculated from plotting of absorption maximum (A) *vs* concentration (C) represented into the following Beer-Lambert law equation:

$$A = \varepsilon bc$$

2.5.2 Fluorescence spectroscopy

The stock solutions of fluorophores **T1** and **T2** were diluted to the concentration of 1 μM and 5 μM, respectively, with their respective solvents. The emission spectra of fluorophores were recorded from the wavelength at 380 to 600 nm at room temperature using excitation wavelength at 388 nm in $CHCl_3$, and 386 nm in 10%H_2O in THF for **T1**, and 3 75 nm in 30%THF-HEPES buffer (0.002M, pH 7.4) for **T2**.

Fluorescence quantum yield (Φ_F)

The fluorescence quantum yield of fluorophores was performed in $CHCl_3$ and 10% H_2O in THF for **T1**, and 30%THF-HEPES buffer (0.002M, pH 7.4) for **T2** using quinine sulfate (Φ_F = 0.54 in 0.1 M H_2SO_4) as the reference according to a previously reported

method [36]. The UV-Visible absorption spectra of five analytical samples and five reference samples at various concentrations were recorded. The maximum absorbance of all samples should not be more than value of 0.1 in order to prevent the interaction among themselves resulting in the quantum yield values may be perturbed at high concentration. The fluorescence emission spectra of the same solutions using appropriate excitation wavelengths selected were recorded based on the absorption at the excitation wavelength (λ_{max}) of each compound. The graphs of integrated fluorescence intensities were plotted against the absorbance at the respective excitation wavelengths. Each plot should be a straight line with a y-intercept at 0, and gradient m.

Moreover, the fluorescence quantum yields (Φ) were determined by comparison with a standard of known fluorescence quantum yield according to the following equation.

$$\Phi_X = \Phi_{ST}\left(\frac{Slope_x}{Slope_{ST}}\right)\left(\frac{\eta_x^2}{\eta_{ST}^2}\right)$$

Where the subscripts, X refers to the unknown samples and ST refers to the standard quinine sulfate solution in 0.1 M H_2SO_4, whose fluorescence quantum yield is known to be 0.54 [Ref], Φ_X is the fluorescence quantum yield of sample, *Slope* is the slope from the plot of integrated fluorescence intensity versus absorbance, and η is the refractive index of the solvent.

2.6 Fluorescent sensor study

2.6.1 Nitroaromatic sensor studies

2.6.1.1 Selective screening test for nitroaromatic compounds

A solution of the fluorophore **T1** was prepared in $CHCl_3$ and aqueous THF, and then adjusted to the concentration of 1 μM. The maximum absorption wavelength was used as the excitation wavelength of **T1** at 388 nm in $CHCl_3$ solution, and 386 nm in 10%H_2O in THF and the emission was recorded from the wavelength at 390 to 600 nm. Nitroaromatic compounds such as 2,4,6-trinitrotoluene (TNT), 2,4,6-dinitrotoluene (DNT), 2,4-dinitrophenol (DNP), picric acid (PA), 2-or 3- or 4-nitrophenol (NP),

nitrobenzene (NB), and 4-nitrobenzoic acid (NBA), and non-nitroaromatic analogs such as benzoic acid (BA), benzophenol (BP), and 2-chlorobenzoic acid (CBA) were prepared in $CHCl_3$ and H_2O at concentrations of 10 mM.

2.6.1.2 Fluorescence titration of T1 with 2-NP in $CHCl_3$

A 1μM $CHCl_3$ solution of **T1** was prepared through dilution of its 100 μM $CHCl_3$ solution. This solution with a volume of 1 mL was pipetted into a 1 cm standard quartz cell and titrated with stepwise addition of 2-NP at various concentration from 0 μM to 2 mM. The fluorescence emission spectra were measured at room temperature at an excitation wavelength of 388 nm.

2.6.1.3 Fluorescence titration of T1 with TNP in aqueous THF

5 μM of **T1** in a mixture of THF in water (9:1) solution was added to quartz cell with a 1 mL volumetric pipette and titrated with stepwise addition of TNP at a concentration from 0 to 100 μM. The fluorescence emission spectra were measured at room temperature at an excitation wavelength of 386 nm.

2.6.1.4 Effect of water content on fluorescent quenching efficiency of T1 by picric acid

The excitation wavelength was 386 nm and the fluorescence emission was recorded from the wavelength at 400 to 700 nm at room temperature. 1 μM of **T1** solution was prepared in THF. The stock solution of picric acid (PA) was prepared in water at concentration of 1 mM. The **T1** (1 μM) was transferred to the quartz cuvette in volume 1 mL, and then picric acid (100 μM) was added into the **T1** solution. The final volume of the mixture was adjusted to 1000 μL by varied water content between 5%-50% water in THF.

2.6.1.5 pH effect depending on the ionization of PA in aqueous medium

1 μM and 100 μM of mixture solution of **T1** and PA prepared in THF with 10% aqueous buffer of various pHs were investigated by measuring the fluorescence emission spectra of buffer solutions in the pH range of 4 to 12.

2.6.1.6 LOD (limit of detection)

The detection limit of an individual analytical procedure is the lowest amount of analytes in a sample which can be detected but not necessarily quantitated as an exact value.

The limit of detection (LOD) is determined by the analysis of samples with known concentrations of analyte which may be expressed as:

$$\text{The limit of detection (LOD)} = 3\sigma/K_{SV}$$

Where; σ refers to the standard deviation of the blank measurement deriving from the intensity of fluorophores at 1 μM of 9 samples (n = 9). K_{sv} (Stern-Volmer constant) is the slope of calibration curve obtained from the fluorescence titration spectra.

2.6.2 Metal ion sensor studies

2.6.2.1 Effect of water content depending on solubility of T2

The solution of **T2** was prepared at concentration of 50 μM in THF, then adjusted to 5 μM and added into the 1 mL cuvette. The final volume of the solution was adjusted to 1mL by varying the ratio of water in THF from 10% to 90% to afford the final concentration of 5 μM of **T2**. The fluorescence spectra were measured with an excitation wavelength of 375 nm at room temperature and recorded from the wavelength at 390 to 700 nm.

2.6.2.2 Cation sensing ability of T2

The solution of fluorophore **T2** was prepared at concentration 50 μM in THF and adjusted to the concentration of 10 μM. The excitation wavelength was 374 nm and the emission spectrum was recorded from the wavelength at 390 to 700 nm. Metal ions were used as analytes such as K^+, Na^+, Li^+, Ba^{2+}, Mg^{2+}, Ca^{2+}, Cu^{2+}, Ni^{2+}, Zn^{2+}, Al^{3+}, Hg^{2+}, $Fe^{3+,}$ Co^{2+}, Cr^{3+}, Cd^{2+}, and Pb^{2+}. All metal stock solutions were prepared in 0.002

M HEPES buffer pH 7.4 at concentrations of 2 mM. Concentration of each metal solution was adjusted to 50 μM and was transferred to **T2** solution in the cuvette with a volume of 1 mL. The fluorescence emission spectra were measured at room temperature at an excitation wavelength of 375 nm.

2.6.2.3 Complexation studies of T2 with various anions in the presence of copper (II) ion

A mixture of **T2** (5 μM) in 30%THF-HEPES buffer (0.002M, pH 7.4) and 10 equivalent of Cu^{2+} ion was prepared and added to the cuvette in volume 1 mL and stirred for 1 min before adding each anion. The anions selected in this study which were HPO_4^-, ClO_4^-, HSO_4^- ,NO_3^-, OAc^-, SO_3^{2-}, CN^-, CO_3^{2-}, Cl^-, F^-, I^-, and Br^- were prepared in water at concentrations of 2 mM. The 10 equivalent of each anionic guest solution was transferred to the mixture solution of complex in the cuvette and stirred for 1 min before each scan.

CHAPTER III

RESULTS AND DISCUSSION

Our design of new truxene-based chemosensors (**T1** and **T2**) relied on the reactivity of truxene which can be deprotonated at the position 5, 10, and 15 and react towards electrophilic reagent at the position 2, 7, and 12. The structures of these compounds are shown in **Figure 3.1**. Compound **T1** will be decorated with six hydrophobic *n*-butyl groups to facilitate its solubility in organic solvent, and three ethynylpyrene groups as receptors for nitroaromatic analyte. On the other hand, compound **T2** will be alkylated by six diglycol groups to enhance the water solubility. The metal-ion receptor units for **T2** are dipicolyl anilines. The synthesis of both compounds are described herein.

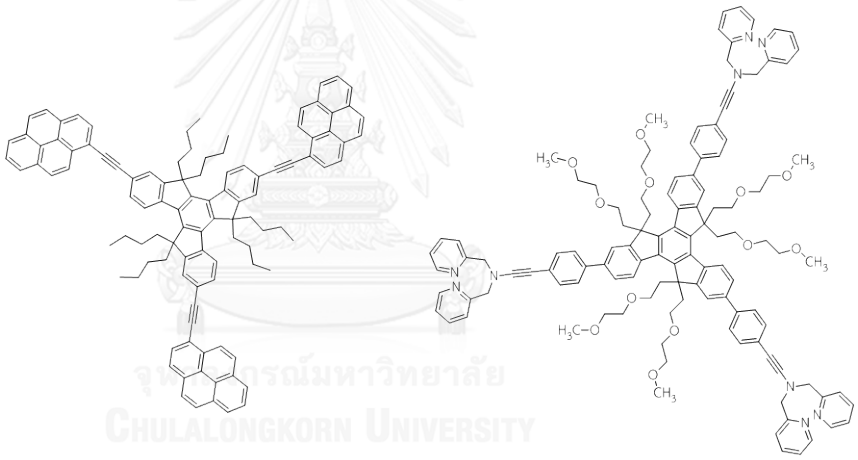

T1 T2

Figure 3.1 Structure of fluorophores

3.1 Synthesis and Characterization of fluorophores

3.1.1 Fluorophores T1

The synthesis of fluorophores **T1** and **T2** began with the preparation of truxene core as shown in **Scheme 3.1**. The commercially available dihydrocinnamic acid was treated with polyphosphoric acid (PPA) at 160°C for 8 h. The reaction generated indanone *in situ*, which then underwent aldol condensation to provide truxene as a

light-yellow solid in 49% yield after recrystallization in tolulene. The structure of truxene was verified by comparing the ^{1}H-NMR data with the literature report [28].

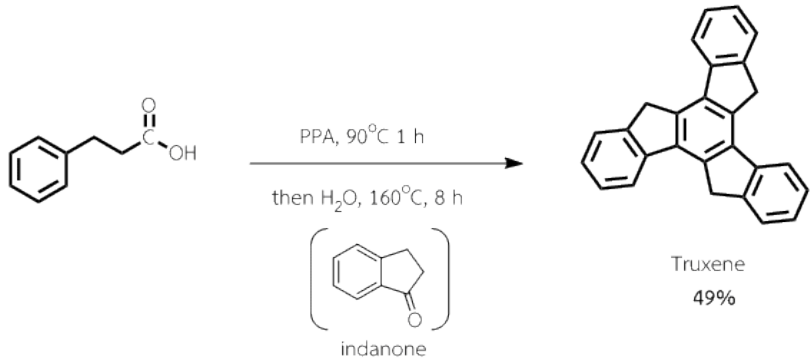

Scheme 3.1 Synthesis of Truxene

The ^{1}H NMR spectrum of truxene in $CDCl_3$ **(Figure 3.2)** shows a signal for methylene protons (e) at 4.30 ppm as a singlet. The four signals at 7.98 (d), 7.71 (a), 7.51 (b), and 7.40 (c) ppm correspond to the four aromatic protons.

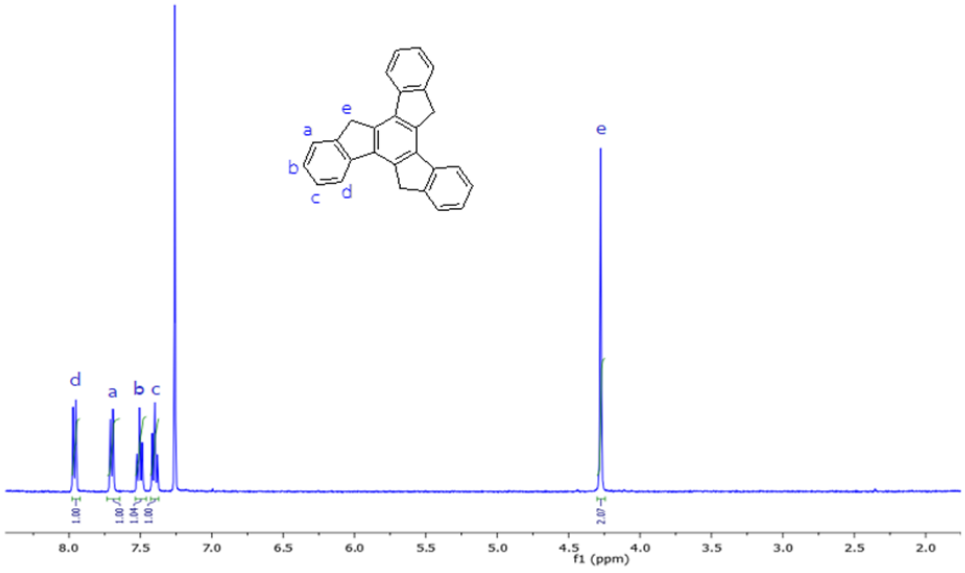

Figure 3.2 ^{1}H NMR spectrum of Truxene (400 MHz, in $CDCl_3$)

Since its structure is relatively planar and it is highly hydrophobic, truxene has poor solubility in most common solvents and tends to aggregate at high concentration which lead to poor optical properties. To overcome this issue, the methylene positions

(C-5, C-10 and C-15) of truxene was alkylated by either hydrophobic *n*-butyl groups or hydrophilic 2-(2′-methoxy) ethoxyethyl groups. This structural modification should hinder molecular aggregation via π-π stacking resulting in better solubility in nonpolar and polar solvents.

Hexa-alkylation at the 5, 10 and 15-positions of truxene was achieved by treatment with NaH and n-butyl bromide to provide the hexabutylated truxene core **1** in 75% yield. The compound was obtained as a white solid after a simple chromatography on silica gel column. Regioselective iodination of **1** with KIO_3 and I_2 in a mixed solvent of CH_3COOH, H_2SO_4, H_2O, and CCl_4 afforded the triiodo **2** in an excellent yield of 93% after crystallization in ethanol (**Scheme 3.2**).

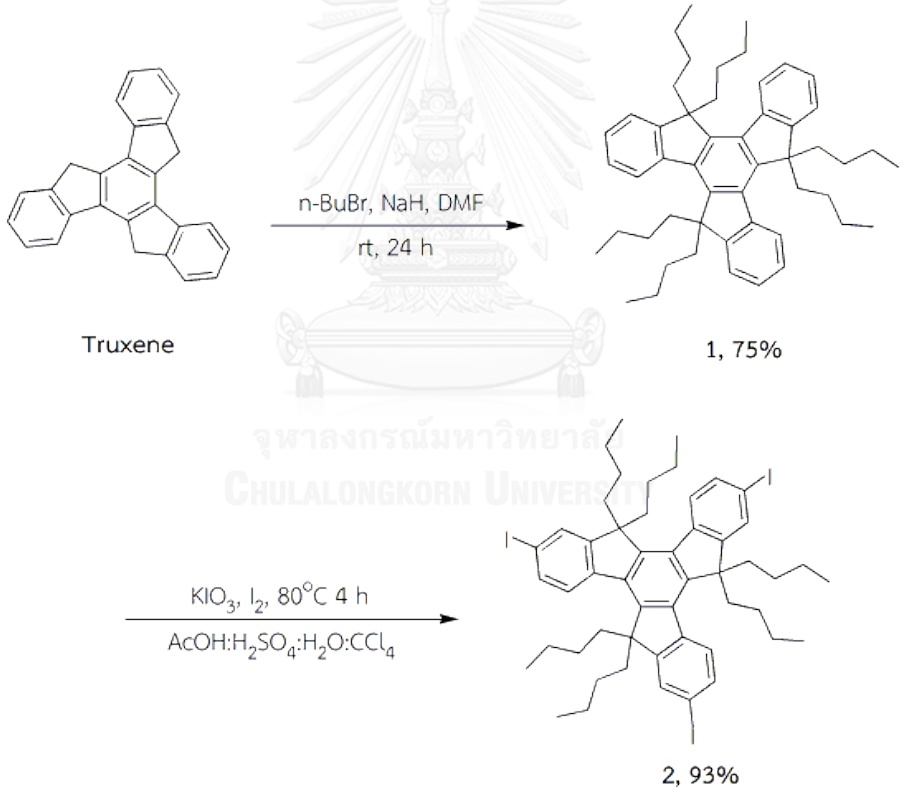

Scheme 3.2 Synthesis of the hexabutylated truxene **1** and the triiodo truxene **2**

The ^{1}H-NMR spectrum of **1** and **2** in $CDCl_3$ are shown in **Figure 3.3**. Compound **1** showed three signals for aromatic protons at 8.38 (d, *J* = 7.4 Hz), 7.46 (dd, *J* = 7.1 and 1.3 Hz) and 7.40-7.35 (m) ppm. Signals for the methylene groups closest to the

aromatic rings are separated into two groups as the truxene structure is not completely flat. All of the aliphatic protons appeared around 0.4 to 3.0 ppm. The ^{1}H-NMR spectrum of **2** shows one singlet signal at 7.76 and two doublets signals at 8.07, 7.71 for the aromatic protons. The multiplet in the range 0.4-2.8 ppm can be assigned to all of methyl and methylene protons on the butyl chains.

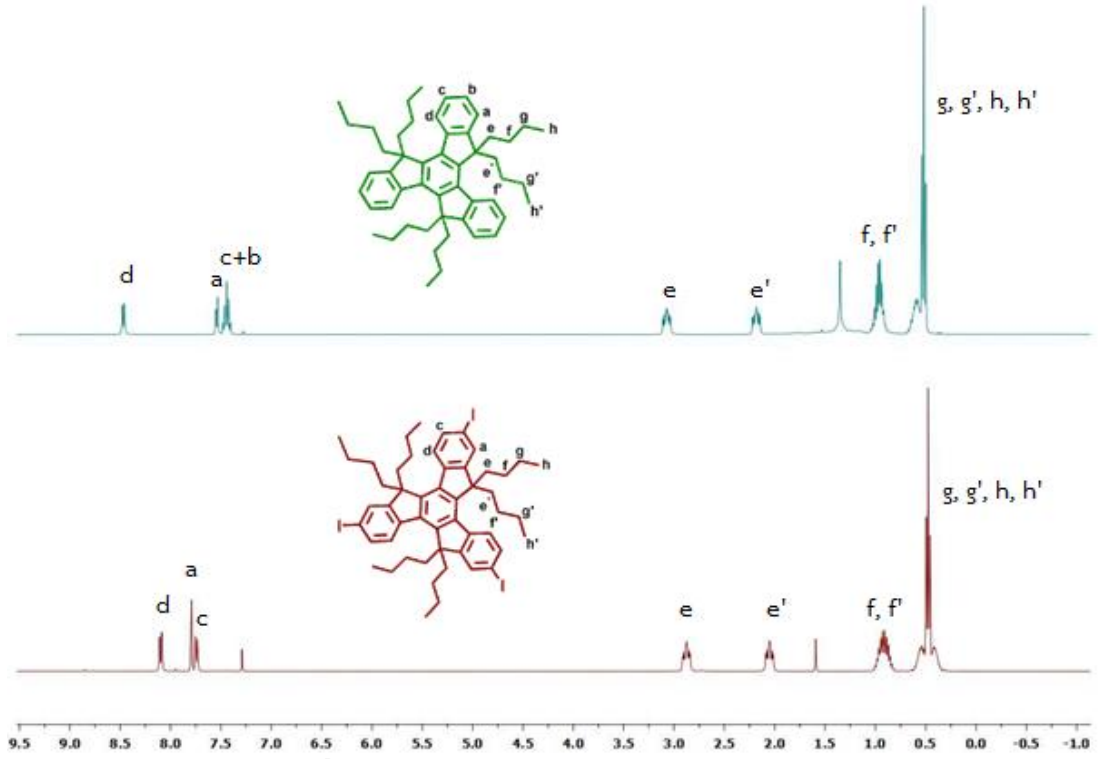

Figure 3.3 ^{1}H NMR spectrum of **1** and **2** (400 MHz, in $CDCl_3$)

The synthesis of target molecule **T1** is shown in **Scheme 3.3**. Sonogashira coupling of the triiodo truxene **2** with 1-ethylnylpyrene was achieved using $Pd(PPh_3)_2Cl_2$ and CuI catalytic system. Fluorophore **T1** was obtained in 40% yield after a silica gel column chromatography as a yellow solid (m.p. >300 °C).

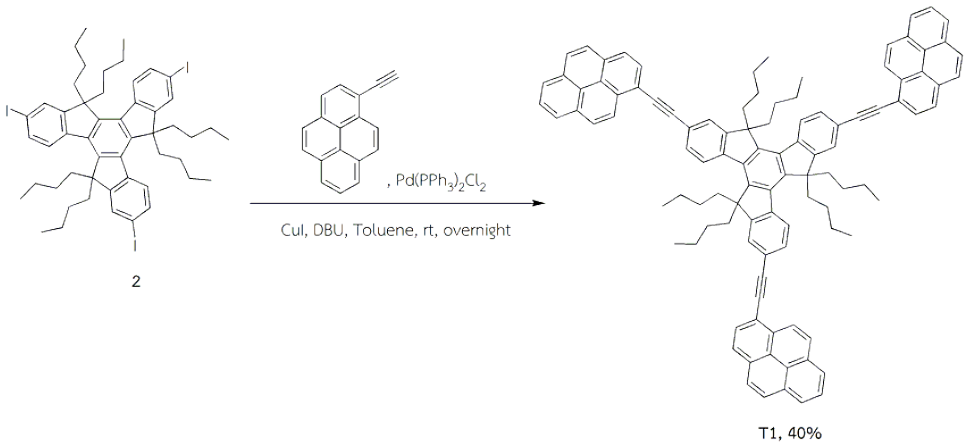

Scheme 3.3 Synthesis of fluorophore **T1**

Fluorophore **T1** was identified by IR, ^{1}H NMR, ^{13}C NMR and MALDI-TOF-MS. The MALDI-TOF-MS analysis revealed a molecular ion peak $[M+H]^+$ at *m/z* 1352.91 which validated the molecular formula of $C_{105}H_{90}$ **(Figure 3.4)**.

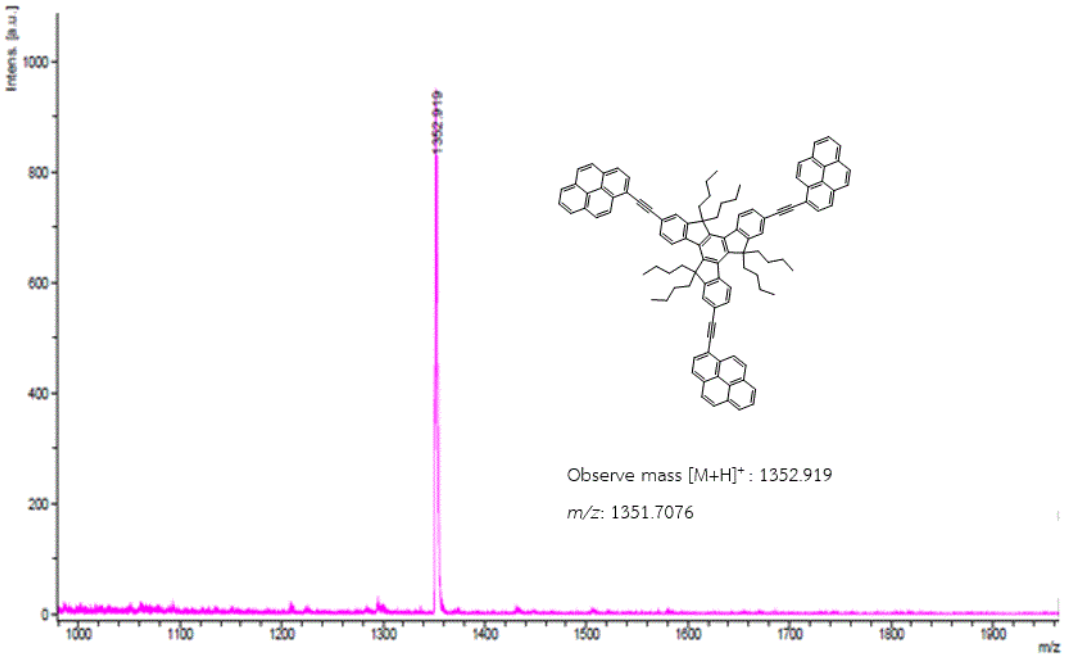

Figure 3.4 MALDI-TOF Mass spectrum of **T1**

The ^{1}H NMR spectrum of **T1** is shown in **Figure 3.5.** The signals of pyrene groups appeared as a doublet at 8.82 (3H) and multiplet signals at 8.35-8.03 (24H) ppm.

The aromatic protons of truxene core appeared at 8.51 (3H) and 7.86-7.84 (m, 6H) ppm. The signals at 0.49 to 3.11 ppm belonged to the butyl chain. The appearance of both truxene and pyrene fragments in the ^{1}H-NMR spectrum of **T1** suggested that the coupling reaction was successful.

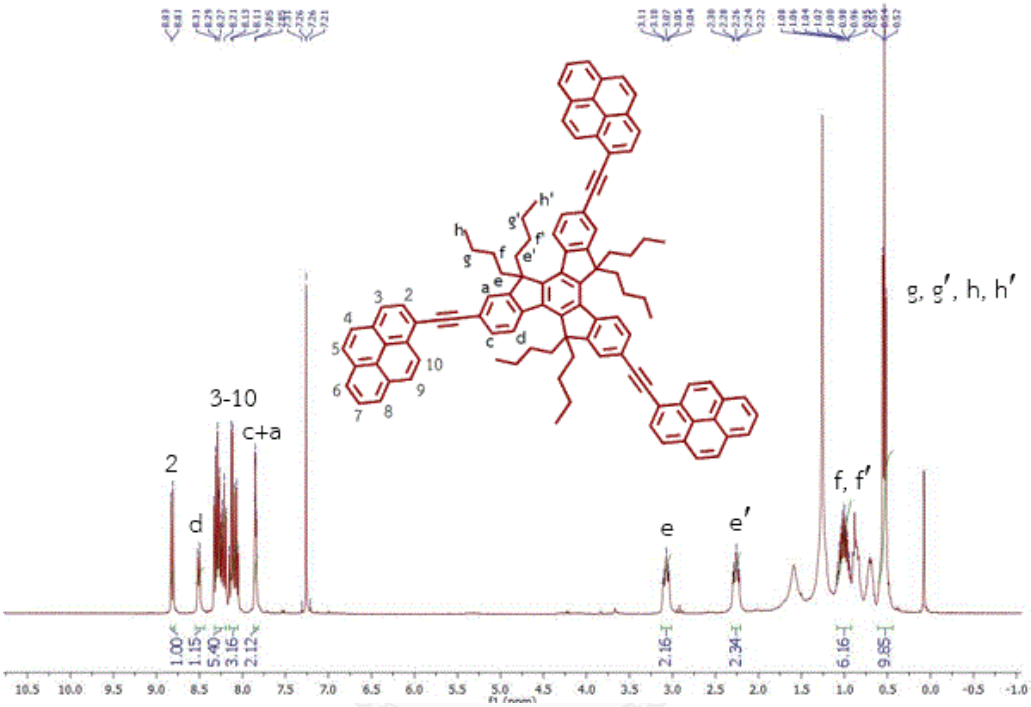

Figure 3.5 ^{1}H NMR spectrum of **T1** (400 MHz, in $CDCl_3$)

3.1.2 Fluorophores T2

3.1.2.1 Synthesis of water-soluble truxene core

To enhance the water solubility of the truxene fluorophore, six hydrophilic 2-(2′-methoxy) ethoxyethyl groups were installed at the methylene positions of truxene core **(Scheme 3.4)**. Hexa-alkylation of truxene was accomplished by treatment with NaH and 2-(2′-methoxy) ethoxyethyl iodide in DMF at room temperature with stirring for 24 h. The product was purified by silica gel column chromatography to give the hexaalkylated truxene core **6** in 66% yield as a white solid. The selective iodination of **6** using KIO_3 and I_2 in mixed solvent between CH_3COOH, H_2SO_4, H_2O, and CCl_4 gave rise to the 2,7,12-triiodo **7** as a single regiosiomer in excellent yield of 96% as yellow solid.

This synthetic method was prepared following a literature reported previously by Earmrattana et al. [28].

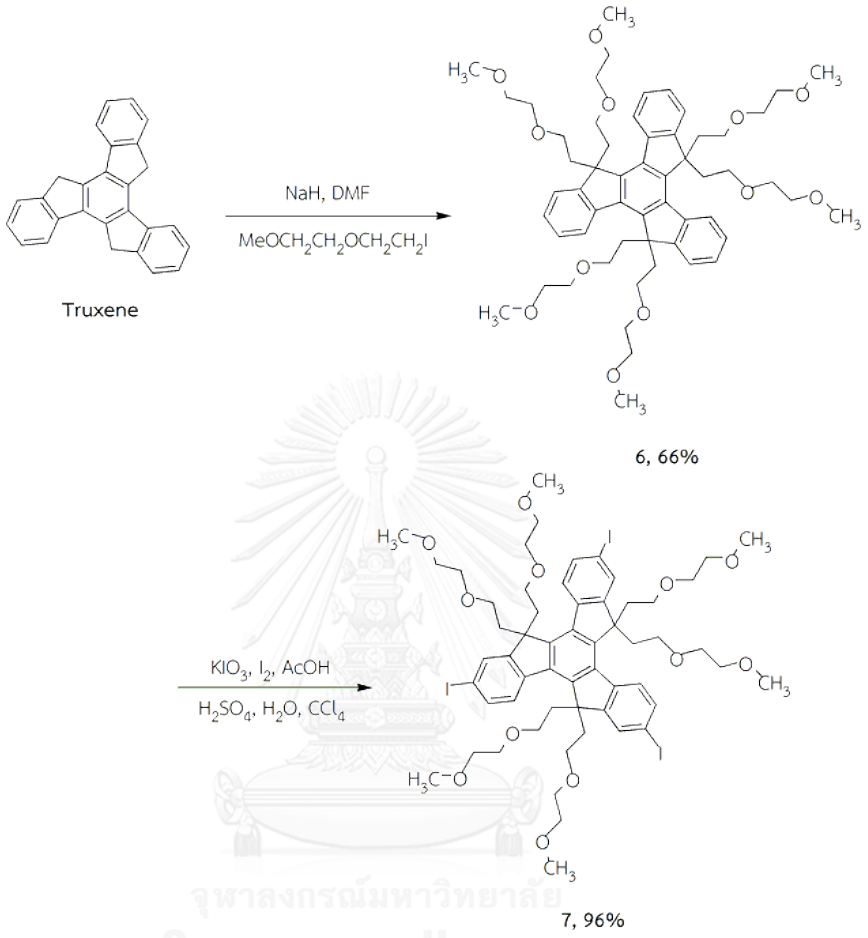

Scheme 3.4 Synthesis of hydrophilic truxene core

The compound **6** and **7** was characterized by ^{1}H NMR and ^{13}C NMR spectroscopy which were in good agreement with the literature reports**.** The ^{1}H NMR spectrum of **6** showed characteristic peaks of the glycol chains signal in the range of 2.5 to 3.7 ppm (m, 66H) and the aromatic protons appeared as at 7.41 (m, 6H, H-b and H-c), 8.34 (d, 3H, H-d) and 7.58 ppm (d, 3H, H-a) (**Figure 3.6**). For compound **7**, there is a new low-field signal at 7.85 ppm (s, 3H, H-a), 7.97 (d, 3H), and 7.68 ppm (d, 3H) which was identified as aromatic protons. The multiplet signal in the regions of 2.44 to 3.01 were assigned as methylene and methyl protons of the diglycol chains **(Figure 3.7)**.

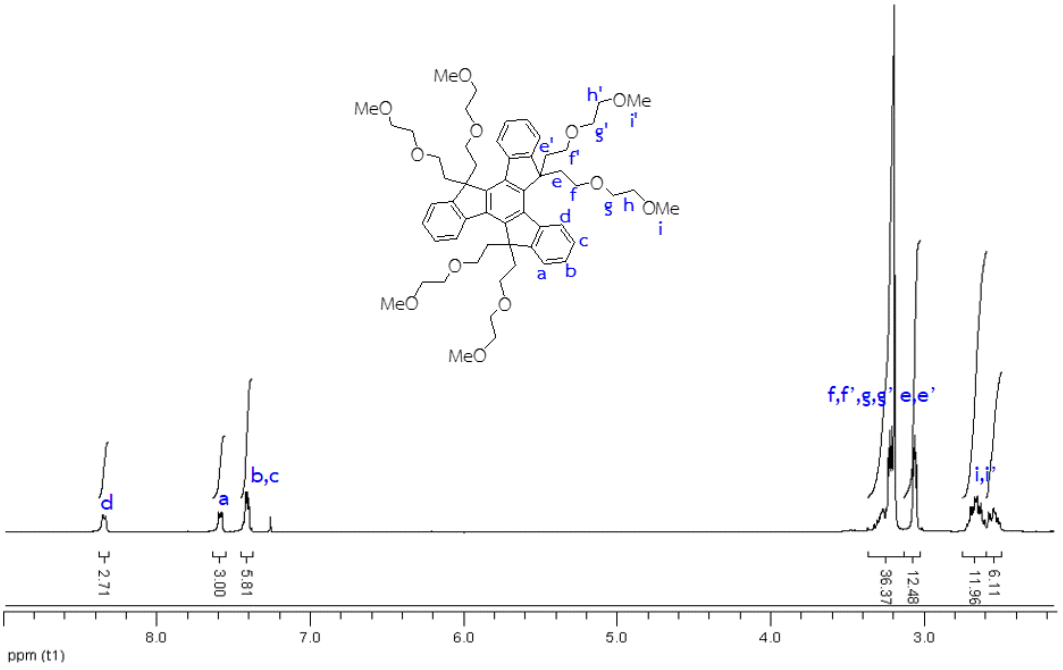

Figure 3.6 ^{1}H-NMR spectrum of 5,5',10,10',15,15'-Hexa-2-(2-methoxyethoxy) ethane-truxene **6** (400 MHz, in $CDCl_3$)

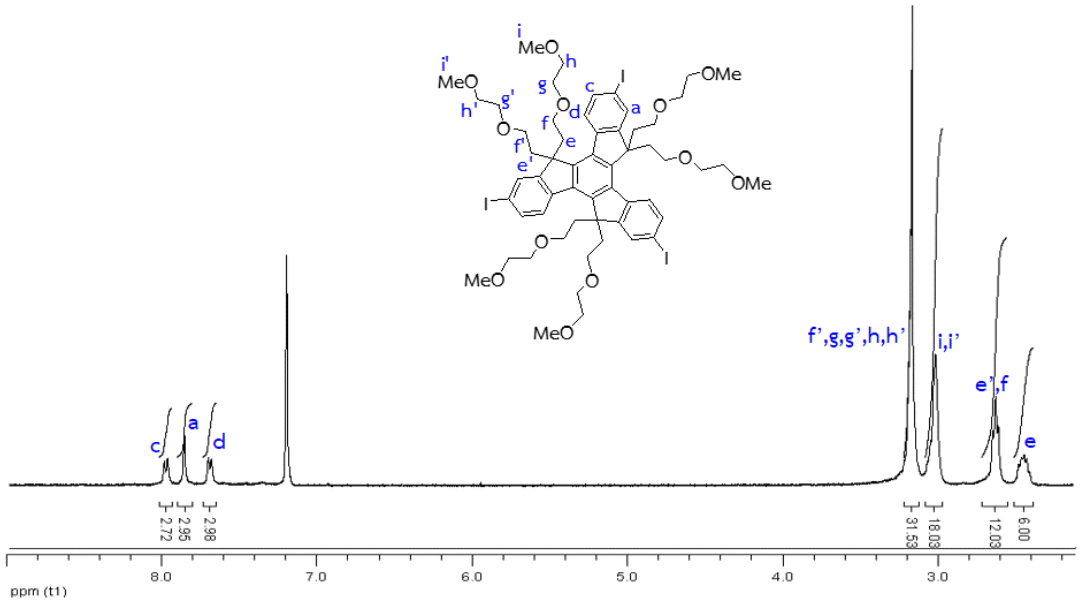

Figure 3.7 ^{1}H-NMR spectrum of 2,7,12-Triiodo-5,5',10,10',15,15',-hexa-2-(2-methoxy ethoxy) ethanetruxene **7** (400 MHz, in $CDCl_3$)

3.1.2.2 Synthesis of the peripheral group

Synthetic pathway of the peripheral group (compound **5**) was outlined in **Scheme 3.5.** Starting from a reaction between the commercially available 4-iodoamine and 2-(chloromethyl) pyridinium chloride in a mixture of H_2O and CH_3CN according to a published procedure [16], the disubstituted *p*-iodoaniline product **3** was obtained after stirring at room temperature for 4 days as a yellow needle crystal in 44% yield. It should be noted that there was a side product (15%) in this reaction which was identified as monosubstituted *p*-iodoaniline. Next, the Sonogashira cross coupling between compound **3** and trimethylsilylacetylene using Pd complex and CuI as catalyts provided trimethylsiyl dipicolyl amine **4** in 75% yield [16, 35]. The desilylation was achieved using excess KOH (in THF/MeOH 1:10 v/v) at room temperature to afford the aryl acetylene **5** as a pale yellow crystal in 89% yield. Compound **5** was then used for coupling with the 2,7,12-triiodo **7** to generate fluorophore **T2**.

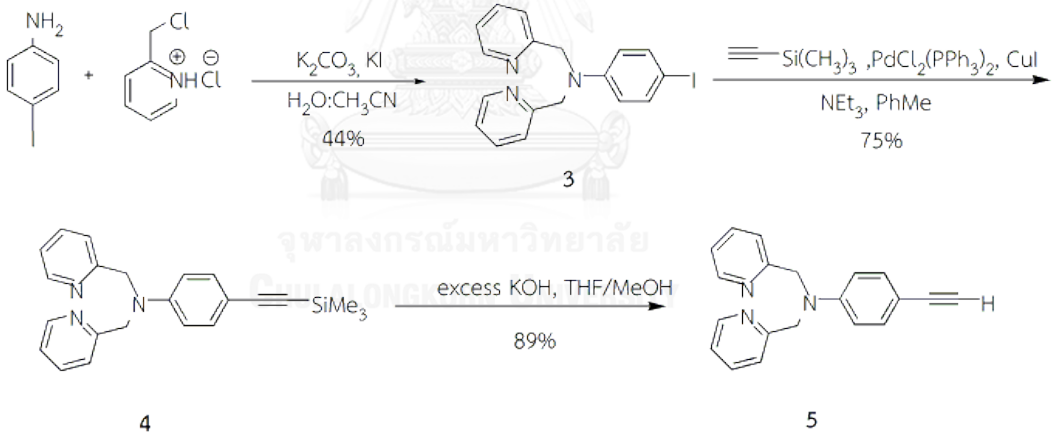

Scheme 3.5 Synthesis of peripheral group

Characterizations of **3**-**5** by IR, NMR, and HR-MS confirmed the successful synthesis of these compounds. For **3**, a singlet signal at 4.85 ppm belonged to the methylene protons of dipicolyl moieties, while the aromatic protons resonated at 6.46 to 8.59 ppm **(Figure 3.8)**. After a successful Sonogashira coupling, a singlet signal of trimethylsilyl group at 0 ppm appeared in the ^{1}H-NMR spectrum of **4**. This signal then

disappeared after the silylation to afford the terminal alkyne **5 (Figure 3.9 and Figure 3.10)**.

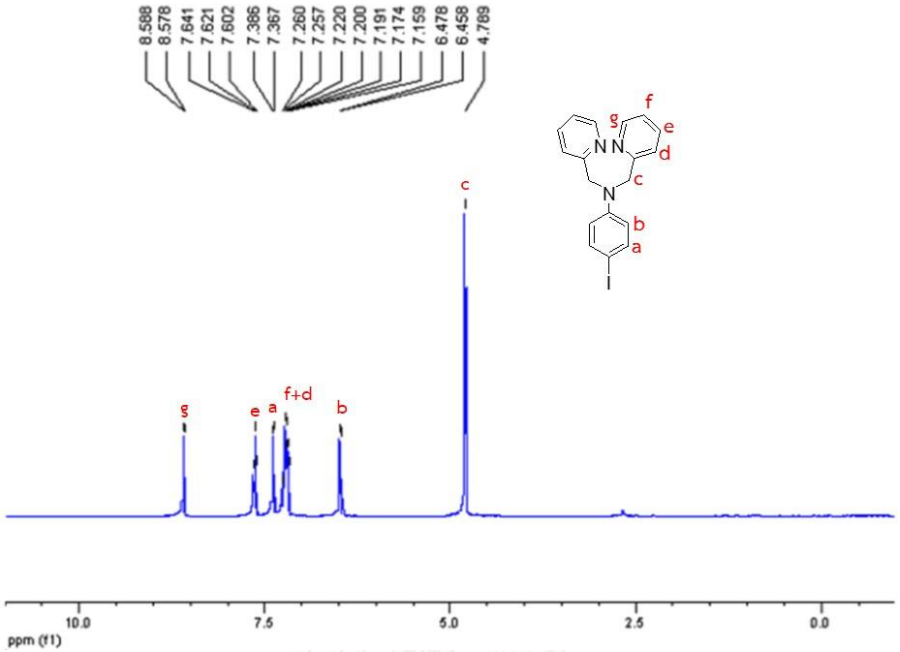

Figure 3.8 ^{1}H-NMR spectrum of **3** (400 MHz, in $CDCl_3$)

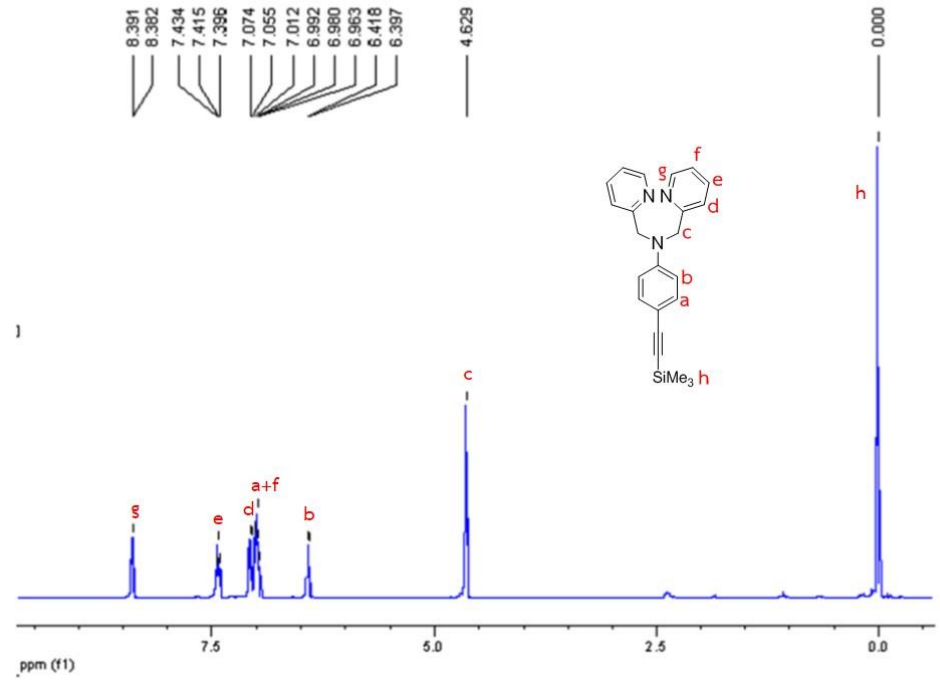

Figure 3.9 ^{1}H-NMR spectrum of **4** (400 MHz, in $CDCl_3$)

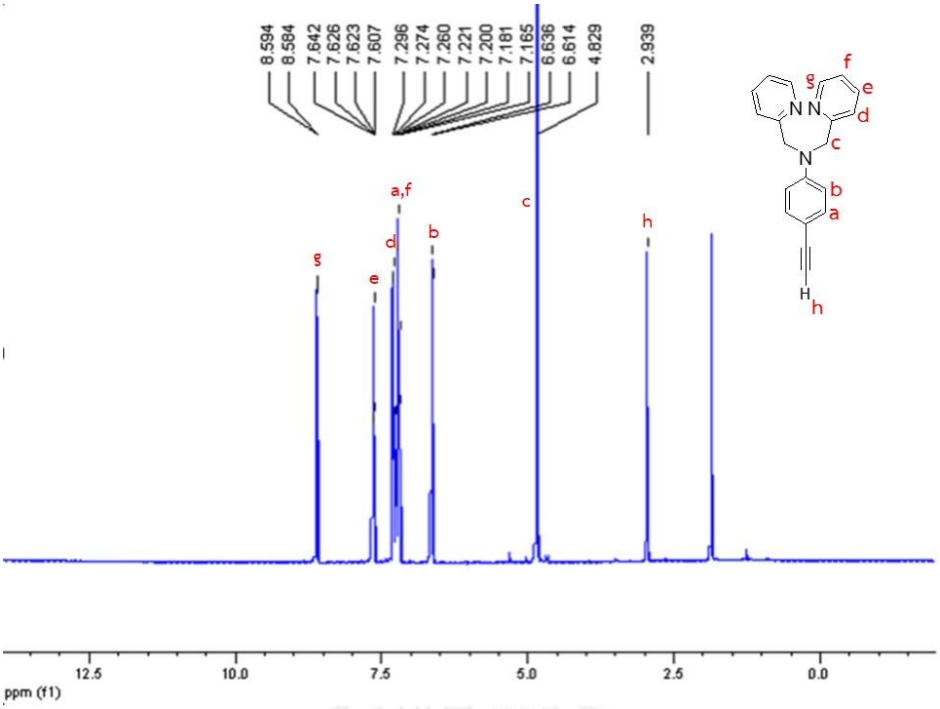

Figure 3.10 ^{1}H-NMR spectrum of **5** (400 MHz, in $CDCl_3$)

3.1.2.3 Final assembly of T2

The synthesis of target molecule **T2** also relied on the Sonogashira coupling between the 2,7,12-triiodo **7** and terminal alkyne **5**. The reaction was carried out using $Pd(PPh_3)_2Cl_2$ and CuI catalytic system to provide **T2** as a yellow solid in 42% yield **(Scheme 3.6)**. The formation of **T2** was verified by several spectroscopic techniques involving IR, ^{1}H-NMR, ^{13}C-NMR, MALDI-TOF, and HR-MS.

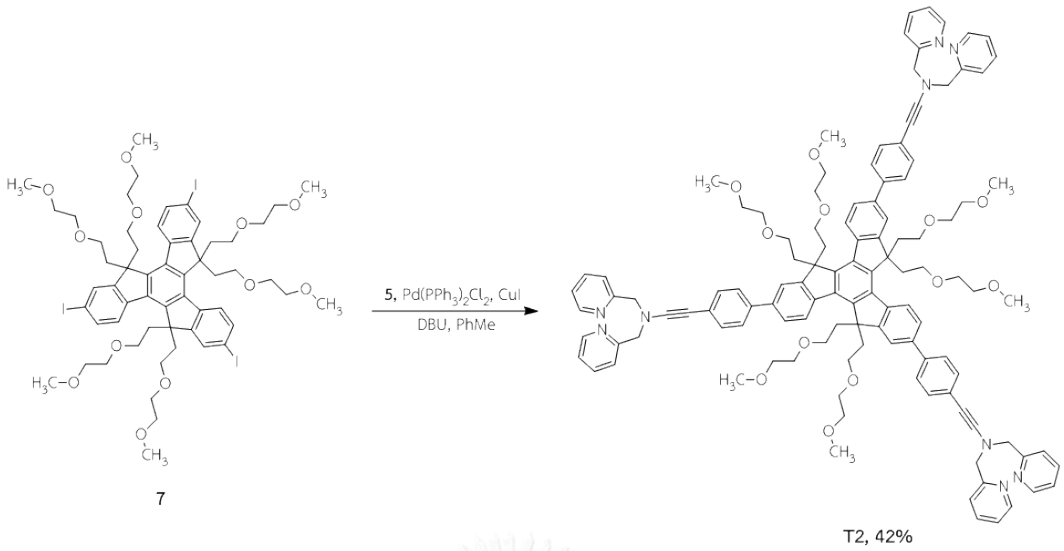

Scheme 3.6 Synthesis of target molecule **T2**

The ^{1}H NMR spectrum of fluorophore **T2 (Figure 3.11)** exhibited the signals of dipicolyl groups at 4.86, 7.12, 7.26, 7.66 and 8.59 ppm. The aromatic protons of phenyl groups appeared as doublets at 6.68 and 7.39 ppm. Signals of the aromatic protons on the truxene core appeared at 7.45, 7.62 and 8.21, whereas the aliphatic proton signals of hydrophilic chains displays in the regions of 2.98 to 3.2 ppm.

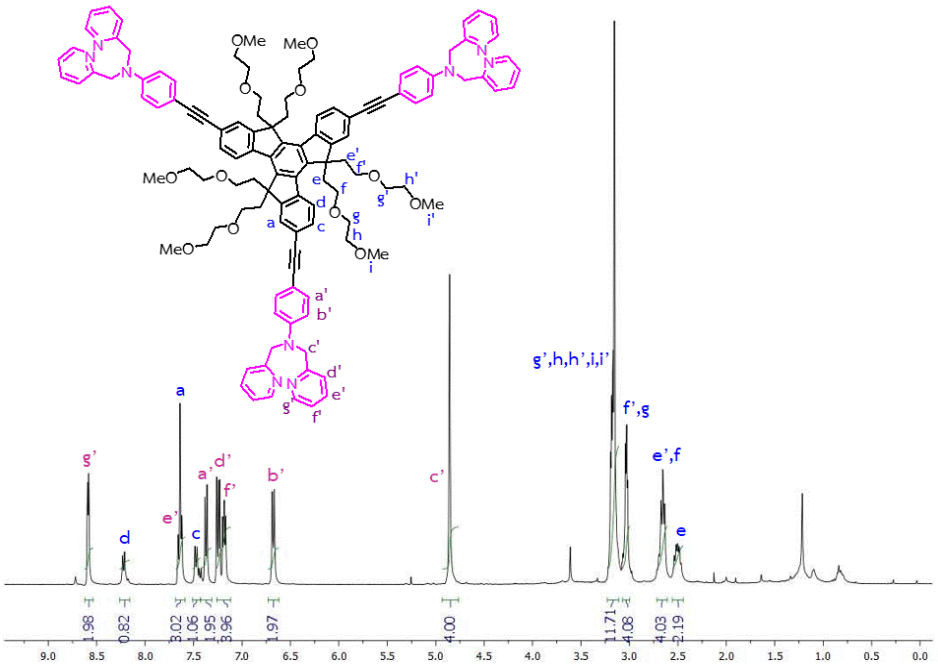

Figure 3.11 ^{1}H-NMR spectrum of **T2** (400 MHz, in $CDCl_3$)

The MALDI-TOF and HR-MS mass analysis confirmed the structure of **T2** by showing an apparent molecular ion peak at 1847.949 $[M+H]^+$, which confirmed the molecular mass of compound with a molecular formula of $C_{117}H_{123}N_9O_{12}$ **(Figure 3.12 and 3.13)**.

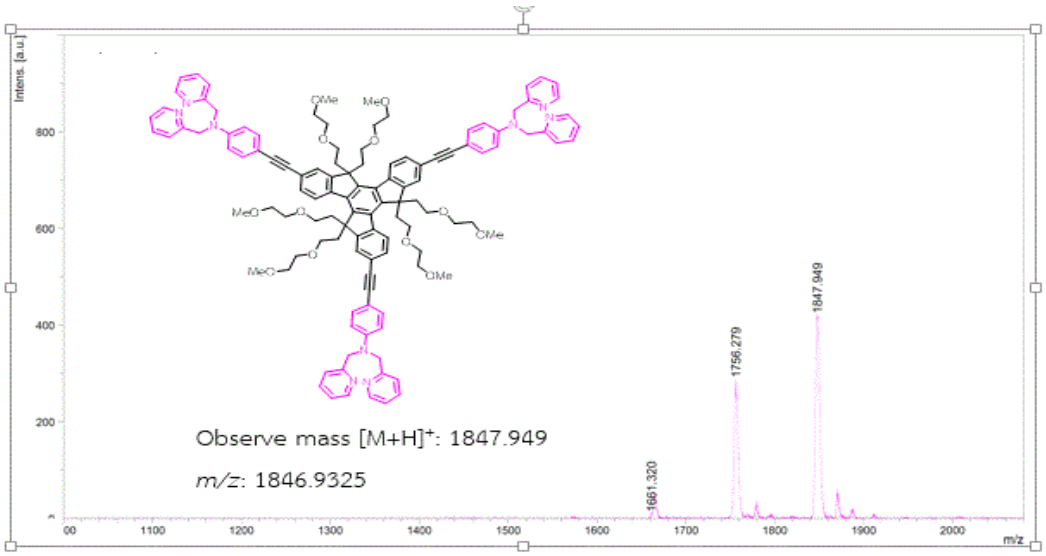

Figure 3.12 MALDI-TOF Mass spectrum of **T2**

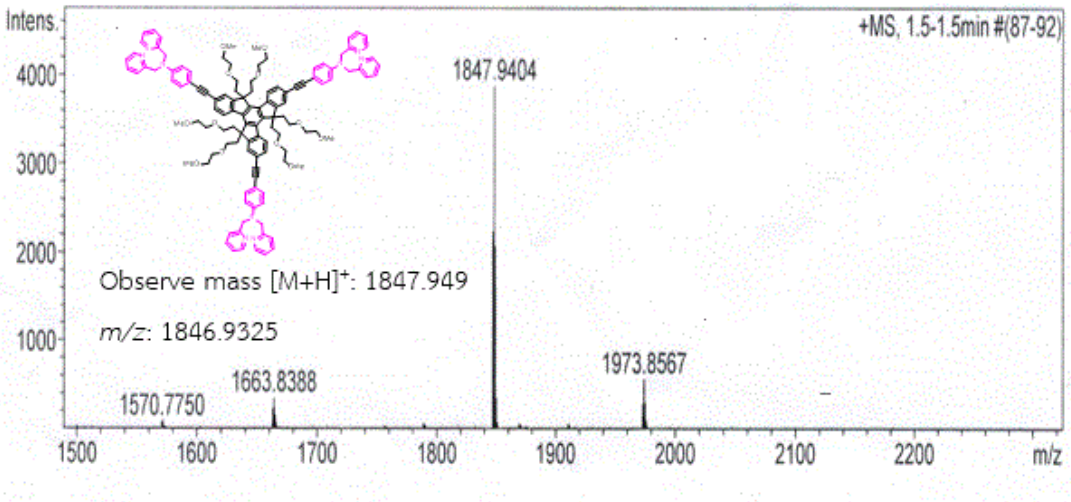

Figure 3.13 HR-MS spectrum of **T2**

3.2 Nitroaromatic sensor

3.2.1 Photophysical properties of T1

The UV-Spectrum of **T1** in $CHCl_3$ and 10% H_2O in THF was studies. From the normalized absorption and emission spectra in both solvents are relatively similar. They show two maximum absorption peaks at 388 and 412 nm in $CHCl_3$ solution, and 386 and 410 nm when dissolved in 10% H_2O in THF **(Figure 3.14 and Table 3.1).** However, the molar extinction coefficients in two solvents are significantly different, probably due to the lower solubility of the compound in aqueous THF. The two absorption maxima suggested two distinctly different conformations due to the rotation of the bond between the truxene and pyrene pendant which may allow a full or partial conjugation. The fluorophore also possesses two maximum emission peaks at 414 to 442 nm in $CHCl_3$ solution with high quantum yield of 71%. The emission spectrum of fluorophore in 10% H_2O in THF remained quite similar to that of the $CHCl_3$ solution but the quantum efficiency decreased to 53%. This indicated that the compound may aggregated in aqueous solution resulting in self-quenching and lower quantum yield. In addition, the higher polar solvent could stabilize the fluorophore in the excited state, causing higher degree of geometrical relaxation and loss of energy in non-radiative pathways. In comparison with the parent truxene, the absorption and emission of fluorophore **T1** shifted towards visible range which can benefit its applications as naked-eye fluorescent chemosensor for detection of nitroaromatic compounds.

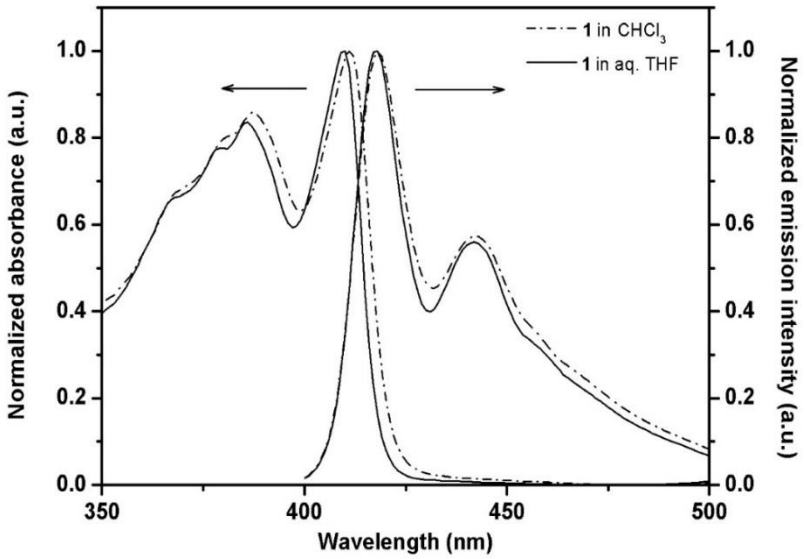

Figure 3.14 Normalized absorption and emission spectra of **T1** in $CHCl_3$ and aqueous THF

Table 3.1 Photophysical property of truxene and **T1** in $CHCl_3$ and 10% H_2O in THF

Compound	Absorption		Emission	
	λ_{max} (nm)	log ε (M^{-1} cm^{-1})	λ_{max} (nm)	Φ (%)
Truxene ($CHCl_3$)	275	4.21	359	< 0.01
Truxene (THF-H_2O)	273	4.23	357	6[a]
T1 ($CHCl_3$)	388, 412	5.27	415, 442	71[b]
T1 (THF-H_2O)	386, 410	4.95	415, 440	53[b]

[a]2-Aminopyridine in 0.1 M H_2SO_4 (Φ = 60%) was used as the standard.
[b]Quinine sulfate in 0.1 M H_2SO_4 (Φ = 54%) was used as the standard.

3.2.2 Selectivity screening for nitroaromatic compounds

Next, the sensing selectivity of **T1** in $CHCl_3$ (1 μM) and aqueous THF towards various analytes including nitroaromatic compounds such as 2,4,6-trinitrotolulene (TNT), 2,4-dinitrotolulene (DNT), 2,4-dinitrophenol (DNP), picric acid (PA), 2- or 3- or 4-nitrophenol (NP), nitrobenzene (NB), 4-nitrobenzoic acid (NBA), and non-nitroaromatic

analogs such as benzoic acid (BA), benzophenol (BP) and 2-chlorobenzoic acid (CBA) was investigated. The fluorescence signal of **T1** in $CHCl_3$ could be selectively quenched by 2-NP **(Figure 3.15)**, whereas the selectivity towards PA was observed for the aqueous THF solution **(Figure 3.16)**.

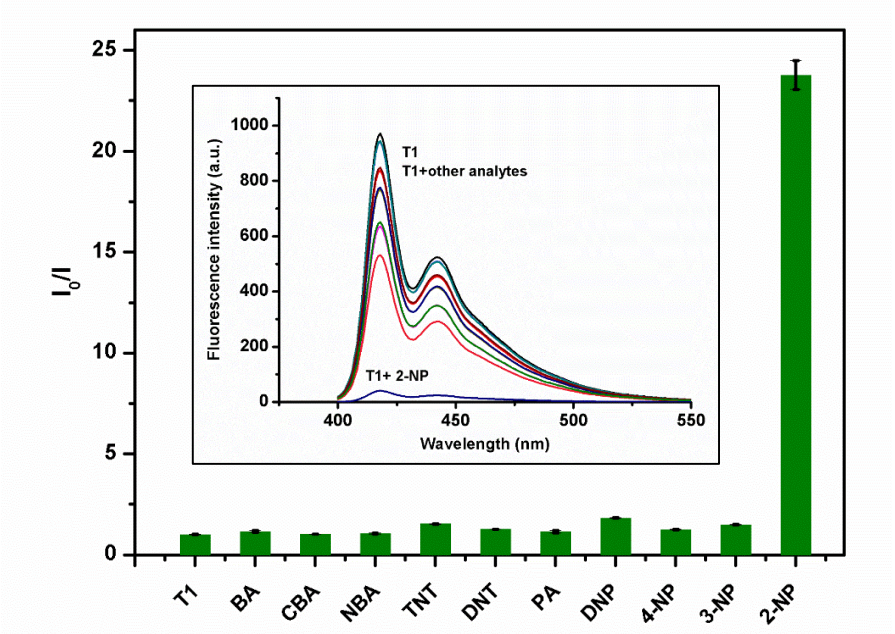

Figure 3.15 Fluorogenic responses and emission spectra (inset) of **T1** (1 μM) towards various analytes (1 mM) in $CHCl_3$

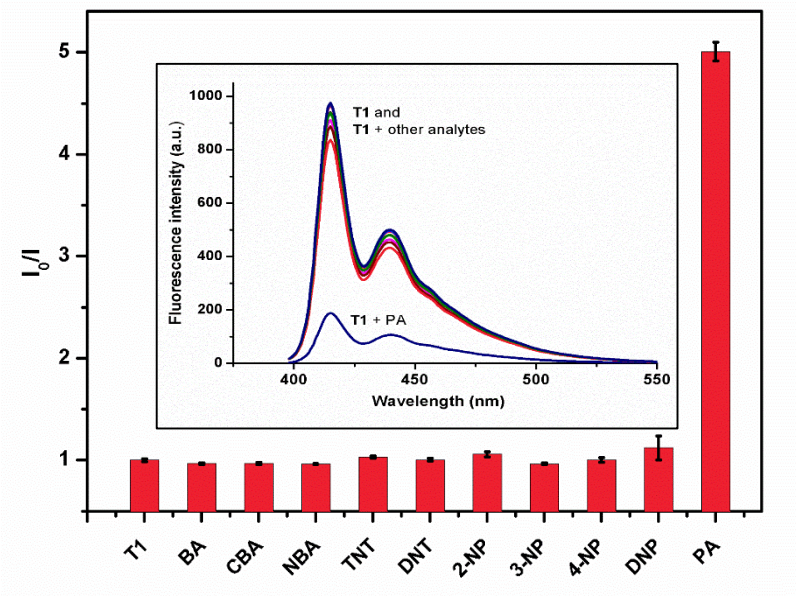

Figure 3.16 Fluorogenic responses and emission spectra (inset) of T1 (1 μM) towards various analytes (0.1 mM) in 10% H_2O in THF

3.2.3 Effect of water content on fluorescent quenching efficiency of T1 by picric acid (PA)

On the other hands, the quenching efficiency by PA in aqueous THF could be enhanced by the addition of water but the water content above 50% led to detrimental aggregation that diminished the initial fluorescence signal **(Figure 3.17)**. Upon an optimization of the water content, the highest quenching efficiency was obtained when 10% H_2O in THF was used as the solvent **(Figure 3.18).**

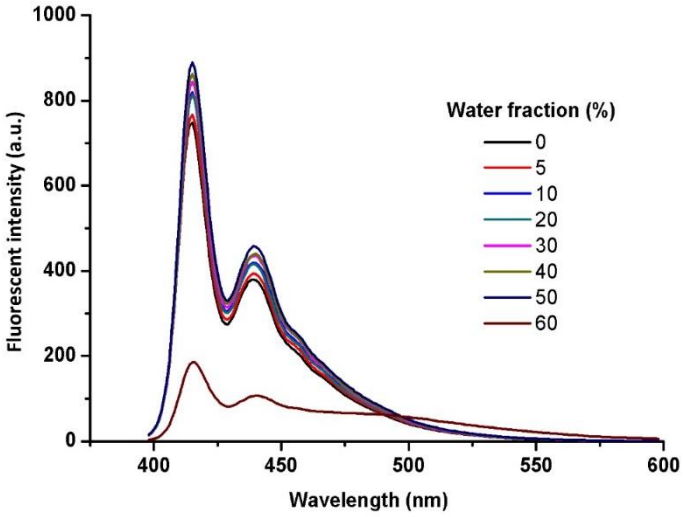

Figure 3.17 Fluorescent spectra of **T1** in THF with various water contents

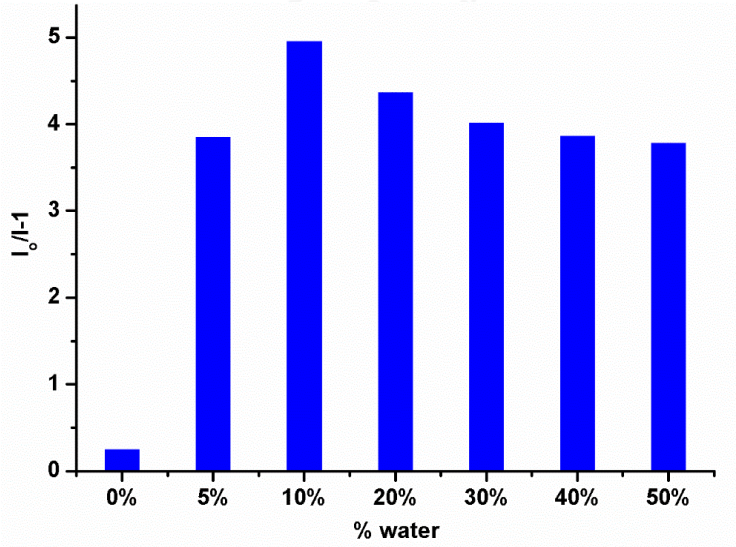

Figure 3.18 Effect of water content in THF on fluorescent quenching efficiency of **T1** (1 μM) by picric acid (0.1 mM)

3.2.4 pH effect depend on the ionization of PA in aqueous medium

In addition, the fluorescent quenching efficiencies of **T1** in THF with 10% buffer of various pHs were investigated. Data from **Figure 3.19** indicated that the sensitivity was independent to the pH of the medium. This suggested that this sensing system could be operated under a pH range of 4.4-12.4. Since the pKa of picric acid is around 0.4, the sensing mechanism in aqueous THF may involve the absorption of excitation light by picrate anion.

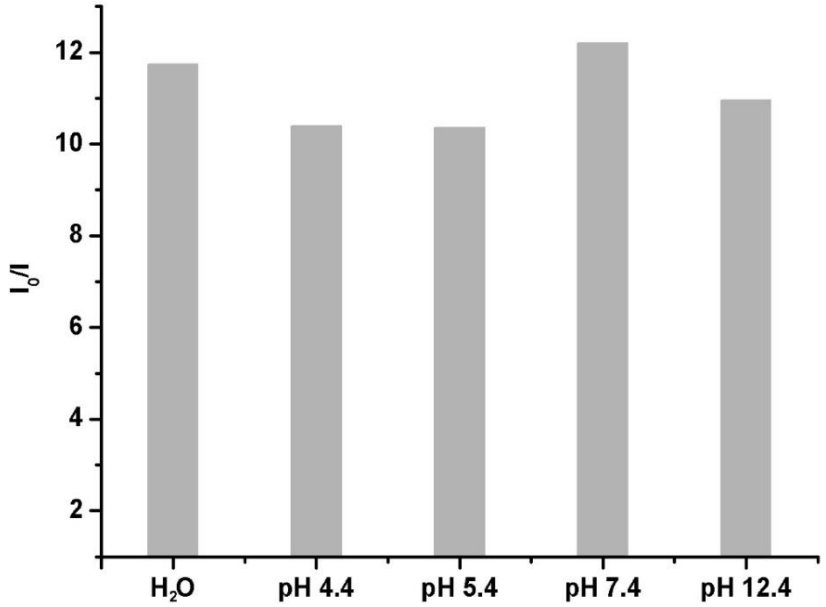

Figure 3.19 Fluorogenic responses of **T1** by picric acid in THF with 10% aqueous buffer of various pHs.

In order to access a quantitative measurement of the fluorescence quenching, Stern-Volmer plots were made from the fluorescence data. Thus, the fluorescence intensity of **T1** (1 μM) in $CHCl_3$ and in aqueous THF with varied concentrations of 2-NP and PA was performed, respectively **(Figure 3.20** and **Figure 3.21)**. A Stern-Volmer plot revealed a linear relationship between the fluorescence quenching ratio (I_0/I) and the concentration of 2-NP and PA in the range below 250 μM and 16 μM, respectively. From the plots in **Figure 3.22** and **Figure 3.23**, the Stern-Volmer constants of **T1** in $CHCl_3$ and in aqueous THF were 3.2×10^3 M^{-1} and 3.6×10^4 M^{-1}, respectively. The

limits of detection of 2-NP and PA at three-time noise were determined as 1.54 ppm and 0.15 ppm, respectively.

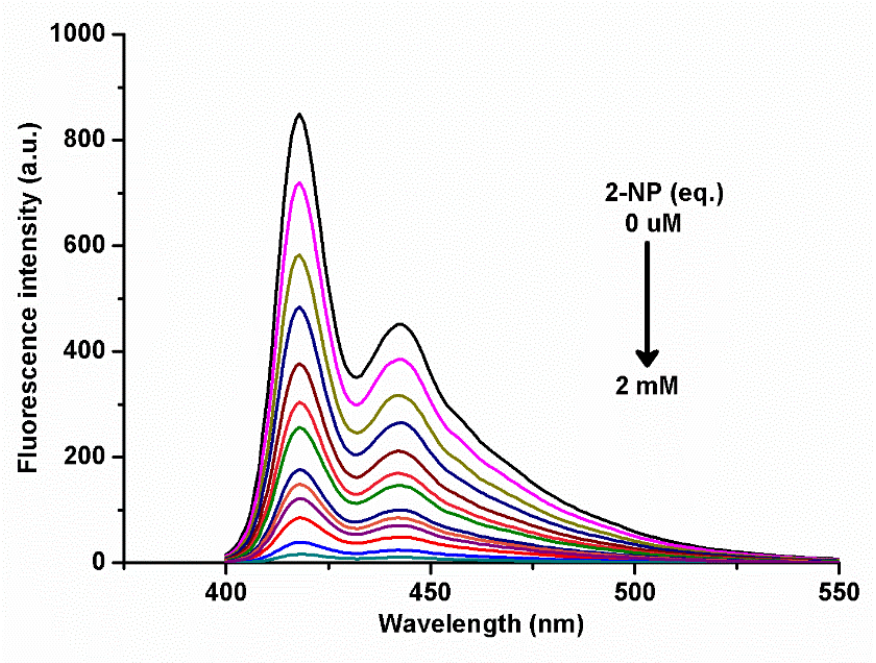

Figure 3.20 The fluorescence intensity of **T1** (1 μM) with 2-NP titration (0-2 mM) in $CHCl_3$

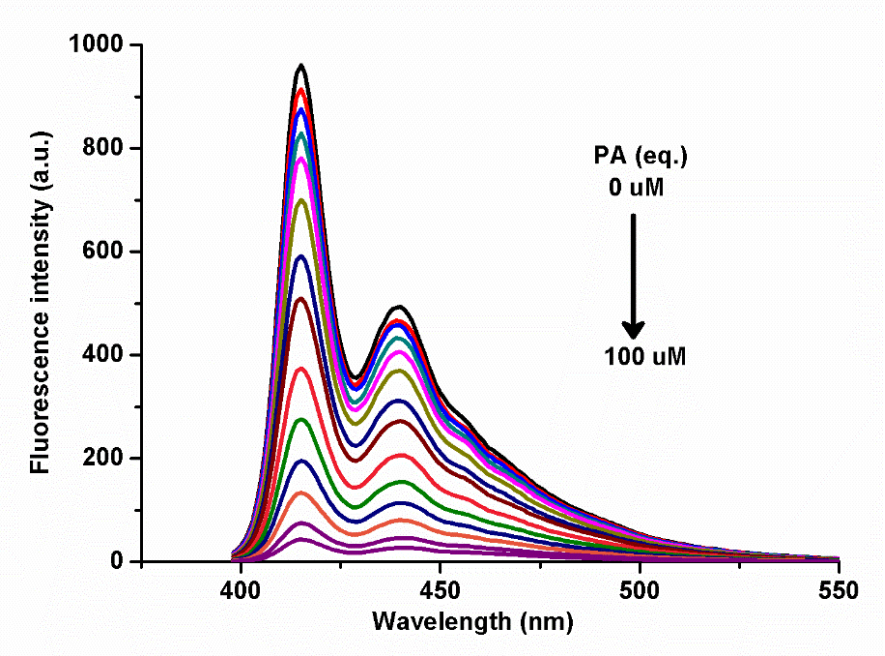

Figure 3.21 The fluorescence intensity of **T1** (1 μM) with PA titration (0-0.1 mM) in aqueous THF

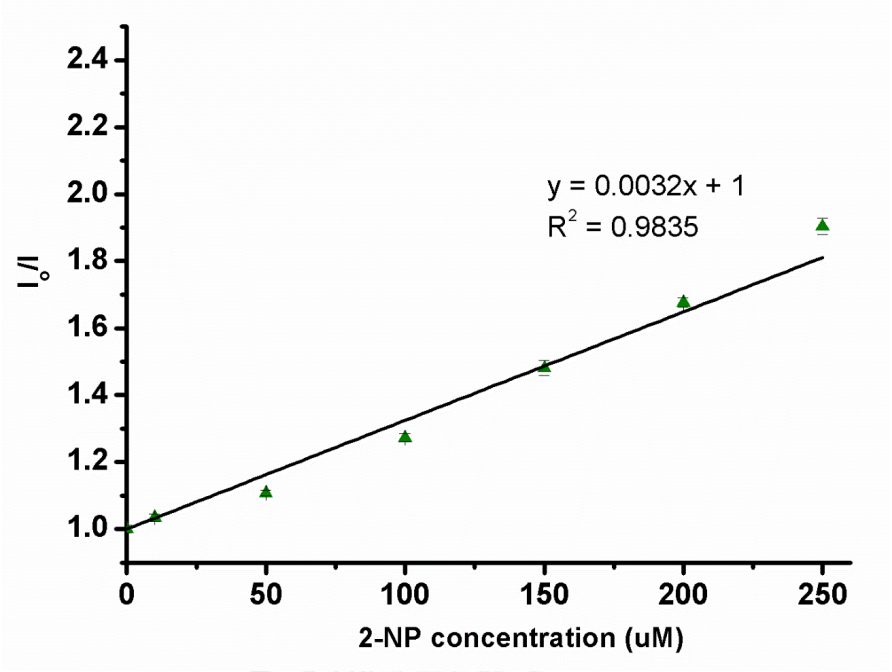

Figure 3.22 Stern-Volmer plot for fluorescence quenching of **T1** (1 μM) by 2-NP in $CHCl_3$

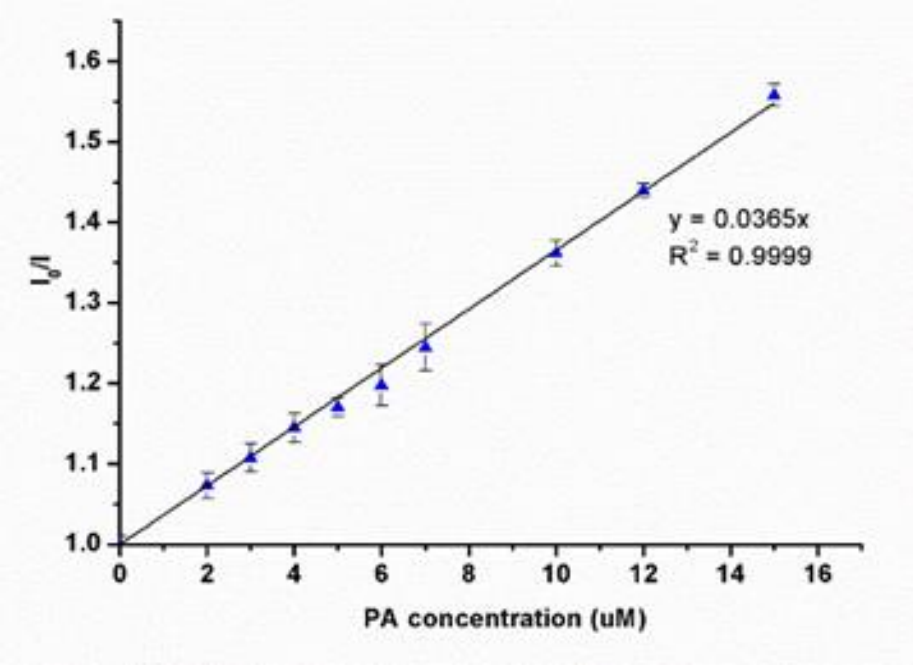

Figure 3.23 Stern-Volmer plot for fluorescence quenching of **T1** (1 μM) by PA in 10% H_2O in THF

3.2.5 Investigation of sensing mechanism

From the absorption spectra of **T1** and **2-NP** in $CHCl_3$ and absorption spectra of **T1** and PA in 10% H_2O in THF. As the result, both absorption spectra of 2-NP and PA overlap with absorption of **T1** might result from the inner filter effect (IFE) or the competitive absorption **Figure 3.24**.

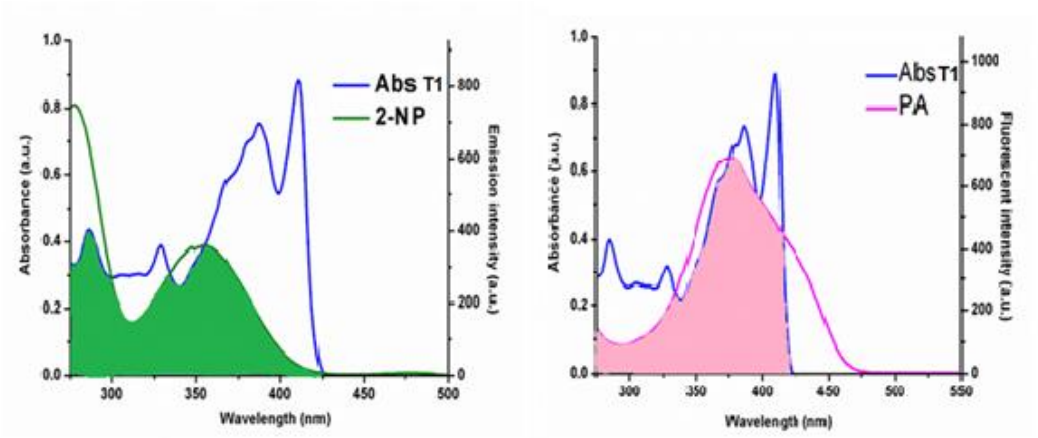

Figure 3.24 (left) Absorption spectra of **T1**, 2-nitrophenol in $CHCl_3$ (Right) Absorption spectra of **T1**, picric acid in 10% H_2O in THF

We thus performed an empirical analysis in order to determine whether the fluorescence quenching was caused solely by the IEE. Hence, we constructed a plot between the absorbance of **T1** ($A_{T1}/(A_{T1}+A_{NAC})$) [37] against the ratios of emission integals in the presence and absence of analytes **(Figure 3.25)**. The data indicated that the fluorescent response decreased when fraction of photons absorbed by **T1** was lowered, but the decreasing rates of these two parameters were unequal. Therefore, there should be other quenching mechanisms apart from the competitive absorption taking place in these systems, for instance, p-stacking and subsequent photo-induced energy transfer.

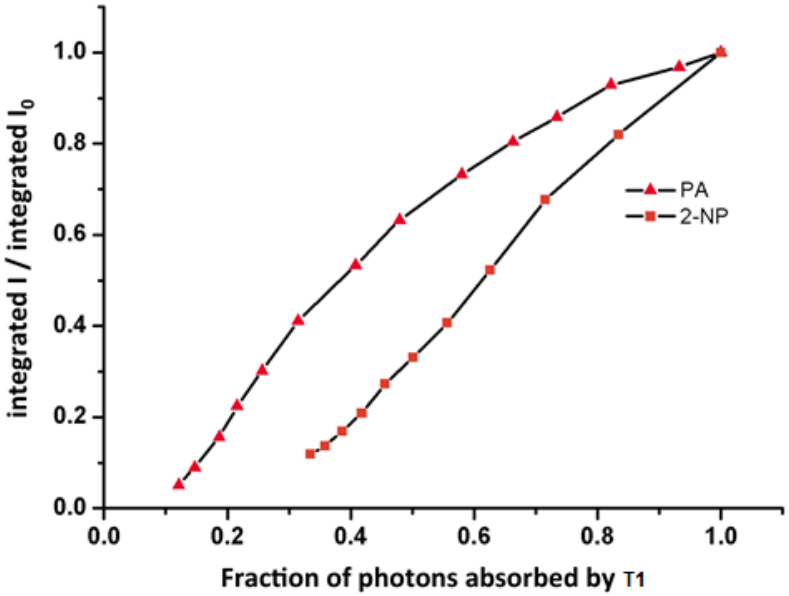

Figure 3.25 A plot between fraction of photons absorbed by T1 versus the quenching efficiencies calculated by the integrated emission intensities in the absence and presence of analytes

Moreover, the quenching mechanism of **T1** interacted with 2-NP and PA was further examined from the Stern-Volmer plots at different temperature (**Figure 3.26** and **Figure 3.27**). It was found that the quenching efficiency decreased as the temperature increased from 25 to 50°C. This suggested a static mode of quenching in which the pyrene units in the fluorophore may interact with electron-deficient analyst by means of π-stacking. This complex may dissociate upon increasing of the temperature, thus resulting in lower quenching efficiency.

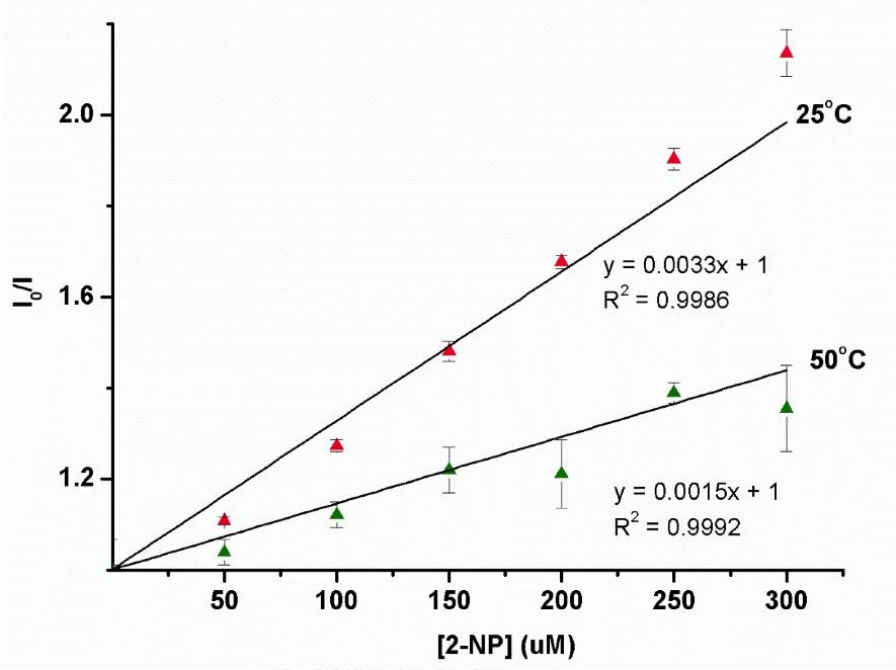

Figure 3.26 Stern-Volmer plots for the fluorescent responses of T1 towards 2-nitro phenol in $CHCl_3$ at 25 and 50 °C

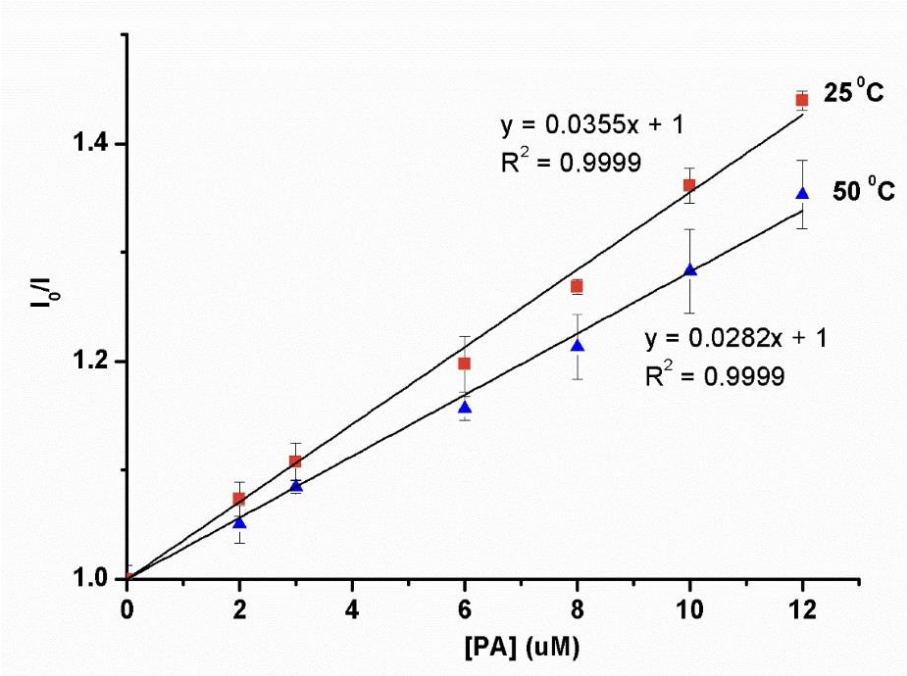

Figure 3.27 Stern-Volmer plots for the fluorescent responses of **T1** towards picric acid in 10% H_2O in THF at 25 and 50 °C.

3.3 Metal ion sensor

3.3.1 Photophysical properties of T2

Normalized absorption-emission spectra of **T2** were recorded in 30% THF-HEPES buffer (0.002 M, pH 7.4) as shown **Figure 3.28 and Table 3.2**. Compound **T2** exhibited characteristic absorption band of phenylacetylene-conjugated truxene at 375 nm with the molar extinction coefficient of 4.85 $M^{-1}cm^{-1}$. Upon excitation at the absorption maxima, **T2** showed emission peak at 474 nm in 30% THF-HEPES buffer (0.002 M, pH 7.4) with an outstanding quantum yield of 58%. This compound has a large stoke shift (99 nm) due to the rotation of the three dipicoyl peripheries resulting in non-radiative energy loss of the excited fluorophore.

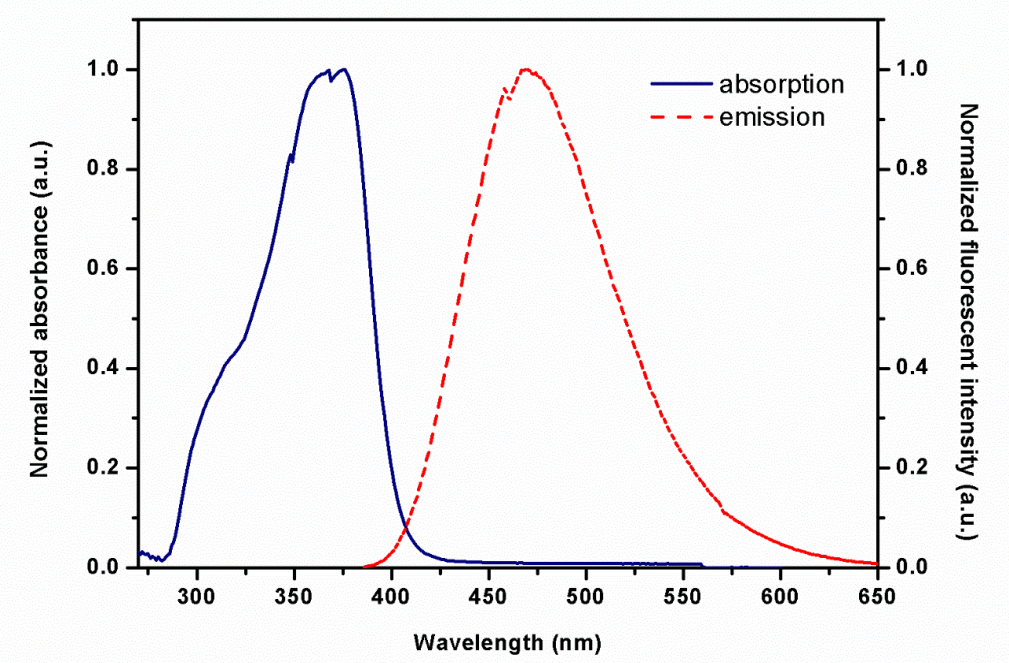

Figure 3.28 Normalized absorption and emission spectra of **T2** in 30% THF-HEPES buffer (0.002 M, pH 7.4).

Table 3.2 Photophysical property of **T2** in 30% THF-HEPES buffer (0.002 M, pH 7.4)

Compound	Absorption		Emission	
	λ_{max} (nm)	log ε (M^{-1} cm^{-1})	λ_{max} (nm)	Φ (%)
7 (core unit)	306, 317	4.23, 4.49	364, 378	0.47[a]
5 (periphery)	212	3.86	-	-
T2	375	4.85	474	58[b]

[a] 2-aminopyridine in 0.1 M H_2SO_4 (Φ = 60%) was used as the standard.

[b] Quinine sulfate in 0.1 M H_2SO_4 (Φ = 54%) was used as the standard.

3.3.2 Effect of water content on solubility of T2

Since the incorporation of three hydrophobic peripheries on one hydrophilic truxene core may decrease the overall polarity of **T2** molecule, the solubility and emission properties of this compound must be investigated. The water solubility was studied by varying the water content in THF from 10 to 90% **(Figure 3.29).** The results showed when the water contents were below 70%, the fluorescence intensities of **T2** remained relatively equal. When the water content was higher than 70 %, the fluorescence signal significantly dropped due to its poor solubility. Therefore, 70% of water in THF was chosen to be the solution media in further studies.

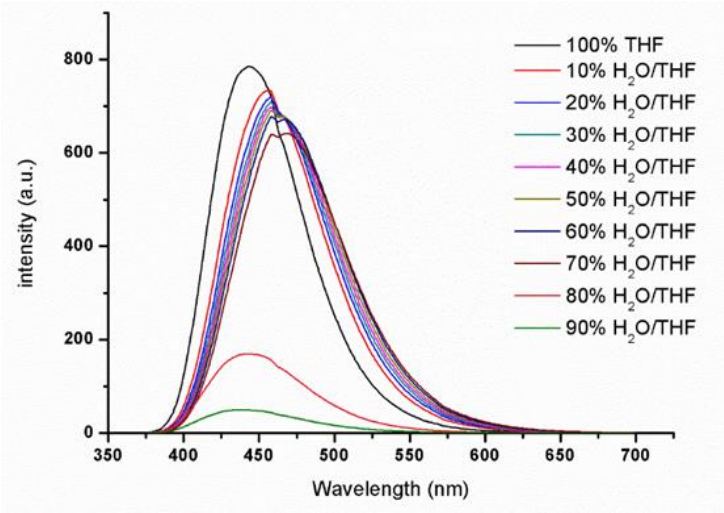

Figure 3.29 Fluorescence spectra of T2 (5 μM) in THF with various water content.

3.3.3 T2 as cation sensor

The sensing abilities of **T2** toward various metal ions (K^+, Na^+, Li^+, Ba^{2+}, Mg^{2+}, Ca^{2+}, Cu^{2+}, Ni^{2+}, Zn^{2+}, Al^{3+}, Hg^{2+}, Fe^{3+}, Co^{2+}, Cr^{3+}, Cd^{2+} and Pb^{2+}) were investigated in 30% THF-HEPES buffer (0.002M, pH 7.4) by UV-Vis and fluorescence spectrophotometry. Unlike other cations, the addition of copper (II) ion caused an absorption spectral shift from 375 nm to 336 nm **(Figure 3.30)**. This possibly resulted from a selective and stronger coordination between Cu^{2+} and dipicolylamine moiety.

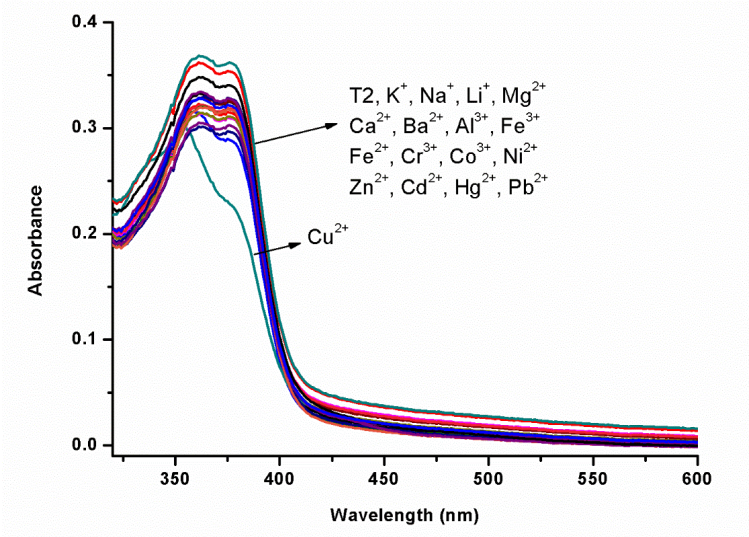

Figure 3.30 Absorbance spectra of **T2** (5 μM) in the presence of various metal ions (25 μM)

Based on the emission spectra **(Figure 3.31)**, it was clear that the fluorescence signal of **T2** (5 μM) in 30% THF-HEPES buffer (0.002 M, pH 7.4) could be selectively quenched by Cu^{2+} (25 μM). The fluorogenic responses of **T2** towards various metal ions along with the corresponding images of each solution mixture are shown in **Figure 3.32**.

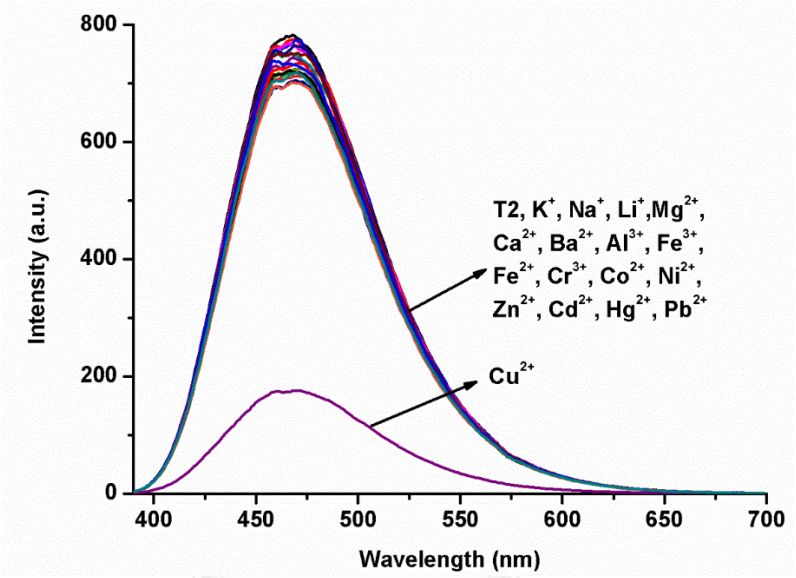

Figure 3.31 Fluorescence spectra of T2 (5 μM) in 30% THF-HEPES buffer (0.002 M, pH 7.4) with metal ions (5 eq)

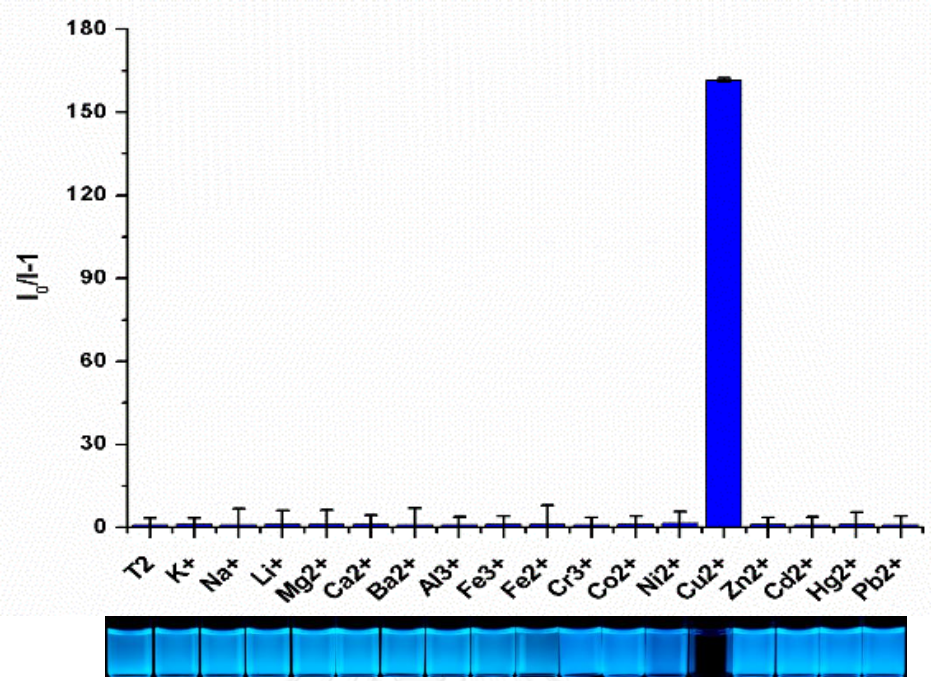

Figure 3.32 Fluorescence responses of **T2** (5 μM) upon the addition of various metal ions (25 μM) in 30% THF-HEPES buffer (0.002M, pH 7.4). Inset: photos of **T2** (5 μM) upon the addition of various metal ions (50 μM) in 30% THF-HEPES buffer (0.002M, pH 7.4).

3.3.4 Spectral titration of T2 by Cu^{2+} ion

The UV-vis and fluorescence titration experiments were carried out using solution of **T2** in 30% THF-HEPES buffer (0.002M, pH 7.4). From **Figure 3.33**, the addition of Cu^{2+} caused the UV-vis spectra shift from 377 nm to 336 nm with an isobestic point at 357 nm. When Cu^{2+} was added to 20 equivalents, the change in absorption spectra was nearly negligible. Results from the fluorescence titrations in **Figure 3.34** display gradual decrease in fluorescence intensity as the Cu^{2+} concentration increased and the signal was almost completely quenched by addition of Cu^{2+} up to 20 equivalents.

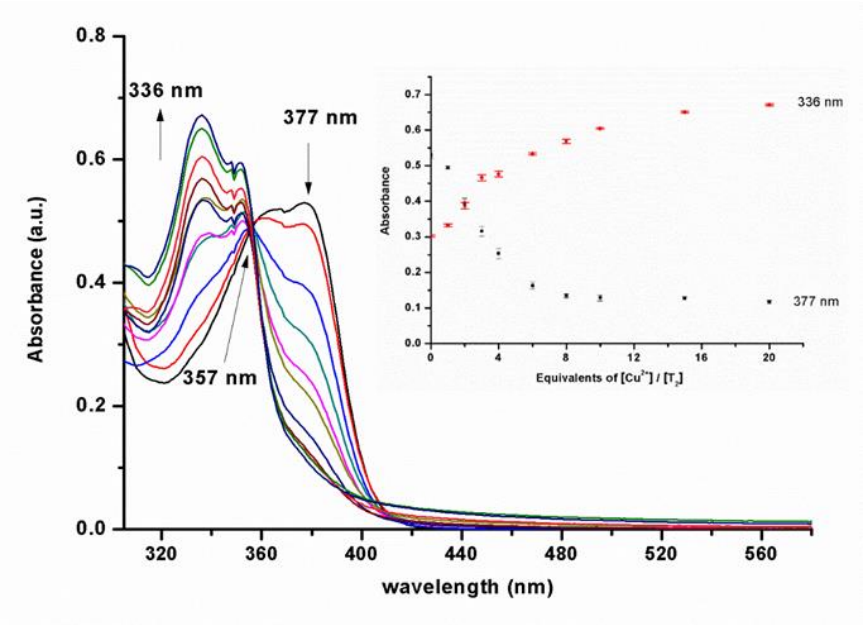

Figure 3.33 UV-vis absorption changes of **T2** (10 μM) upon gradual addition of Cu^{2+} in 30% THF-HEPES buffer (0.002M, pH 7.4)

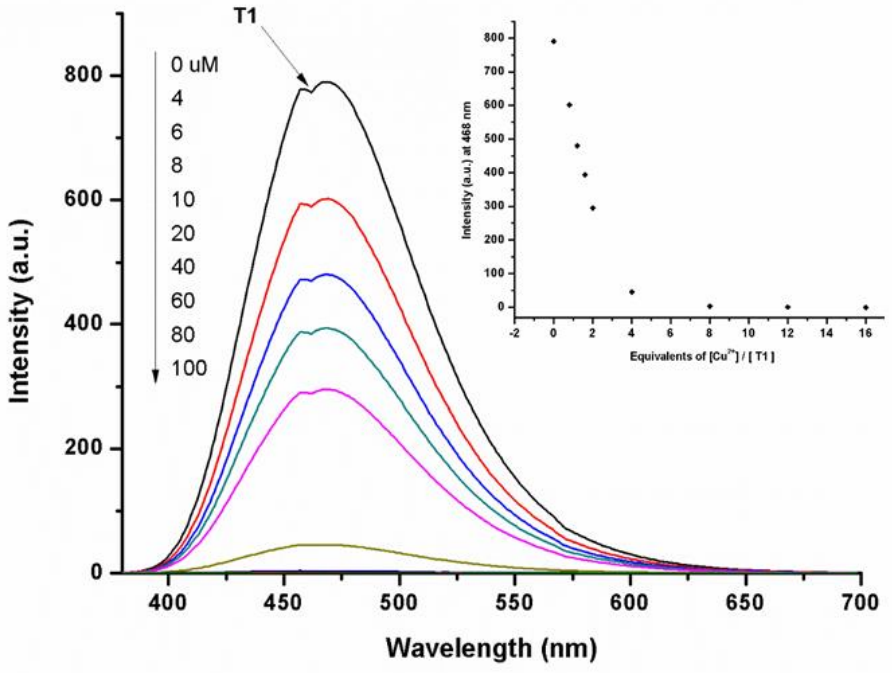

Figure 3.34 Fluorescence spectral changes during the titration of **T2** (5 μM) with Cu^{2+} in 30% THF-HEPES buffer (0.002M, pH 7.4)

3.3.5 Proposed sensing mechanism

In order to determine the binding stoichiometry between **T2** with Cu^{2+}, a Job's plot was established **(Figure. 3.35)**. The result suggested that the maximum quenching efficiency was observed at 0.5 molar fraction of Cu^{2+}, indicating that the stoichiometry of binding between **T2** and Cu^{2+} is 1:1. However, this information is contradicted to presence of three binding sites in **T2**. Therefore, it might be possible that the first binding between **T2** and Cu^{2+} is the only event that causes fluorescence quenching.

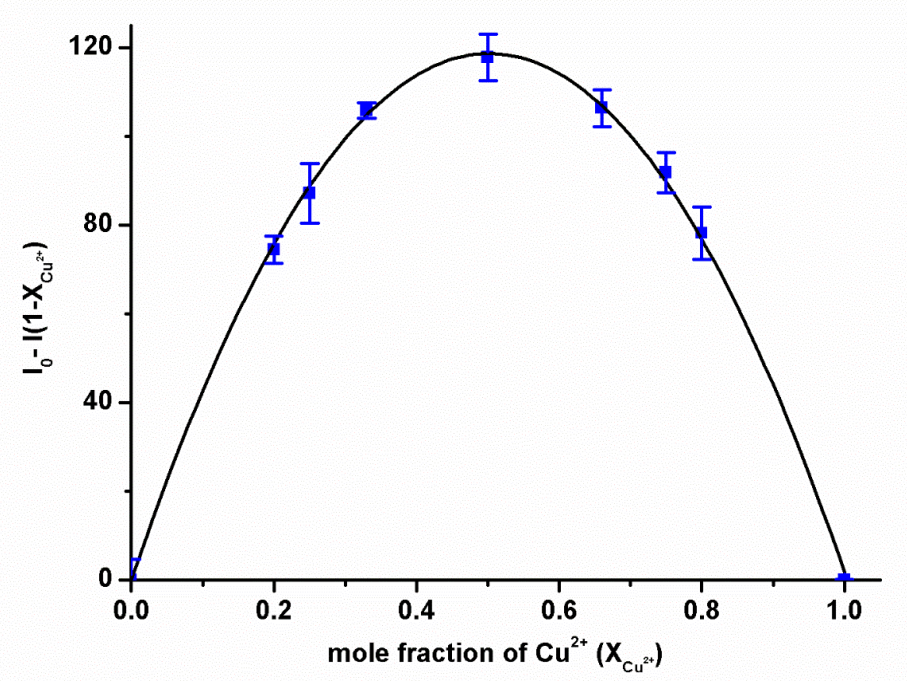

Figure 3.35 Job's plot of the complexation between **T2** and Cu^{2+} in 1:1 Stoichiometry with Cu^{2+}

In order to validate the stoichiometry of binding mentioned above, a mixture of **T2** (10 μM) and Cu^{2+} (100 μM) was subjected to MALDI-TOF analysis. A molecular ion with m/z of 1910.704 was detected (**Figure 3.36**). This corresponds to the molecular mass of **T2**+Cu^{2+} (1910.8265).

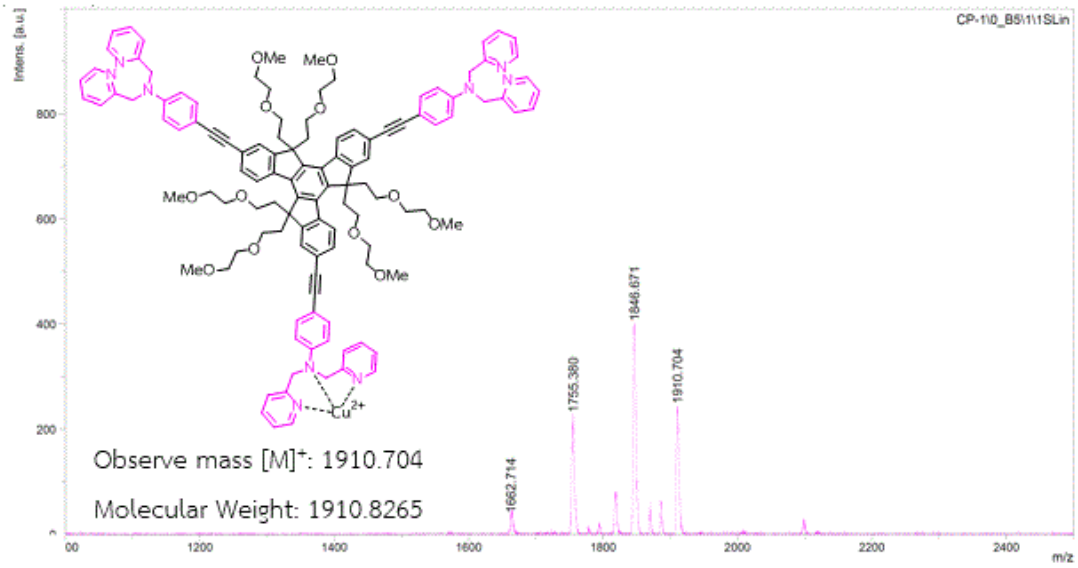

Figure 3.36 MALDI-TOF Mass spectrum of **T2**+Cu^{2+}

Furthermore, we investigated the optimal concentration of **T2** for the detection of Cu^{2+}. When the concentration of **T2** in 30% THF-HEPES buffer (0.002M, pH 7.4) was varied between 5 to 50 μM, the addition of Cu^{2+} at 5 equivalent led to different quenching efficiencies **(Figure 3.37)**. The highest sensitivity (I_0/I) was observed when the concentration of **T2** was at 10 μM or 20 μM. Higher concentration of T2 resulted in lower quenching efficiency because the sensor became less soluble. Thus, the concentration of **T2** at 10 μM was selected for further studies.

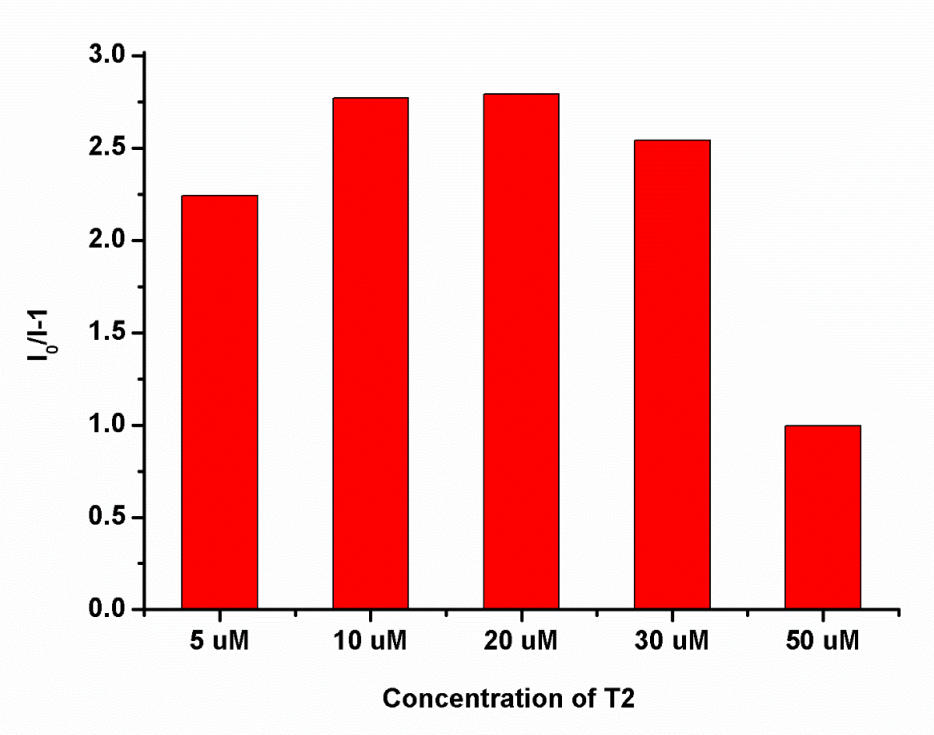

Figure 3.37 Quencing efficiencies of various concentration of **T2** with Cu^{2+} (5 eq) in 30% THF-HEPES buffer (0.002M, pH 7.4)

3.3.6 Detection limit of Cu^{2+} by T2

The increase of Cu^{2+} concentrations resulted in fluorescence quenching of **T2** as shown in **Figure 3.38**. The non-linearity of this plot suggested that the quenching mechanism involves several phenomena. At higher Cu^{2+} concentrations, higher quenching efficiencies were observed. Since the absorption maxima of aqueous Cu^{2+} solution appeared at 263 nm, it is less likely that the signal quenching was caused by competitive absorption by Cu^{2+}. Therefore, we postulate that the sudden increase in quenching efficiency was probably due to the high ionic strength of sample media forcing **T2** to aggregate via hydrophobic interaction.

The Stern-Volmer plot between (I_0/I) and the concentration of Cu^{2+} in the range below 7 μM showed a linear plot with a slope of 5.4×10^4 M^{-1} (K_{SV}) **(Figure 3.39)**. The limit of detection (LOD = 3σ/K) of Cu^{2+} at three-time-noise was determined as 0.06 ppm.

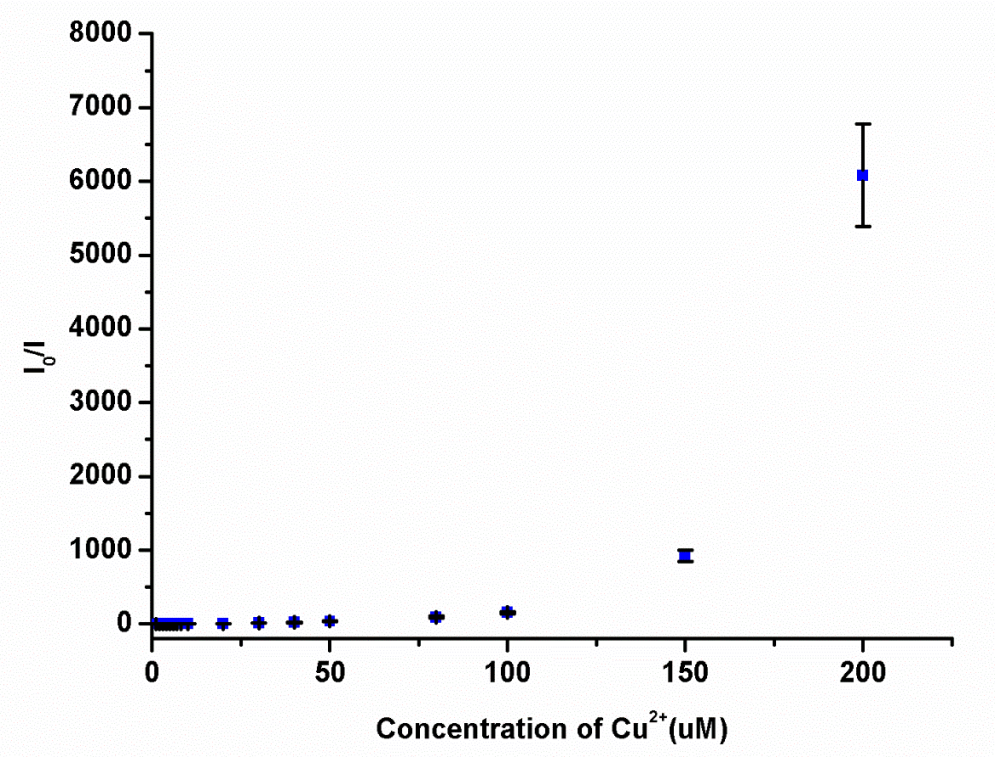

Figure 3.38 The Stern-Volmer plot for fluorescence quenching of **T2** with Cu^{2+} upon the addition of 200 μM of Cu^{2+}

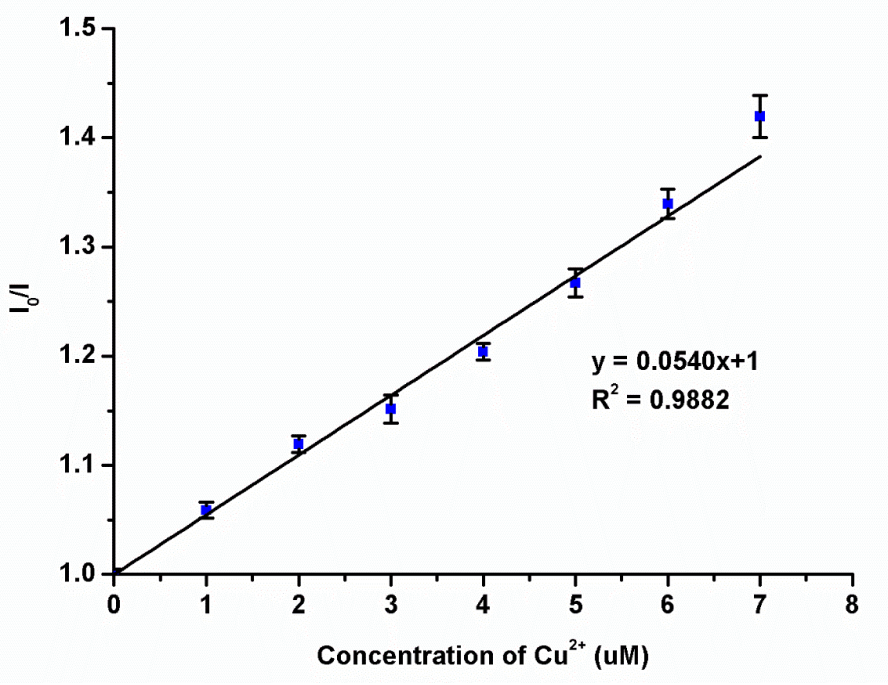

Figure 3.39 The Stern-Volmer plot at lower conc. (up to 7 μM.) of Cu^{2+}

3.3.7 Anion sensing ability of T2-Cu^{2+}

The selective fluorescence quenching of **T2** by Cu^{2+} led us to investigate the use of **T2**-Cu^{2+} mixture as an anion sensor. We thus added various anions such as HPO_4^{-}, ATP, ADP, AMP, ClO_4^{-}, SO_4^{2-}, NO_3^{-}, OAc^{-}, SO_3^{2-}, CN^{-}, CO_3^{2-}, Cl^{-}, F^{-}, I^{-} and Br^{-} to solution composed of **T2** (10 μM) and Cu^{2+} (100 μM) in 30% THF-HEPES buffer (0.002M, pH 7.4). Interestingly, both UV-vis absorption and fluorescence spectra (**Figure 3.40 to 3.41**) showed that the signal of **T2**-Cu^{2+} could be altered by HPO_4^{-} and other biological phosphate substances such as ATP, ADP and AMP. It appeared that HPO_4^{-} and the biological phosphates could bind with Cu^{2+} and release **T2** from the **T2**-Cu^{2+} complex.

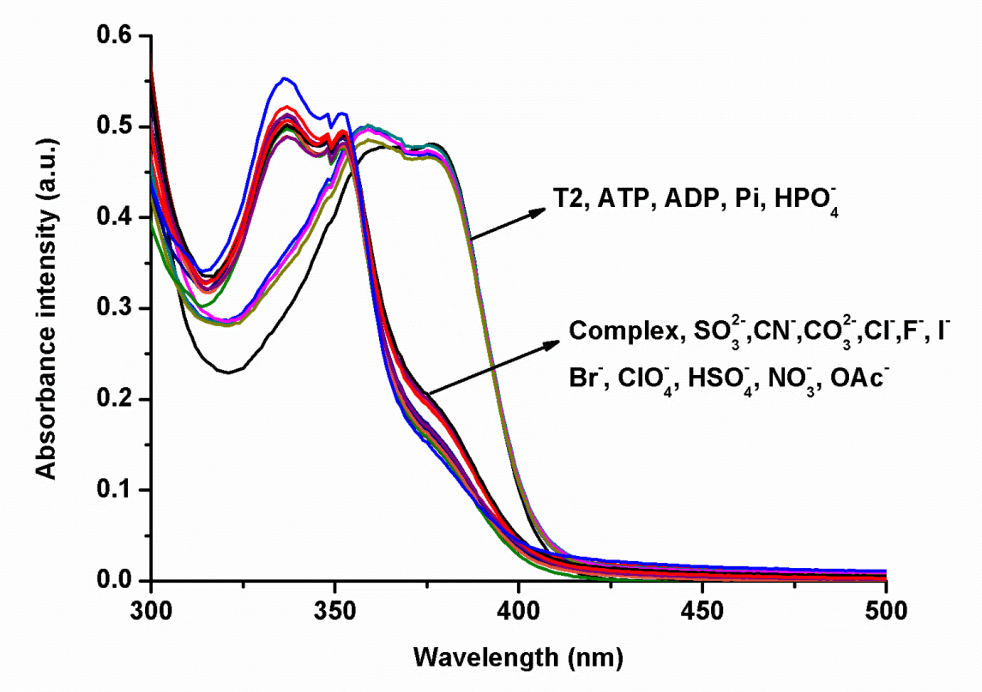

Figure 3.40 Absorbance spectra of complex (**T2-Cu^{2+}**) (10 μM) in the presence of various anions (100 μM, 10 eq.) in 30% THF-HEPES buffer (0.002M, pH 7.4)

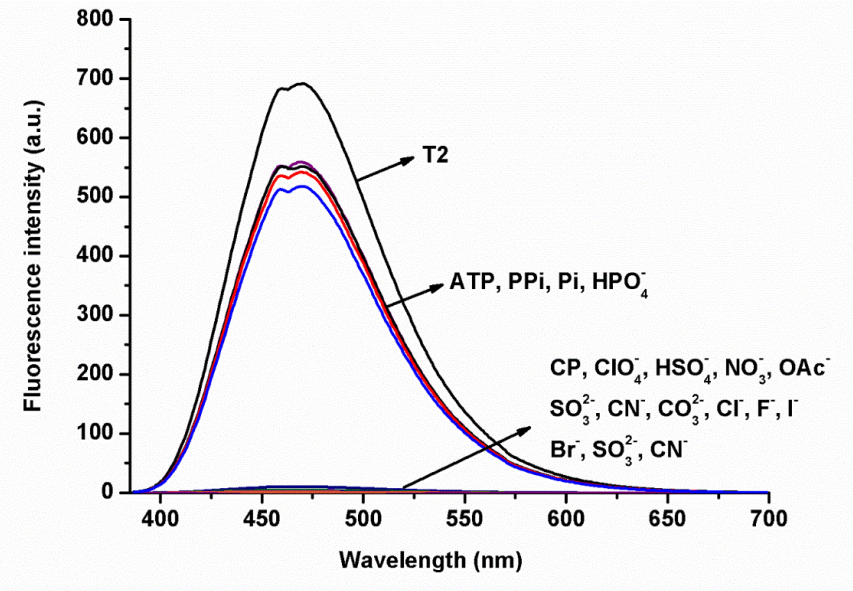

Figure 3.41 Fluorescence responses of complex (T2-Cu^{2+}) (10 μM) in the presence of various anions (100 μM, 10 eq.) in 30% THF-HEPES buffer (0.002M, pH 7.4)

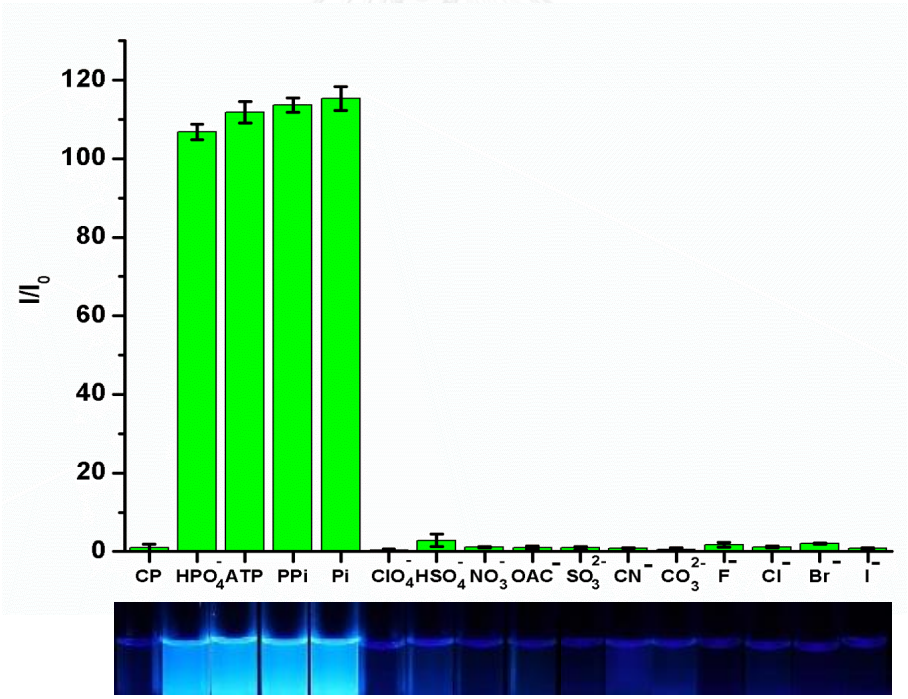

Figure 3.42 The bar represent the fluorescence enhancement ratio (I/I_0) of complex (T2-Cu^{2+}) (10 μM), after addition of each anions (100 μM, 10 eq.) in 30% THF-HEPES buffer (0.002M, pH 7.4). The photograph below shows the fluorescence appearance under black light of complex (T2-Cu^{2+}) (10 μM) upon addition of anions (100 μM, 10 eq.)

3.3.8 Studying the pH effect for sensing anions

Due to the amphoteric properties of HPO_4^-, we also decided to investigate the pH effect on sensitivity of T2- Cu^{2+} complex towards HPO_4^-. For this study, HEPES buffer at pH 6.6, 7.4 and 8.8 were prepared and used as sensing media along with THF. **Figure 3.43** reveals that the fluorescence intensity of **T2** was slightly lower in acidic pH due to partial protonation on the dipicolyl groups. Upon addition of Cu^{2+}, the intensity was lowered most at pH 6.6 and 7.4 while the signal was quenched by 2/3 at pH 8.8. This data indicates that some Cu^{2+} forms hydroxide salt under basic pH, leaving some free **T2** in the solution. When mixtures of **T2** and Cu^{2+} were added anions, it is obvious that only the HPO_4^- could enhance the fluorescence intensity at every pH. However, the maximum sensitivity of HPO_4^- sensing ($I_{T2+Cu+HPO4}$ / I_{T2+Cu}) could be observed at pH 7.4.

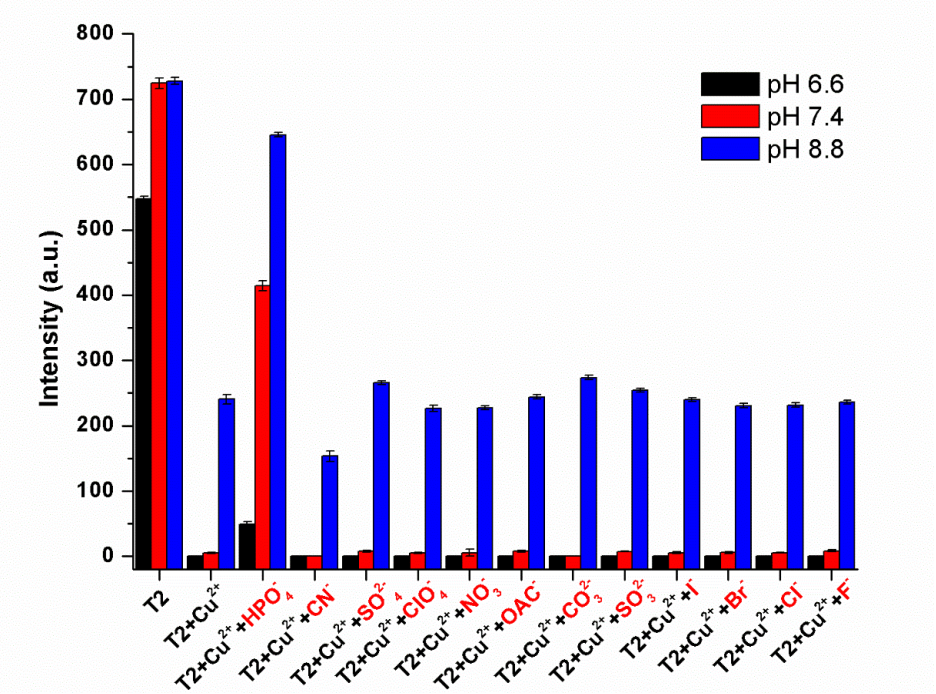

Figure 3.43 The fluorescence intensity of **T2** (5 μM) before and after the addition of Cu^{2+} (50 μM) and various anions (50 μM) in 30% THF-HEPES buffer at various pH

CHAPTER IV
CONCLUSION

Two fluorescence sensors containing truxene as signal transducer were successfully synthesized using Sonogashira coupling. The selectivities of these sensors depend on the interaction between peripheral groups and targeted analytes. For the nitroaromatic sensor, sensor **T1** was decorated by hydrophobic butyl groups on the truxene core and 1-ethynylpyrenes at the peripheries. The synthesis was accomplished in an overall yield of 14% from 4-step process. The compound exhibits the absorption and emission maxima at longer wavelengths than the parent pyrene due to the extended conjugated systems. In comparison with the parent truxene, the quantum efficiency of **T1** is also enhanced to 71 and 53% in $CHCl_3$ and aqueous THF, respectively. As a $CHCl_3$ solution, **T1** displayed a selective fluorescence turn off towards 2-nitrophenol with a detection limit of 1.54 ppm. In aqueous THF, on the other hands, its fluorescent signal was selectively quenched by picric acid with the detection limit of 0.15 ppm. An investigation on the fractions of photons absorbed by the fluorophore in the presence of analytes versus the quenching efficiencies suggested that the inner filter effect was responsible for the fluorescence quenching; however, several other mechanisms might also take place. The Stern–Volmer plots at different temperatures revealed that the signal turn-off involved a static quenching, presumably due to the π-π interaction between the **T1** and analytes.

As a metal ion sensor used in aqueous media, sensor **T2** comprises hydrophilic diglycol units on the truxene core and dipicolyl amine as binding sites for cation. The greater synthetic efficiency was witnessed as **T2** was produced in the overall yield of 42% after 4 steps. **T2** exhibits the absorption maxima at 375 nm and the emission maxima at 474 nm with an outstanding quantum efficiency of 58%. The sensor showed a selective fluorescence response to Cu^{2+} by exhibiting a blue-shift of absorption band from 375 to 336 nm and a quenching of emission signal. The fluorescent quenching possibly resulted from a selective and stronger coordination between Cu^{2+} and the dipicolylamine moiety. The Stern-Volmer constant (K_{sv}) was calculated to be 5.4×10^4

M^{-1} with the detection limit of 0.06 ppm. Interestingly, the **T2**-Cu^{2+} exhibited selective fluorescence enhancement in the presence of HPO_4^{-} and other biological phosphate substances such as adenosine triphosphate (ATP), adenosine diphosphate (ADP) and adenosine monophosphate (AMP). The increase of fluorescent signal of **T2**-Cu^{2+} was presumably due to the fact that HPO_4^{-} and the other biological phosphates could bind with Cu^{2+} and consequently led to the removal of Cu^{2+} from the complex.

REFERENCES

1. Bai, H., C. Li, and G. Shi, *Rapid nitroaromatic compounds sensing based on oligopyrene.* Sensors and Actuators, B: Chemical, 2008. **130**(2): p. 777-782.
2. Khayamian, T., M. Tabrizchi, and M.T. Jafari, *Analysis of 2,4,6-trinitrotoluene, pentaerythritol tetranitrate and cyclo-1,3,5-trimethylene-2,4,6-trinitramine using negative corona discharge ion mobility spectrometry.* Talanta, 2003. **59**(2): p. 327-333.
3. Ma, Y., S. Huang, and L. Wang, *Multifunctional inorganic-organic hybrid nanospheres for rapid and selective luminescence detection of TNT in mixed nitroaromatics via magnetic separation.* Talanta, 2013. **116**: p. 535-540.
4. Deng, X. and D. Wu, *Highly sensitive photoluminescence energy transfer detection for 2,4,6-trinitrophenol using photoluminescent carbon nanodots.* RSC Advances, 2014. **4**(79): p. 42066-42070.
5. Germain, M.E. and M.J. Knapp, *Optical explosives detection: from color changes to fluorescence turn-on.* Chemical Society Reviews, 2009. **38**(9): p. 2543-2555.
6. Ju, K.-S. and R.E. Parales, *Nitroaromatic Compounds, from Synthesis to Biodegradation.* Microbiology and Molecular Biology Reviews : MMBR, 2010. **74**(2): p. 250-272.
7. Toal, S.J. and W.C. Trogler, *Polymer sensors for nitroaromatic explosives detection.* Journal of Materials Chemistry, 2006. **16**(28): p. 2871-2883.
8. Wang, Y., et al., *Novel signal-amplifying fluorescent nanofibers for naked-eye-based ultrasensitive detection of buried explosives and explosive vapors.* Advanced Functional Materials, 2012. **22**(17): p. 3547-3555.
9. Du, H., et al., *Preparation of pyrene-functionalized fluorescent film with a benzene ring in spacer and sensitive detection to picric acid in aqueous phase.* Journal of Photochemistry and Photobiology A: Chemistry, 2011. **217**(2-3): p. 356-362.

10. Kumar, S., N. Venkatramaiah, and S. Patil, *Fluoranthene based derivatives for detection of trace explosive nitroaromatics.* Journal of Physical Chemistry C, 2013. **117**(14): p. 7236-7245.
11. Shanmugaraju, S., S.A. Joshi, and P.S. Mukherjee, *Fluorescence and visual sensing of nitroaromatic explosives using electron rich discrete fluorophores.* Journal of Materials Chemistry, 2011. **21**(25): p. 9130-9138.
12. Bhalla, V., et al., *Triphenylene derivatives: Chemosensors for sensitive detection of nitroaromatic explosives.* Dalton Transactions, 2013. **42**(4): p. 969-974.
13. Zhang, S., et al., *Fluorescent film sensors based on SAMs of pyrene derivatives for detecting nitroaromatics in aqueous solutions.* Spectrochimica Acta - Part A: Molecular and Biomolecular Spectroscopy, 2012. **97**: p. 31-37.
14. Singh, R., et al., *Heavy metals and living systems: An overview.* Indian Journal of Pharmacology, 2011. **43**(3): p. 246-253.
15. Hatai, J. and S. Bandyopadhyay, *Altered selectivity of a dipicolylamine based metal ion receptor.* Chemical Communications, 2013. **50**(1): p. 64-66.
16. Luo, H.Y., et al., *Synthesis of dipicolylamino substituted quinazoline as chemosensor for cobalt(II) recognition based on excited-state intramolecular proton transfer.* Spectrochimica Acta - Part A: Molecular and Biomolecular Spectroscopy, 2008. **70**(2): p. 337-342.
17. O'Neil, E.J. and B.D. Smith, *Anion recognition using dimetallic coordination complexes.* Coordination Chemistry Reviews, 2006. **250**(23-24): p. 3068-3080.
18. Zhang, J.F., et al., *Pyrophosphate-Selective Fluorescent Chemosensor Based on 1,8-Naphthalimide–DPA–Zn(II) Complex and Its Application for Cell Imaging.* Organic Letters, 2011. **13**(19): p. 5294-5297.
19. Lakowicz, J.R., *Principles of Fluorescence Spectroscopy. (3rd ed.) New York: Springer Science & Business Media*. 2006.
20. Hong, Y., J.W.Y. Lam, and B.Z. Tang, *Aggregation-induced emission: Phenomenon, mechanism and applications.* Chemical Communications, 2009(29): p. 4332-4353.

21. Diring, S., et al., *Star-shaped multichromophoric arrays from bodipy dyes grafted on truxene core.* Journal of the American Chemical Society, 2009. **131**(17): p. 6108-6110.

22. Kao, M.T., et al., *Facile synthesis of 5,10,15-hexaaryl truxenes: Structure and properties.* Organic Letters, 2011. **13**(7): p. 1714-1717.

23. Montgomery, N.A., et al., *Dynamics of fluorescence depolarisation in star-shaped oligofluorene- truxene molecules.* Physical Chemistry Chemical Physics, 2012. **14**(25): p. 9176-9184.

24. Wang, J., et al., *Truxene-cored **π**-expanded triarylborane dyes as single- and two-photon fluorescent probes for fluoride.* Analyst, 2014. **139**(6): p. 1541-1549.

25. Yuan, M.S., et al., *Symmetrical and asymmetrical (multi)branched truxene compounds: Structure and photophysical properties.* Dyes and Pigments, 2012. **95**(2): p. 236-243.

26. Yuan, S.C., et al., *Star-shaped oligo(fluorene ethynylene)-functionalized truxene derivatives: synthesis, characterization, and their size effects.* Tetrahedron, 2009. **65**(21): p. 4165-4172.

27. Yang, Z., et al., *Solution-processable and thermal-stable triphenylamine-based dendrimers with truxene cores as hole-transporting materials for organic light-emitting devices.* Organic Electronics, 2009. **10**(5): p. 954-959.

28. Earmrattana, N., M. Sukwattanasinitt, and P. Rashatasakhon, *Water-soluble anionic fluorophores from truxene.* Dyes and Pigments, 2012. **93**(1-3): p. 1428-1433.

29. Lee, Y.H., et al., *Dipyrenylcalix[4]arene-A fluorescence-based chemosensor for trinitroaromatic explosives.* Chemistry - A European Journal, 2010. **16**(20): p. 5895-5901.

30. Bhalla, V., A. Gupta, and M. Kumar, *Fluorescent nanoaggregates of pentacenequinone derivative for selective sensing of picric acid in aqueous media.* Organic Letters, 2012. **14**(12): p. 3112-3115.

31. Park, K., et al., *Calix[2]pyreno[2]pyrrole as a fluorescence chemical probe for polynitroaromatics.* Bulletin of the Korean Chemical Society, 2012. **33**(2): p. 675-677.

32. Niamnont, N., et al., *Tunable star-shaped triphenylamine fluorophores for fluorescence quenching detection and identification of nitro-aromatic explosives.* Chemical Communications, 2013. **49**(8): p. 780-782.

33. Yuan, M.-S., et al., *Symmetrical and asymmetrical (multi)branched truxene compounds: Structure and photophysical properties.* Dyes and Pigments, 2012. **95**(2): p. 236-243.

34. Kang, Y., et al., *Blue luminescent rigid molecular rods bearing N-7-azaindolyl and 2,2′-dipyridylamino and their Zn(II) and Ag(I) complexes.* Inorganic Chemistry, 2003. **42**(8): p. 2789-2797.

35. Thorand, S. and N. Krause, *Improved procedures for the palladium-catalyzed coupling of terminal alkynes with aryl bromides (Sonogashira coupling).* Journal of Organic Chemistry, 1998. **63**(23): p. 8551-8553.

36. Fery-Forgues, S. and D. Lavabre, *Are fluorescence quantum yields so tricky to measure? A demonstration using familiar stationery products.* Journal of Chemical Education, 1999. **76**(9): p. 1260-1264.

37. *The number of absorbed photons was calculated from the concentration and molar absorptivity at excitation wavelength of T1. The fraction of photons absorbed byT1 was calculated based on the total number of photons absorbed by T1 and each analyte.*

APPENDIX

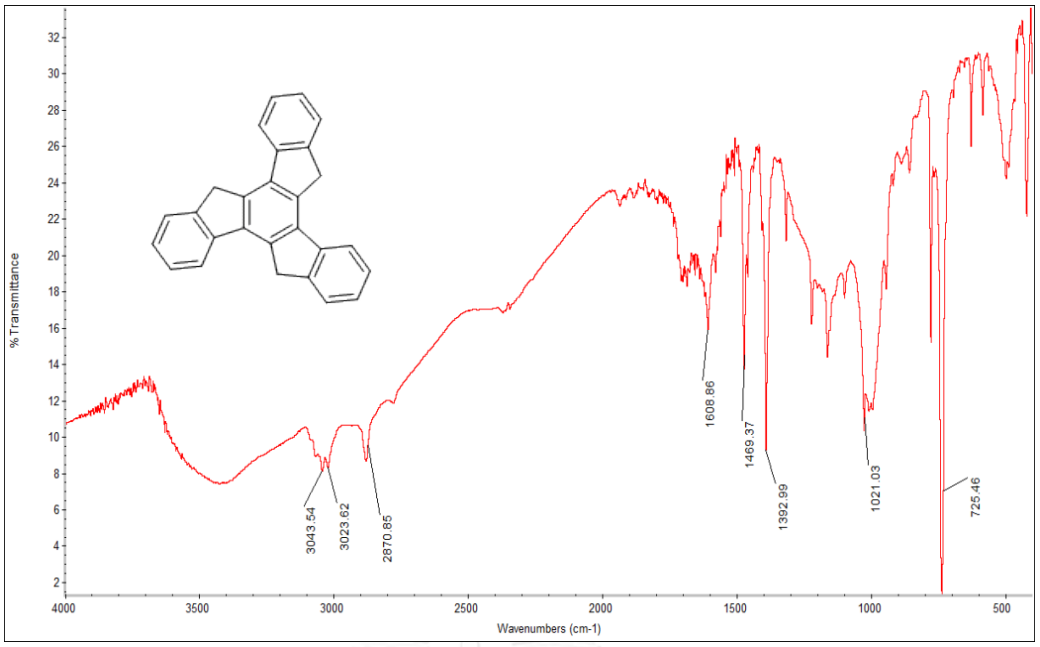

Figure A.1 IR spectrum of **Truxene**

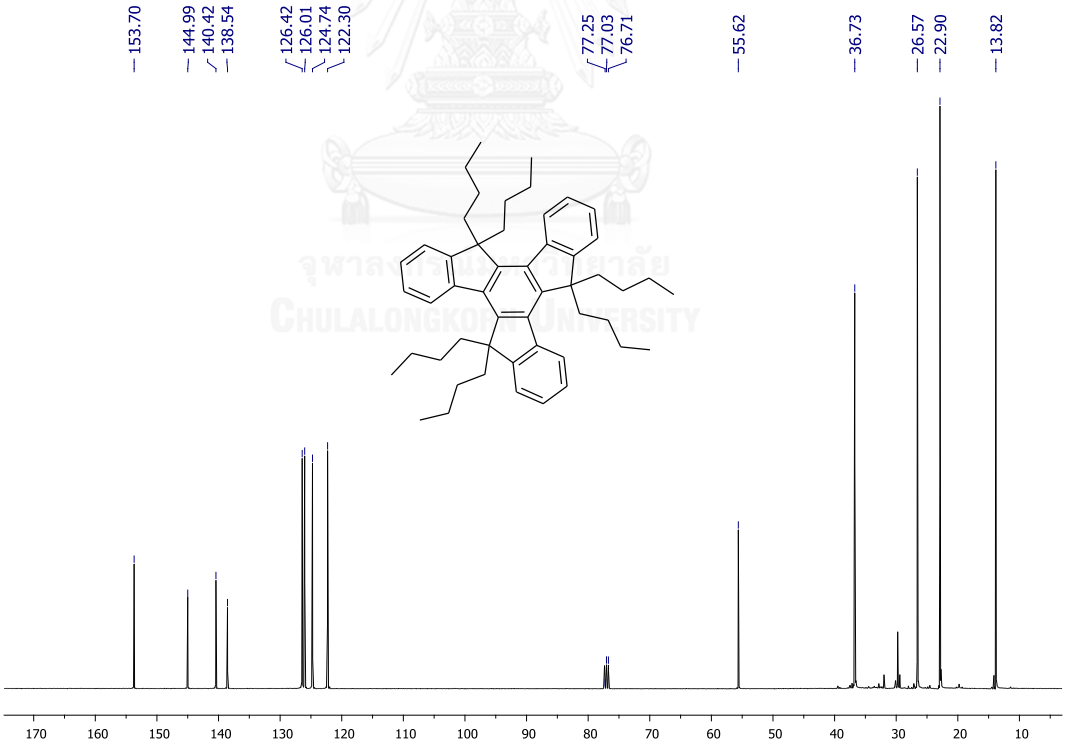

Figure A.2 ^{13}C NMR spectrum of **1** (400 MHz, in $CDCl_3$)

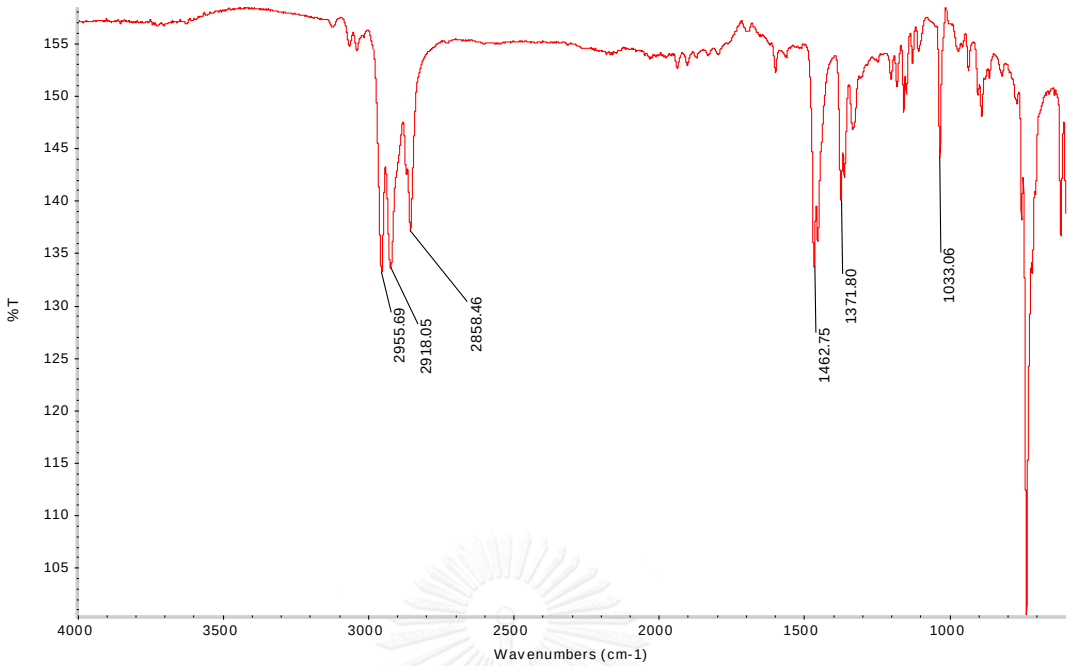

Figure A.3 IR spectrum of **1**

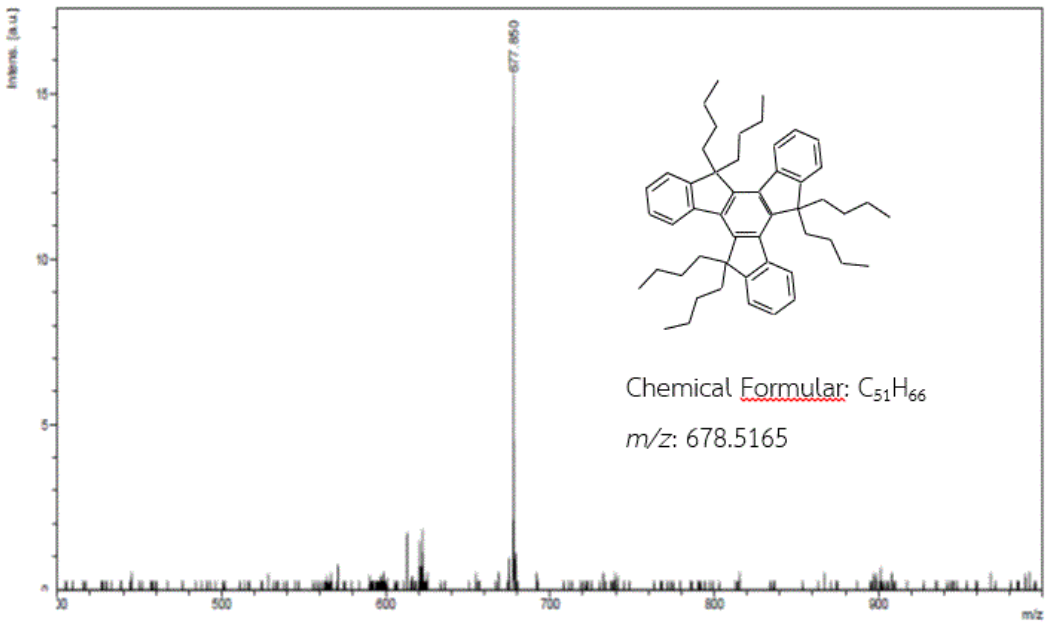

Figure A.4 MALDI-TOF Mass spectrum of **1**

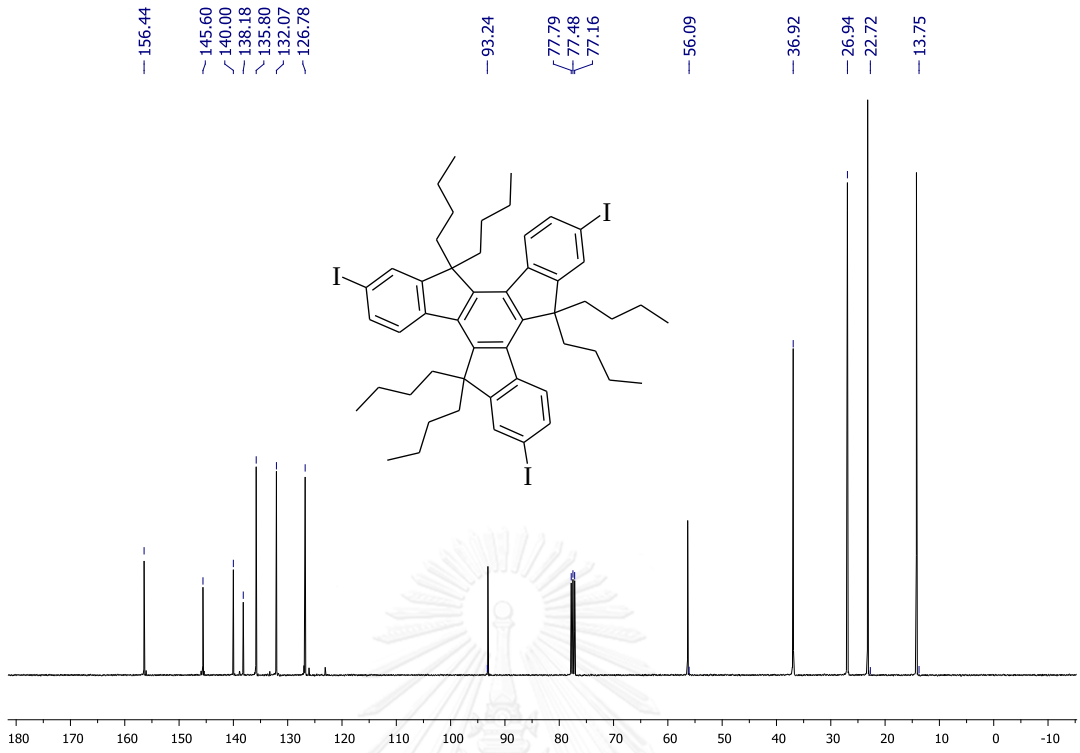

Figure A.5 ^{13}C NMR spectrum of **2** (400 MHz, in $CDCl_3$)

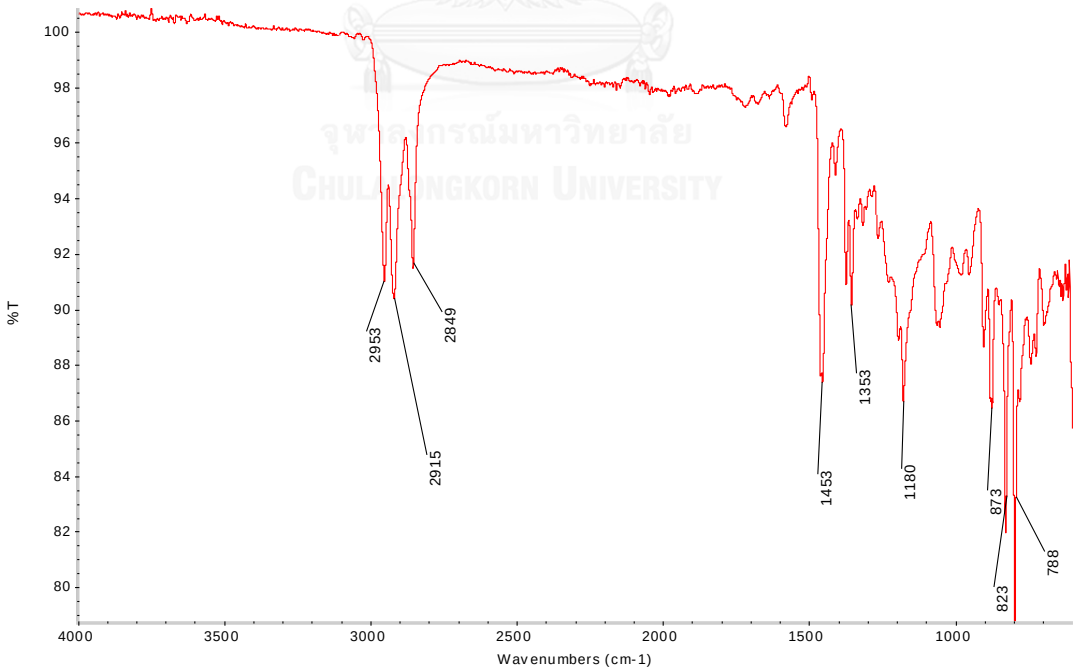

Figure A.6 IR spectrum of **2**

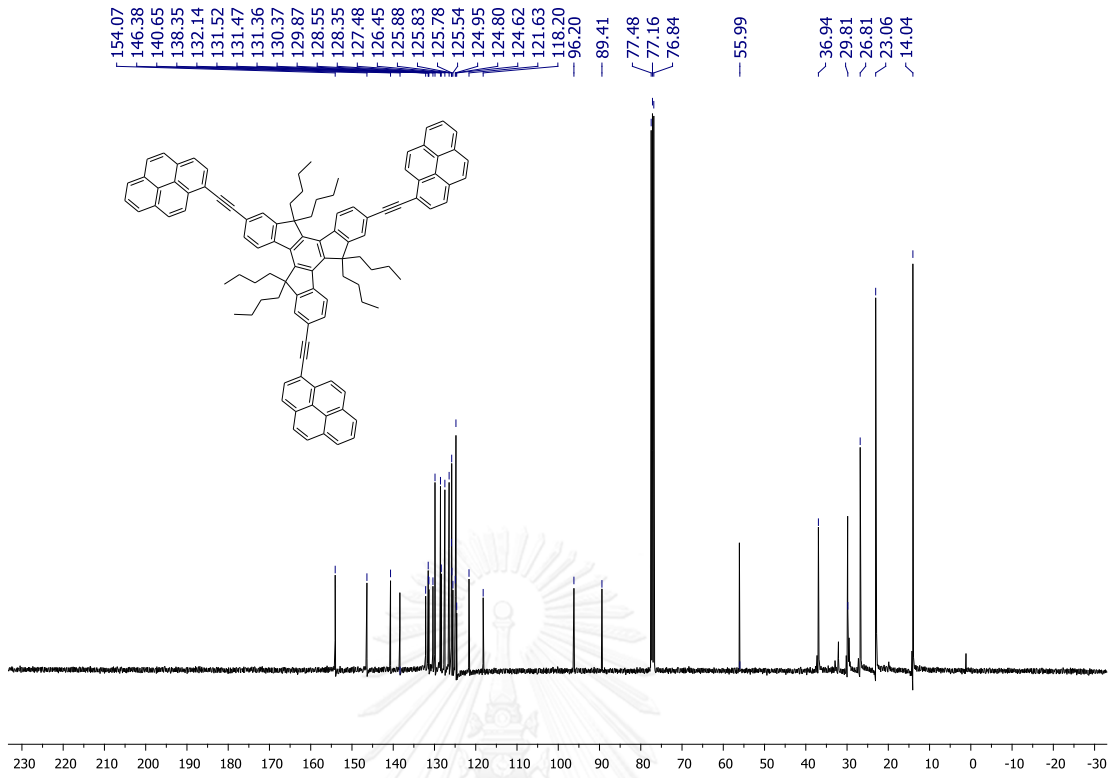

Figure A.7 ^{13}C NMR spectrum of **T1** (400 MHz, in $CDCl_3$)

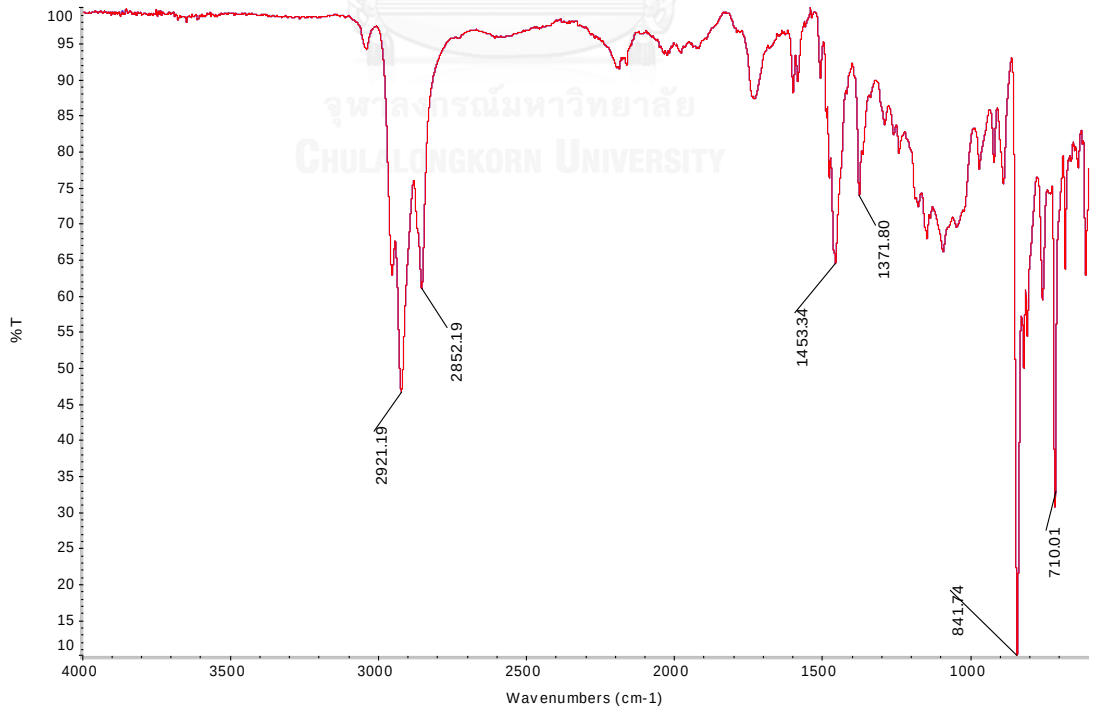

Figure A.8 IR spectrum of **T1**

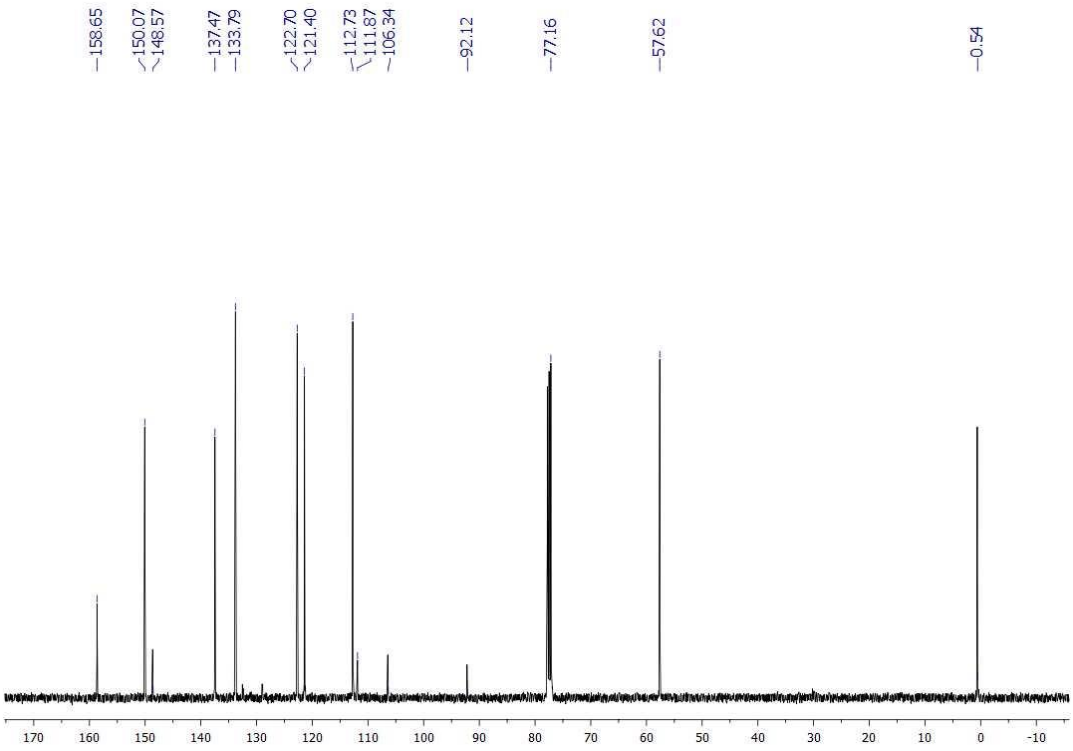

Figure A.9 ^{13}C NMR spectrum of **4** (400 MHz, in $CDCl_3$

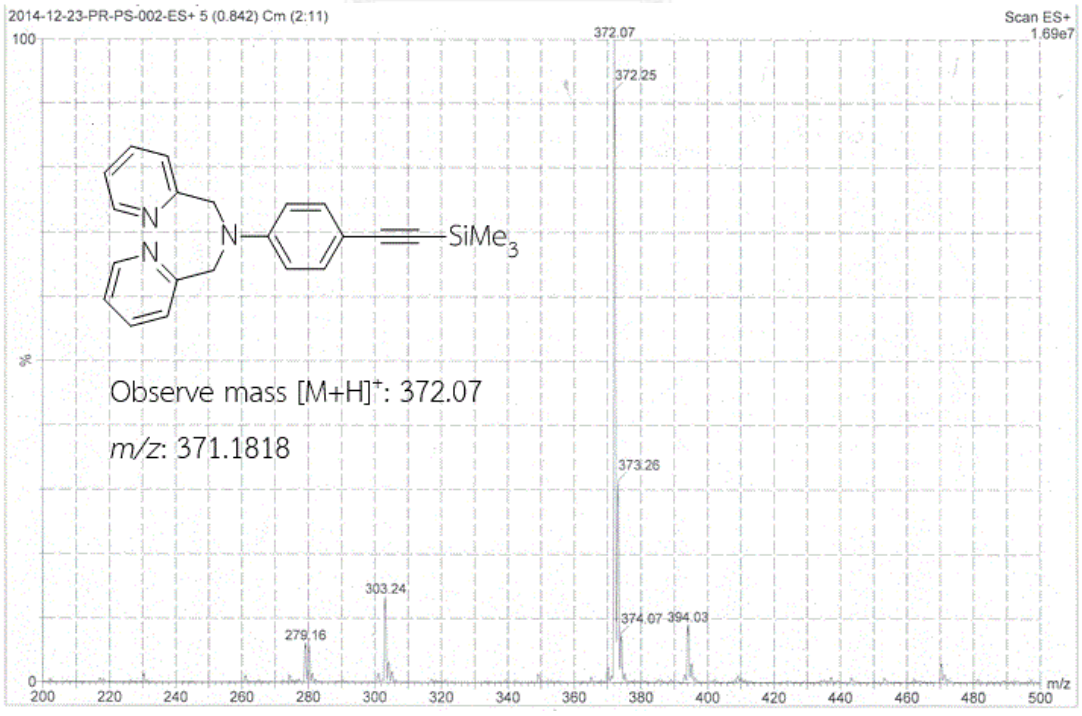

Figure A.10 LR-MS Mass spectrum of **4**

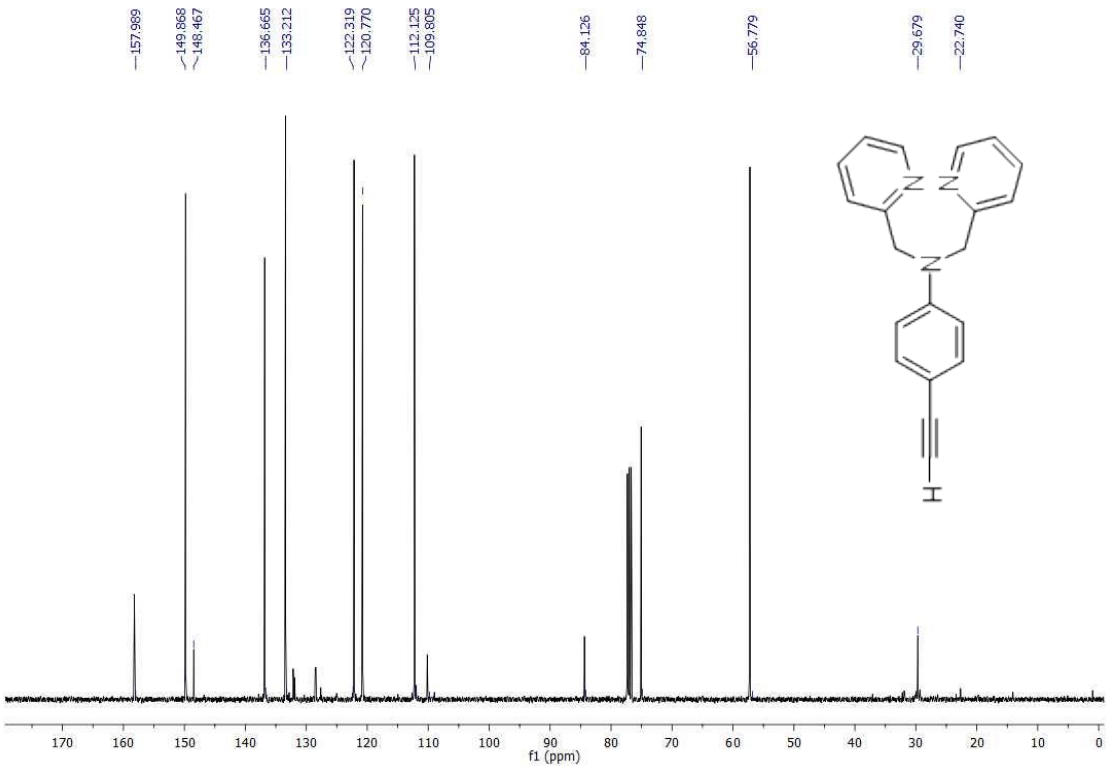

Figure A.11 ^{13}C NMR spectrum of **5** (400 MHz, in $CDCl_3$)

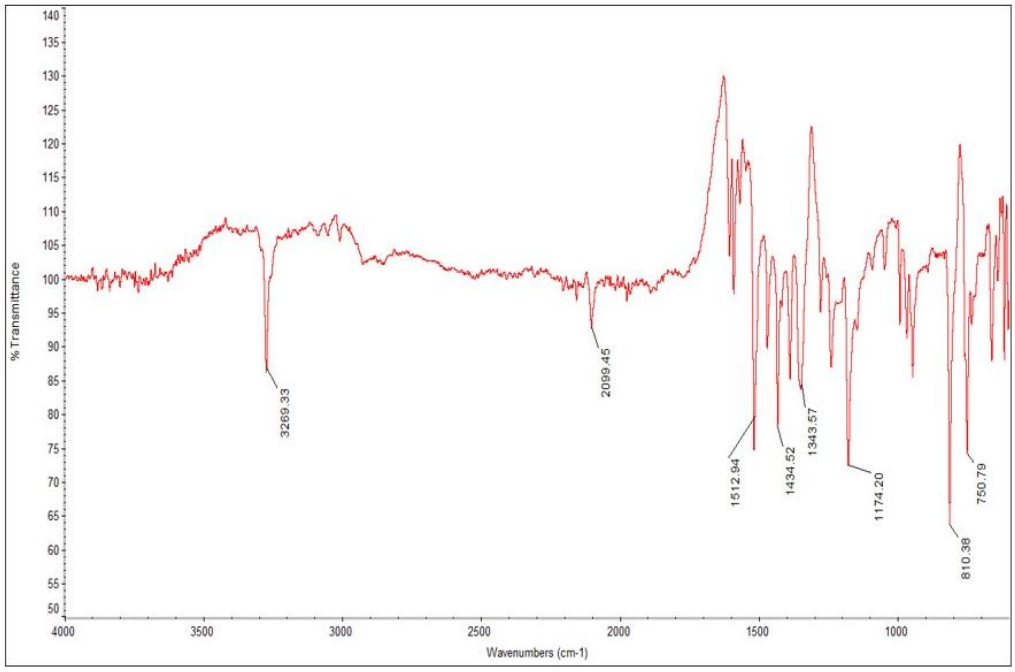

Figure A.12 IR spectrum of **5**

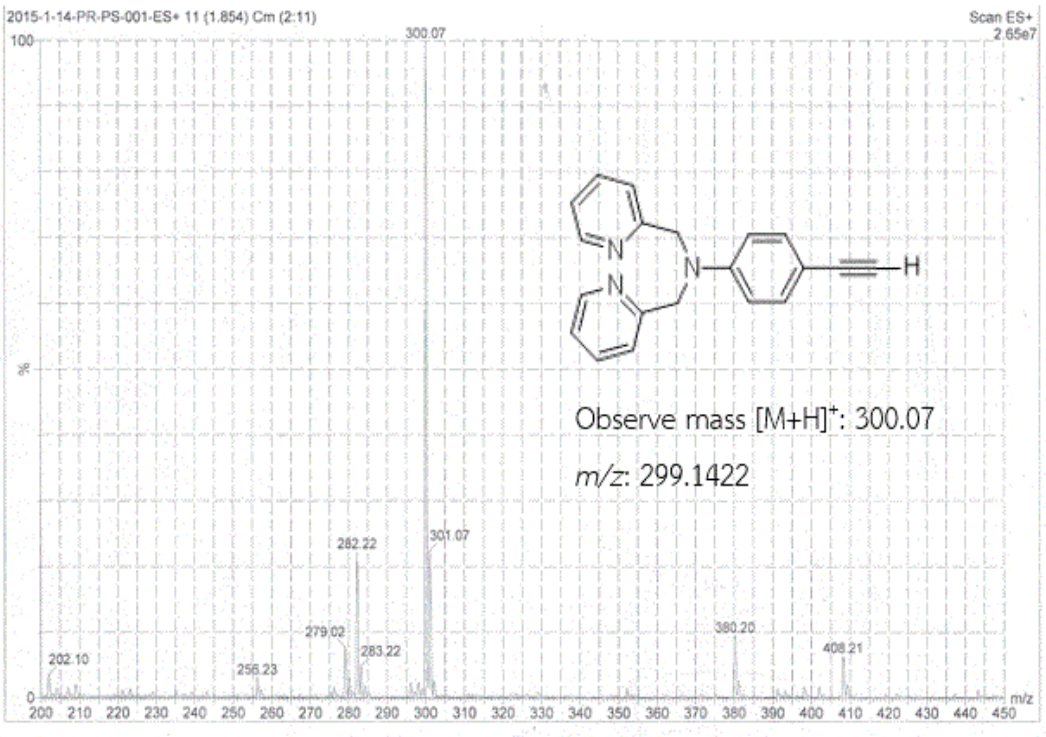

Figure A.13 LR-MS Mass spectrum of **5**

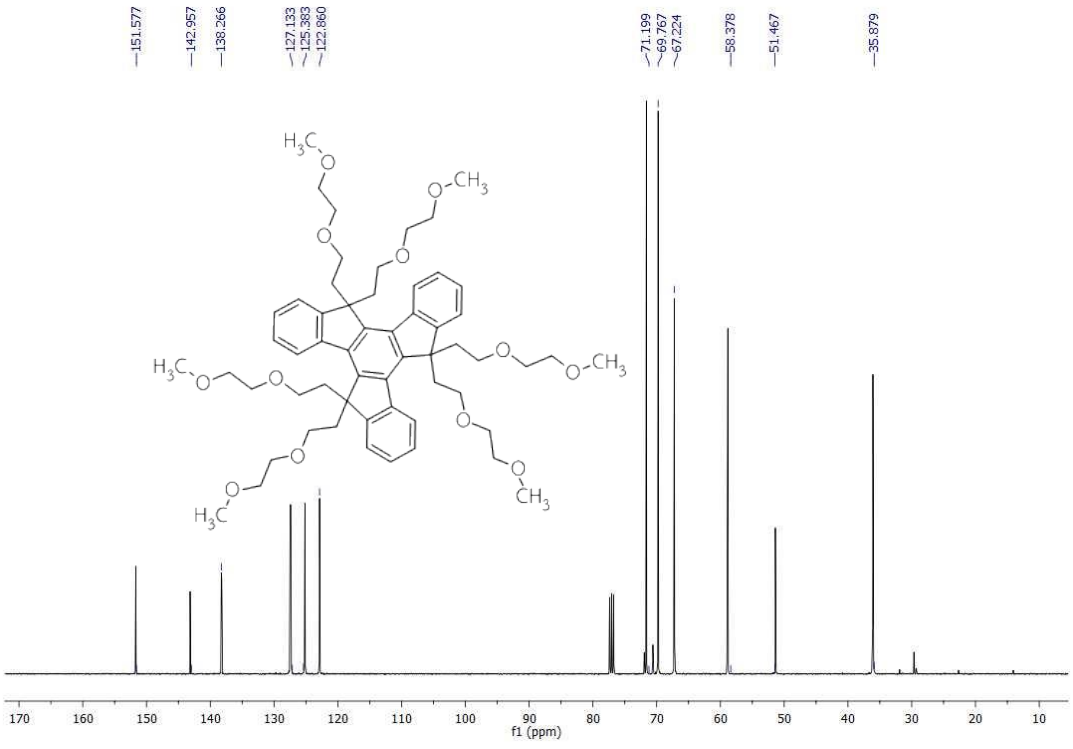

Figure A.14 ^{13}C NMR spectrum of **6** (400 MHz, in $CDCl_3$)

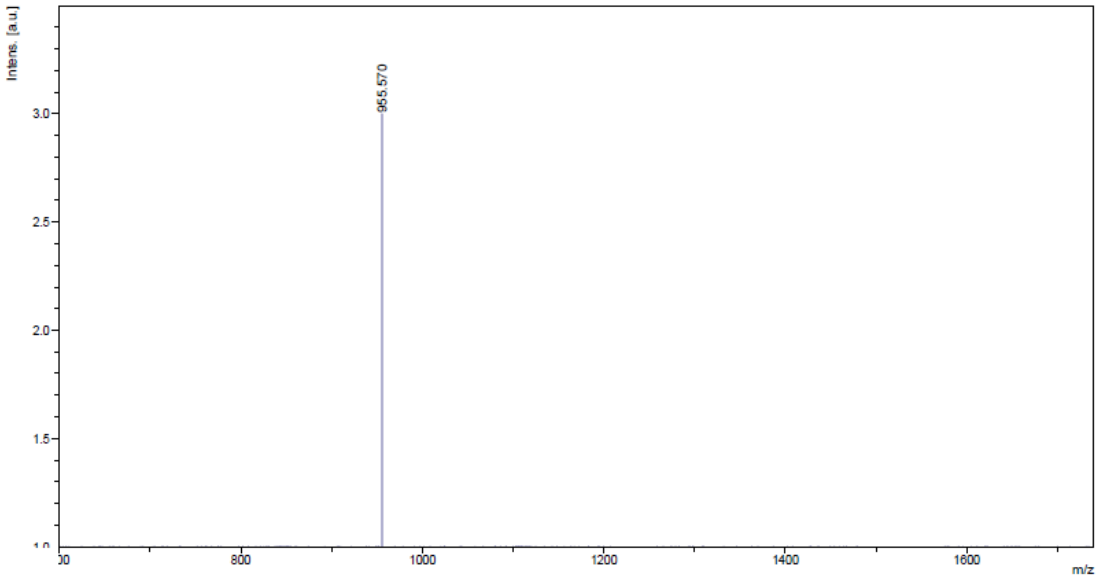

Figure A.15 MALDI-TOF Mass spectrum of **6**

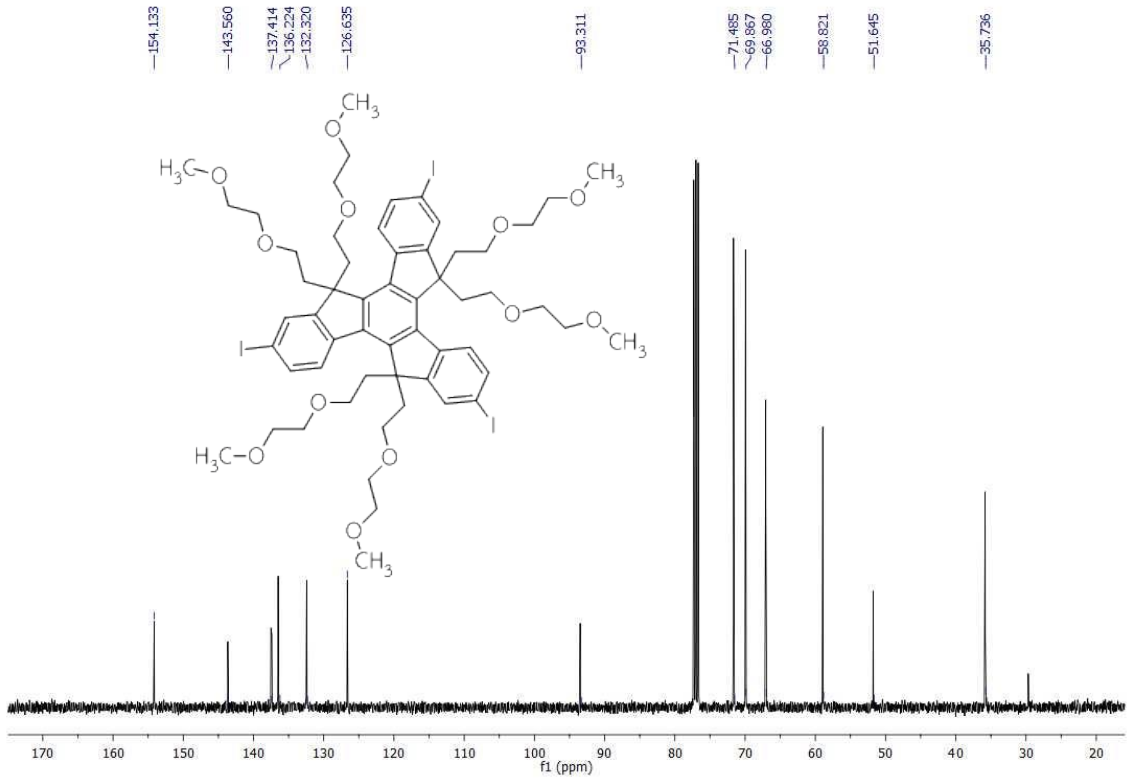

Figure A.16 ^{13}C NMR spectrum of **7** (400 MHz, in $CDCl_3$)

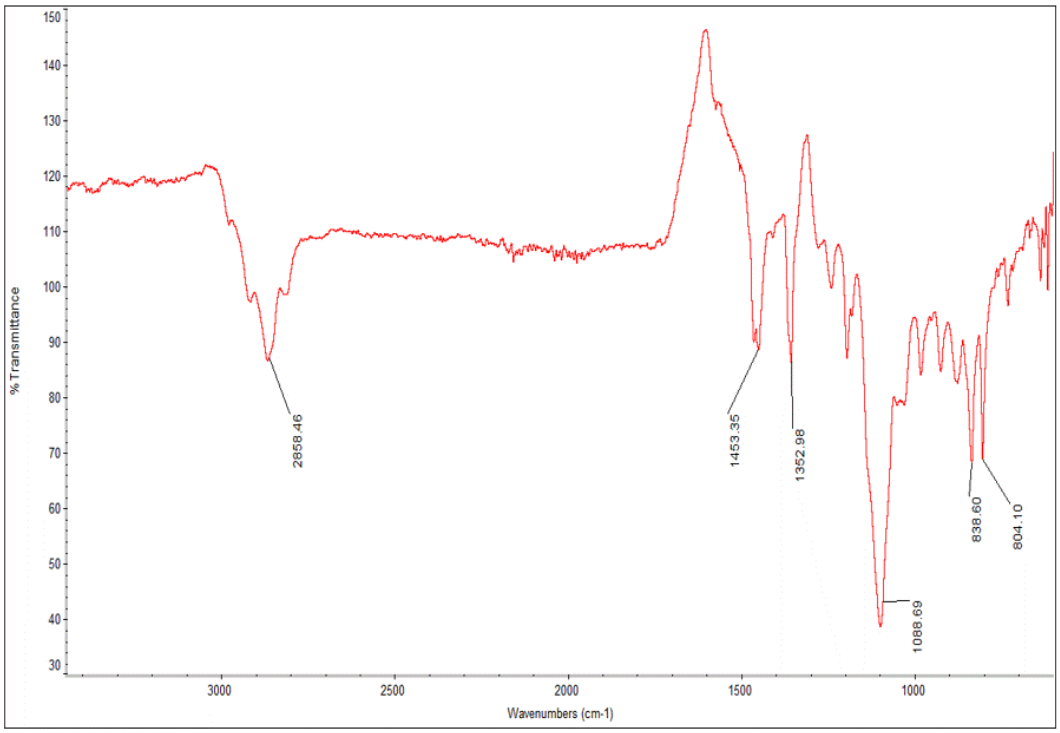

Figure A.17 IR spectrum of **7**

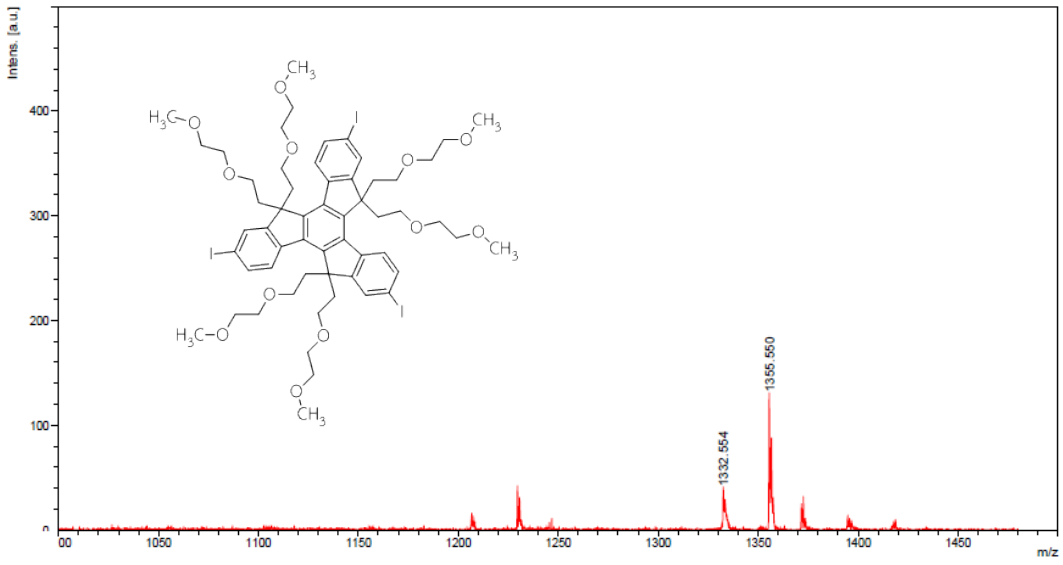

Figure A.18 MALDI-TOF Mass spectrum of **7**

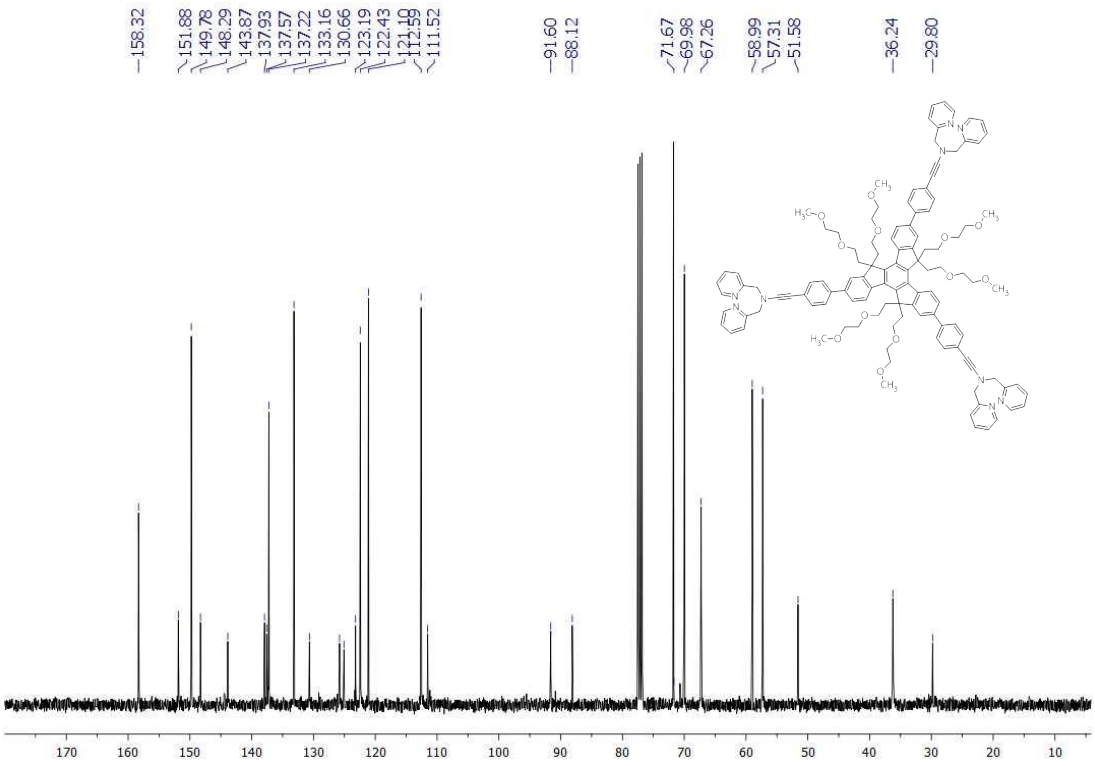

Figure A.19 ^{13}C NMR spectrum of **T2** (400 MHz, in $CDCl_3$)

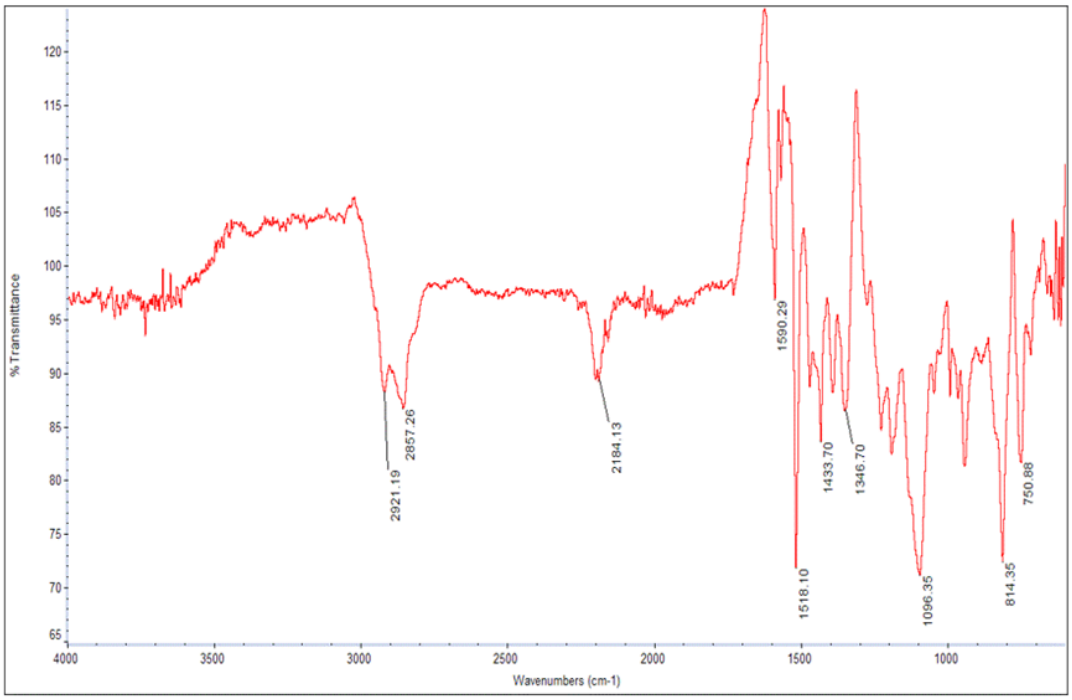

Figure A.20 IR spectrum of **T2**

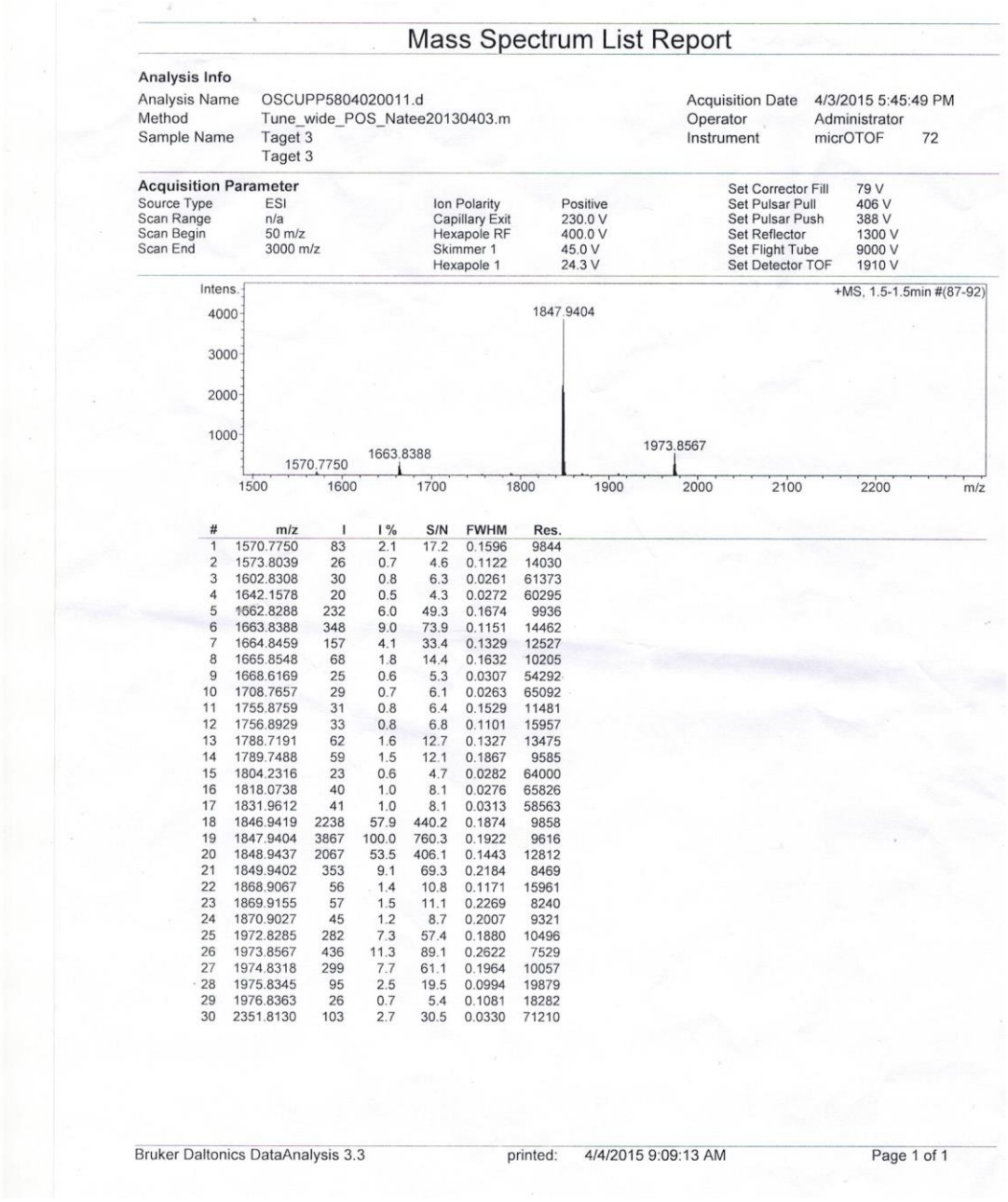

Mass Spectrum List Report

Analysis Info

Analysis Name	OSCUPP5804020011.d	Acquisition Date	4/3/2015 5:45:49 PM
Method	Tune_wide_POS_Natee20130403.m	Operator	Administrator
Sample Name	Taget 3 Taget 3	Instrument	micrOTOF 72

Acquisition Parameter

Source Type	ESI	Ion Polarity	Positive	Set Corrector Fill	79 V
Scan Range	n/a	Capillary Exit	230.0 V	Set Pulsar Pull	406 V
Scan Begin	50 m/z	Hexapole RF	400.0 V	Set Pulsar Push	388 V
Scan End	3000 m/z	Skimmer 1	45.0 V	Set Reflector	1300 V
		Hexapole 1	24.3 V	Set Flight Tube	9000 V
				Set Detector TOF	1910 V

#	m/z	I	I %	S/N	FWHM	Res.
1	1570.7750	83	2.1	17.2	0.1596	9844
2	1573.8039	26	0.7	4.6	0.1122	14030
3	1602.8308	30	0.8	6.3	0.0261	61373
4	1642.1578	20	0.5	4.3	0.0272	60295
5	1662.8288	232	6.0	49.3	0.1674	9936
6	1663.8388	348	9.0	73.9	0.1151	14462
7	1664.8459	157	4.1	33.4	0.1329	12527
8	1665.8548	68	1.8	14.4	0.1632	10205
9	1668.6169	25	0.6	5.3	0.0307	54292
10	1708.7657	29	0.7	6.1	0.0263	65092
11	1755.8759	31	0.8	6.4	0.1529	11481
12	1756.8929	33	0.8	6.8	0.1101	15957
13	1788.7191	62	1.6	12.7	0.1327	13475
14	1789.7488	59	1.5	12.1	0.1867	9585
15	1804.2316	23	0.6	4.7	0.0282	64000
16	1818.0738	40	1.0	8.1	0.0276	65826
17	1831.9612	41	1.0	8.1	0.0313	58563
18	1846.9419	2238	57.9	440.2	0.1874	9858
19	1847.9404	3867	100.0	760.3	0.1922	9616
20	1848.9437	2067	53.5	406.1	0.1443	12812
21	1849.9402	353	9.1	69.3	0.2184	8469
22	1868.9067	56	1.4	10.8	0.1171	15961
23	1869.9155	57	1.5	11.1	0.2269	8240
24	1870.9027	45	1.2	8.7	0.2007	9321
25	1972.8285	282	7.3	57.4	0.1880	10496
26	1973.8567	436	11.3	89.1	0.2622	7529
27	1974.8318	299	7.7	61.1	0.1964	10057
28	1975.8345	95	2.5	19.5	0.0994	19879
29	1976.8363	26	0.7	5.4	0.1081	18282
30	2351.8130	103	2.7	30.5	0.0330	71210

Bruker Daltonics DataAnalysis 3.3 printed: 4/4/2015 9:09:13 AM Page 1 of 1

Figure A.21 HR-ESI Mass spectrum of **T2**

VITA

Miss Pornpat Sam-ang was born on August 2nd, 1982 in Sukhothai, Thailand. She received a Bachelor's Degree of Science, majoring in Chemistry from Faculty of Science, Chiang Mai University in 2004 and hold a Master's Degree of Science, majoring in Organic Chemistry under the supervision of Prof. Dr. Ngampong Kongkathip at Kasetsart University in 2008. She was a graduate student under the supervision of Assoc. Prof. Dr. Paitoon Rashatasakhon. During her studies towards a Ph.D. program, she got a scholarship from the Office of the Higher Education Commission (OHEC) (2010-2014) for financial support, a teaching assistant scholarship from the Faculty of Science in 2010-2013 and the Overseas Research Experience Scholarship (ORES) for Graduate Student from Graduate School and Faculty of Science, Chulalongkorn University to conduct part of her thesis research under the supervision of Prof. Dr. Quan Jason Cheng at the department of Chemistry, University of California Riverside, starting from August 24th,2015 to October 25th 2015. She graduated with Ph.D. degree in Organic chemistry at Chulalongkorn University in academic year 2015.

Her parents address is 118/3 Moo 9, Tambon Phkumkao, Amphur Sawankalok, Sukhothai, Thailand, 64110

PUBLICATION:

Sam-ang, P.; Raksasorn, D.; Sukwattanasinitt, M.; Rashatasakhon, P. A nitroaromatic fluorescence sensor from a novel tripyrenyl truxene. RSC Adv., 2014, 4, 58077–58082.